The Dissertation Committee for David Brian Johnson
certifies that this is the approved version of the following dissertation:

The Micromaser Theory and Comparison to Experiment

Committee:

William C. Schieve, Supervisor

Jack S. Turner

Linda E. Reichl

Mark G. Raizen

Robert E. Wyatt

The Micromaser Theory and Comparison to Experiment

by

David Brian Johnson, B.S.

DISSERTATION

Presented to the Faculty of the Graduate School of

The University of Texas at Austin

in Partial Fulfillment

of the Requirements

for the Degree of

DOCTOR OF PHILOSOPHY

THE UNIVERSITY OF TEXAS AT AUSTIN

December 2003

The Micromaser Theory and Comparison to Experiment

Publication No. _____

David Brian Johnson, Ph.D.
The University of Texas at Austin, 2003

Supervisor: William C. Schieve

The one-atom maser or micromaser is a quantum optics system that allows the observation of single two-level atoms interacting with a single-mode field. The microscopic nature of the micromaser system and the absence of significant amounts of stochasticity and noise, allows for the observation of behavior that is drastically different from that of macroscopic masers. This dissertation describes theoretical studies of the micromaser system and extensions of the previous micromaser theory to improve its agreement with experimental observations.

Table of Contents

List of Figures

Chapter 1

Introduction

The most basic system of radiation-matter coupling is a single two-level atom interacting with a single mode of an electromagnetic field. This system was first treated theoretically by Jaynes and Cummings in 1963 [29]. Their model predicted an enhancement of the spontaneous emission rate near resonance and Rabi oscillations of energy exchange between the atom and field in agreement with the earlier classical models. The Jaynes-Cummings model also predicts collapse and revivals [42] and fractional revivals [1] of the Rabi oscillations at large interaction times. This system was of purely academic interest until the development of frequency-tunable lasers allowed the study of highly excited Rydberg atoms. The use of Rydberg atoms allows for very strong atom-field coupling and long spontaneous lifetimes. Also, transitions to neighboring levels being coupled to microwave frequency modes allows for the construction of cavities with low-order modes being sufficiently large to insure long interaction times. Enhancement of the spontaneous emission rate of a single atom in a tuned cavity was observed in 1983 [23]. Later in 1985 a group led by H. Walther achieved the construction of a cavity of sufficiently high Q that the oscillatory energy exchange between the atom and field could be observed [41]. Their system consists of a series of identically prepared Rydberg atoms injected into a maser cavity at a rate small enough so that it is rare for more than one atom to interact with the field at the same time. Since then, the Jaynes-Cummings model has been found useful in a number of other applications including quantum nondemolition measurements [7, 8, 27], quantum state teleportation [10, 15], quantum computation [59], ion traps [11], and optical cavity QED [21].

In the one-atom maser or micromaser, as it came to be called the atoms play a dual-purpose role of both pumping the field and also probing the field via measurements made on the outgoing atoms. Any other means of measuring

the field has the detrimental effect of lowering the Q of the cavity. The long photon-storage time of the cavity allows for the build up of a significant field without needing higher pump rates that would include a significant amount of cooperative effects. It also allows for the decay of the field to be negligible during the passage of an atom whose interaction time is much less than the photon-storage time. The dynamics of the micromaser system thus separates into times of pure damping of the field punctuated by the passage of single atoms through the cavity with the atom-field interactions described by the Jaynes-Cummings model. This is the micromaser theory that was first proposed by Filipowicz, Javanainen, and Meystre in 1986 [20]. Their model also included the effect of a highly peaked distribution of atomic velocities. The theory predicts a number of behaviors that are drastically different from that of macroscopic masers due to the microscopic nature of the micromaser system and the absence of significant amounts of stochasticity and noise. These behaviors include sub-Poissonian statistics [20, 37], bistability and hysteresis [20], trapping states [44], and quantum jumps [3].

In 1987 Rempe and Walther *et al.* measured the probability of detecting atoms in the upper maser level and obtained results in good agreement with the theory and observed an effect analogous to the collapse and revivals of the Jaynes-Cummings model [54]. Then in 1990 they argued that the sub-Poissonian statistics of the micromaser field could be observed by the presence of sub-Poissonian statistics in the detection of lower state atoms [53] and measured the Fano-Mandel function for the detection of lower state atoms [52]. They observed sub-Poissonian statistics and obtained results in good agreement with the theory. In 1995 Raithel and Walther *et al.* [50] observed atom-atom correlations and bistability. More recently, Weidinger and Walther *et al.* have reported evidence of trapping states in measurements of the atomic inversion and the Fano-Mandel function [67], though their results show poor agreement with the theory.

In order to increase the regime of applicability of micromaser theory and to improve the comparison with past and future experiments, much work has been done to extend the theory of Filipowicz, Javanainen, and Meystre. Zhu *et al.* have extended the Jaynes-Cummings model to include the effect of atomic damping and discussed its effect on the microamser field statistics [68],

though they assumed zero temperature and gave results only for the case of the two atomic levels having the same decay rate. The micromaser theory has also been extended by determining the detection statistics of the outgoing atoms including the effect of inefficient detection. The evolution of the micromaser field between detection events was derived by Briegel *et al.* [6]. They showed that conditioned evolution of the field is described by a nonlinear master equation. However, a linear master equation and a non-normalized conditioned density operator, as used by Herzog [25], can be used in place of the nonlinear equation and the normalized conditioned density operator. For the case of inefficient detection, the counting statistics [6], the sequence statistics [30], and the waiting-time statistics [30] of detection events were derived. The detection statistics of the emerging atoms have been shown to be sensitive to the photon-number distribution in steady state [53] and the intensity fluctuations [12, 13, 25, 26]. The theory was also extended to include the counter-rotating terms neglected in the rotating-wave approximation by Zheng-Dong *et al.* [35]. We extended the theory to include two-atom events [31] making use of the results of Kolobov and Haake [33] who derived the equivalent of the Jaynes-Cummings model for two atoms interacting with the same field. Even at the pump rates used in Walther's experiments where the occurrence of two-atom events are extremely rare, two-atom events were predicted to affect the visibility of trapping states [47, 66], though our analysis showed that the effect of including of two-atom events was negligible in the experiment of Ref. [67] in which Walther's group reported evidence of trapping states.

Other micromaser arrangements have been proposed. Krause and others [34, 39, 56] have proposed coherently pumped micromasers. Wagner *et al.* [63–65] have proposed introducing a $\pi/2$ pulse on the atomic beam between the exit port of the maser cavity and the detection apparatus. Both of these experiments were proposed in order to break the phase symmetry of the field in order to achieve measurements sensitive to the field coherence properties. They have been shown to allow measurements of the phase diffusion rate and linewidth of the field, but neither has been shown to give the full details of the spectrum. Briegel *et al.* [5] has considered a periodically pumped maser in which the atoms arrive at equal intervals. Such a setup is attractive for its simplicity and is susceptible to analysis using the damping basis [4]. More recently, Varcoe and Walther *et al.* have begun observations

on a pulsed micromaser, in which a packet of excited atoms arrive at a maser cavity containing only a thermal field. With this setup they have been able to observe number states [61].

For good reviews of the micromaser theory and experiments consult Refs. [18, 24, 45, 51, 58].

In Chapter 2 of this dissertation we review background material about electromagnetic fields inside a high-Q cavity. We also discuss the theory of system-reservoir interactions and the damping of the electromagnetic field. In addition, we discuss the eigenstates of the damping operator that were derived by Briegel [4]. We make a small contribution by correcting the errors in the discussion of Ref. [4] and by treating the left eigenstates of the damping operator differently which simplifies the establishment of orthonormality.

In Chapter 3 of this dissertation we review background material about Rydberg atoms in electromagnetic fields. We also discuss the damping of two-level atoms using a density operator approach similar to the theory of system-reservoir interactions used to describe the damping of the field. This approach gives the usual depletion of the atomic levels due to Wigner-Weisskopf spontaneous emission without making the assumption of zero temperature. It also leads to reservoir-induced transitions between the two levels of the two-level atom that cause the atom to approach a steady state inversion. If you were to describe the reservoir-induced transitions between the two levels of the two-level atom as spontaneous emission at zero temperature, you would conclude that the steady state inversion of the atom is -1. Our contribution is therefore to relax this assumption by describing the relaxation of the atom to the exact steady state inversion. We also discuss the Jaynes-Cummings model of a two-level atom interacting with a single mode field. We extend the Jaynes-Cummings model by including the effect of a spacial-dependent atom-field coupling strength, but show that it has no effect for the case of an atom traversing the cylindrical axis of a cylindrical cavity containing the TE mode used in the experiments of Walther *et al.* [41, 50, 52, 54, 67]. We also extend the Jaynes-Cummings model to include depletion damping, obtaining results that agree with Zhu *et al.* [68].

In Chapter 4 of this dissertation we discuss the micromaser system. We first derive a continuous master equation averaged over the Poissonian

arrival times of the injected atoms. This establishes an operator describing the evolution of the microamser field which had been in use but lacked a formal derivation. We then derive a more general steady state of the micromaser field that includes a non-zero temperature, depletion damping, and velocity averaging. Using this, we discuss the effect of depletion damping on the photon statistics of the micromaser field.

In Chapter 5 of this dissertation we discuss the extension of the micromaser theory to include two-atom events. Kolobov and Haake [33] studied the equivalent of the Jaynes-Cummings model including two atoms interacting with the same field. They also considered the effect of two-atom effects on the micromaser, but their subsequent analysis suffered from approximations and their results were dubious. We extend the theory of Kolobov and Haake by making no approximations and derive the evolution operator and steady state of the micromaser field including two-atom events [31]. Earlier Casagrande *et al.* [9] made the same extension using a quantum trajectory method, but their results have errors. A comparison of our results (in which the spacings between the two atoms in two-atom events are averaged over) with the two extreme cases of two-atom events consisting of atoms arriving in pairs and atoms arriving sequentially, places the average result in between the two extreme cases (as a result of the smooth dependence on the arrival spacings of the two atoms). The results of Casagrande *et al.* does not give this result. As a further test, we perform a Monte Carlo simulation and find that the results agree with our theory.

In Chapter 6 of this dissertation we discuss the detection statistics of the outgoing atoms due to inefficient detection. We contribute to the discussion by deriving the sequence statistics and waiting-time statistics of the detection events [30]. We derive the average number of successive detections of atoms in the upper and lower maser level. We also show that the average waiting-times between detections of atoms in the same state are given by the uncorrelated rates of atomic detections, but that the average waiting-times between atoms in different states exhibit correlations. The waiting-time statistics were calculated earlier, but only for particular trapping states [6, 25].

In Chapter 7 of this dissertation we discuss results of calculations of observable quantities. First we discuss results of calculations of the atomic in-

version including non-zero temperature, atomic depletion damping, and velocity averaging for comparison with the experiment of Weidinger *et al.* [67]. We then perform the same comparison between calculations of the Fano-Mandel function and the experimental measurements in Ref. [67]. Despite the effort to perform a comprehensive comparison with the experimental results, the agreement remains very poor. In light of the good agreement between the previous experiments and the theory, the recent lack of agreement is unexpected. We also show results of calculations of various sequence statistics that have not been measured by experiment. We show that the mean number of successive detections of atoms in the upper and lower maser levels are sensitive to the presence of trapping states and might provide a better alternative to measurements of the atomic inversion for observing trapping states. Finally, we show calculations of the average waiting-time statistics between atoms in different states exhibiting atom-atom correlations.

Chapter 2

Cavity Fields

2.1 Classical Cavity Fields

This sections presents some background material that sets the stage for a later discussion of quantized electromagnetic fields in a cavity. A good reference of classical cavity fields and classical electrodynamics in general is the book by J.D. Jackson [28].

Consider a cavity of volume V, enclosed by perfectly conducting walls. The electromagnetic field inside the cavity is described classically by Maxwell's equations. In the absence of charges and currents, they are given by

$$\nabla \cdot \mathbf{E} = 0 \tag{2.1}$$
$$\nabla \cdot \mathbf{B} = 0 \tag{2.2}$$
$$\nabla \times \mathbf{E} = -\frac{\partial \mathbf{B}}{\partial t} \tag{2.3}$$
$$\nabla \times \mathbf{B} = \frac{1}{c^2}\frac{\partial \mathbf{E}}{\partial t} \tag{2.4}$$

(SI units). We may satisfy Eqs. (2.2) and (2.3) if we let

$$\mathbf{E} = -\frac{\partial \mathbf{A}}{\partial t} - \nabla\Phi \tag{2.5}$$
$$\mathbf{B} = \nabla \times \mathbf{A}, \tag{2.6}$$

where $\mathbf{A}$ and Φ are the vector and scalar potentials. Choosing the Coulomb guage condition

$$\nabla \cdot \mathbf{A} = 0 \tag{2.7}$$
$$\Phi = 0, \tag{2.8}$$

Eq. (2.1) is automatically satisfied. By using the vector identity

$$\nabla \times \nabla \times \mathbf{A} = \nabla(\nabla \cdot \mathbf{A}) - \nabla^2 \mathbf{A}, \tag{2.9}$$

the remaining nontrivial equation (2.4) can be put in the form of the wave equation

$$\nabla^2 \mathbf{A} - \frac{1}{c^2} \frac{\partial^2 \mathbf{A}}{\partial t^2} = 0. \tag{2.10}$$

We use the procedure of separation of variables, and assume a solution of the form

$$\mathbf{A}(\mathbf{r}, t) = \frac{1}{\sqrt{\epsilon_0}} \sum_l q_l(t) \mathbf{u}_l(\mathbf{r}). \tag{2.11}$$

where the coefficient $\epsilon_0^{-1/2}$ is used for normalization. If we substitute this into the wave equation (2.10), then for each l we have

$$\ddot{q}_l + \omega_l^2 q_l = 0 \tag{2.12}$$

$$\nabla^2 \mathbf{u}_l + k_l^2 \mathbf{u}_l = 0, \tag{2.13}$$

where the frequencies ω_l are separation constants, and the wavenumbers k_l are given by $k_l = \omega_l / c$. The guage condition (2.7) further requires that

$$\nabla \cdot \mathbf{u}_l = 0. \tag{2.14}$$

The solution to Eq. (2.12) is oscillatory, and can be written in complex form as

$$q_l(t) = q_l(0) e^{-i\omega_l t} \tag{2.15}$$

(the real solution being the real part of this complex solution and $q_l(0)$ being an arbitrary amplitude and complex phase).

The solution to Eq. (2.13) will depend on the boundary conditions. For boundary conditions, we require that at the walls of the cavity the tangential component of $\mathbf{E}$ and the normal component of $\mathbf{B}$ vanish. That is

$$\hat{\mathbf{n}} \times \mathbf{E}|_{\text{wall}} = 0 \tag{2.16}$$

$$\hat{\mathbf{n}} \cdot \mathbf{B}|_{\text{wall}} = 0, \tag{2.17}$$

where $\hat{\mathbf{n}}$ is a unit normal at the wall. The electric and magnetic fields corresponding to the vector potential (2.11) are given by

$$\mathbf{E} = -\frac{1}{\sqrt{\epsilon_0}} \sum_l \dot{q}_l \mathbf{u}_l \tag{2.18}$$

$$\mathbf{B} = \frac{1}{\sqrt{\epsilon_0}} \sum_l q_l \nabla \times \mathbf{u}_l, \tag{2.19}$$

and so the boundary conditions become

$$\hat{\mathbf{n}} \times \mathbf{u}_l|_{\text{wall}} = 0 \tag{2.20}$$

$$\hat{\mathbf{n}} \cdot (\nabla \times \mathbf{u}_l)|_{\text{wall}} = 0. \tag{2.21}$$

Independent of the shape of the cavity, a discrete set of spatial functions $\mathbf{u}_l$ can be found that satisfy the boundary conditions and form a complete, orthonormal set:

$$\int_V dV\, \mathbf{u}_l \cdot \mathbf{u}_m = \delta_{lm}. \tag{2.22}$$

The spatial functions $\mathbf{u}_l$ are then completely specified and describe the normal modes of the cavity, with the amplitude of the lth mode given by the real part of $q_l(t)$.

The Hamiltonian for the field is given by

$$\mathcal{H} = \frac{1}{2} \int_V dV \left(\epsilon_0 \mathbf{E}^2 + \frac{1}{\mu_0} \mathbf{B}^2 \right). \tag{2.23}$$

If we substitute in the electric and magnetic fields (2.18) and (2.19), we have

$$\mathcal{H} = \frac{1}{2} \sum_{l,m} \dot{q}_l \dot{q}_m \int_V dV\, \mathbf{u}_l \cdot \mathbf{u}_m + \frac{c^2}{2} \sum_{l,m} q_l q_m \int_V dV\, (\nabla \times \mathbf{u}_l) \cdot (\nabla \times \mathbf{u}_m). \tag{2.24}$$

Using the orthonormality condition (2.22), the first term becomes $\frac{1}{2} \sum_l \dot{q}_l^2$. By the vector identity

$$(\nabla \times \mathbf{u}_l) \cdot (\nabla \times \mathbf{u}_m) = \mathbf{u}_m \cdot \nabla \times \nabla \times \mathbf{u}_l + \nabla \cdot (\mathbf{u}_m \times \nabla \times \mathbf{u}_l), \tag{2.25}$$

and Gauss's theorem, the last integral in Eq. (2.24) becomes

$$\int_V dV\, \mathbf{u}_m \cdot \nabla \times \nabla \times \mathbf{u}_l + \int_{\partial V} d\mathbf{A} \cdot (\mathbf{u}_m \times \nabla \times \mathbf{u}_l), \tag{2.26}$$

where $d\mathbf{A}$ is an element of area on the cavity wall. The surface integral vanishes because of the boundary condition (2.21). The first integral in Eq. (2.26) is

$$\int_V dV\, \mathbf{u}_m \cdot (\nabla(\nabla \cdot \mathbf{u}_l) - \nabla^2 \mathbf{u}_l) = k_l^2 \int_V dV\, \mathbf{u}_l \cdot \mathbf{u}_m = k_l^2 \delta_{lm}, \tag{2.27}$$

where we have used Eqs. (2.13), (2.14), and (2.22). Putting everything together, we have

$$\mathcal{H} = \frac{1}{2} \sum_l (\dot{q}_l^2 + \omega_l^2 q_l^2), \tag{2.28}$$

which is equivalent to the Hamiltonian for an infinite set of uncoupled harmonic oscillators of unit mass and frequencies ω_l. In this way, we associate a radiation oscillator with each normal mode of the cavity.

We have shown that a cavity with perfectly conducting walls has a discrete set of frequencies of oscillation with a definite spatial mode for each resonance frequency. In actuality, there is a narrow band of frequencies around each resonance frequency over which appreciable excitation of the mode can occur. The principle source of this is the dissipation of energy due to losses in the cavity walls and perhaps in a dielectric filling the cavity. A measure of the sharpness of a cavity's response to excitation near a resonance frequency is the quality factor Q, defined as

$$Q = \omega_0 \frac{\text{Stored energy}}{\text{Power loss}}. \tag{2.29}$$

Here ω_0 is the resonance frequency of the cavity. This says that free oscillations of the field decay at the rate $\gamma_\text{f} = \omega_0/Q$. A damped oscillator driven at a frequency ω near the resonance frequency has an energy response given by the Lorentz line shape

$$E(\omega) = E(\omega_0) \frac{\left(\frac{1}{2}\gamma_\text{f}\right)^2}{(\omega - \omega_0)^2 + \left(\frac{1}{2}\gamma_\text{f}\right)^2}, \tag{2.30}$$

where the decay rate γ_f is also the half-width of the line shape. The modes in a cavity thus have a characteristic width, and, as a matter of practicality, it is best for the dimensions of the cavity to be chosen so that the resonant frequency of operation lies well separated from other resonant frequencies.

2.2 Quantized Cavity Fields

The field is quantized by quantizing each mode of the cavity as a quantum-mechanical harmonic oscillator. For each mode l, we define boson anihilation and creation operators a_l and $a_l^\dagger$ in the usual way:

$$a_l = \frac{1}{\sqrt{2\hbar\omega_l}}(\omega_l q_l + i\dot{q}_l) \tag{2.31}$$

$$a_l^\dagger = \frac{1}{\sqrt{2\hbar\omega_l}}(\omega_l q_l - i\dot{q}_l). \tag{2.32}$$

The Hamiltonian for the field (without the zero-point energy) becomes

$$\mathcal{H} = \hbar \sum_l \omega_l a_l^\dagger a_l, \tag{2.33}$$

and the fields are described by the time-independent operators

$$\mathbf{A} = \sum_l \sqrt{\frac{\hbar}{2\omega_l\epsilon_0}}\mathbf{u}_l(a_l + a_l^\dagger) \tag{2.34}$$

$$\mathbf{E} = i\sum_l \sqrt{\frac{\hbar\omega_l}{2\epsilon_0}}\mathbf{u}_l(a_l - a_l^\dagger) \tag{2.35}$$

$$\mathbf{B} = \sum_l \sqrt{\frac{\hbar}{2\omega_l\epsilon_0}}\nabla \times \mathbf{u}_l(a_l + a_l^\dagger), \tag{2.36}$$

The time-dependence of the field is now given by the action of the operators a_l and $a_l^\dagger$ on the time-dependent state of the field in the Schrödinger picture.

2.3 Hollow Cylindrical Cavities

The discussion here follows closely the discussion of wave guides and resonant cavities in Ref. [28]. We consider a category of resonant cavities consisting of a hollow metallic cylinder with plane end faces perpendicular to the cylindrical axis. Of particular interest here are right circular cylindrical cavities like the one used in the experiments of Walther *et al.* [41, 52, 54, 67]. In order to find the mode structure of such a cavity it is easier, in practice, to work with $\mathbf{E}$ and $\mathbf{B}$ rather than with $\mathbf{A}$ alone (or equivalently, working with $\mathbf{u}_l$

and $\mathbf{w}_l = \nabla \times \mathbf{u}_l$ rather than with $\mathbf{u}_l$ alone). As will be shown, the modes of a hollow cylindrical cavity separate neatly into two distinct categories called transverse magnetic modes and transverse electric modes. Taking the curl of Eqs. (2.3) and (2.4), and making use of the vector identity (2.9) and the vanishing divergences, we find that both $\mathbf{E}$ and $\mathbf{B}$ satisfy the wave equation

$$\left(\nabla^2 - \frac{1}{c^2}\frac{\partial^2}{\partial t^2}\right)\left\{\begin{array}{c}\mathbf{E}\\ \mathbf{B}\end{array}\right\} = 0. \tag{2.37}$$

For a particular mode of frequency ω (dropping the l subscripts for clarity), we set

$$\mathbf{E} = -\frac{1}{\sqrt{\epsilon_0}}\dot{q}\mathbf{u} \tag{2.38}$$

$$\mathbf{B} = \frac{1}{\sqrt{\epsilon_0}}q\mathbf{w}, \tag{2.39}$$

and assume solutions of the form

$$\mathbf{u}(x,y,z) = \mathbf{u}(x,y)e^{\pm ik_z z} \tag{2.40}$$

$$\mathbf{w}(x,y,z) = \mathbf{w}(x,y)e^{\pm ik_z z} \tag{2.41}$$

appropriate for standing waves along the cylindrical axis in the $\hat{\mathbf{z}}$ direction. The wave equation (2.37) becomes

$$\left(\nabla_{\mathrm{t}}^2 + k_t^2\right)\left\{\begin{array}{c}\mathbf{u}\\ \mathbf{w}\end{array}\right\} = 0, \tag{2.42}$$

where

$$\nabla_{\mathrm{t}}^2 \equiv \nabla^2 - \frac{\partial^2}{\partial z^2} \tag{2.43}$$

is the transverse part of the Laplacian operator and

$$k_t^2 = k^2 - k_z^2. \tag{2.44}$$

It is useful to separate the fields into components parallel and transverse to the cylindrical axis:

$$\mathbf{u} = u_z\hat{\mathbf{z}} + \mathbf{u}_t \tag{2.45}$$

$$\mathbf{w} = w_z\hat{\mathbf{z}} + \mathbf{w}_t. \tag{2.46}$$

By applying $\hat{\mathbf{z}}\times$ to the curl equations (2.3) and (2.4), the transverse components of the curl equations can be written as

$$\frac{\partial \mathbf{u}_t}{\partial z} + \hat{\mathbf{z}} \times \mathbf{w}_t = -\nabla_t u_z \tag{2.47}$$

$$\frac{\partial \mathbf{w}_t}{\partial z} + k^2(\hat{\mathbf{z}} \times \mathbf{u}_t) = -\nabla_t w_z. \tag{2.48}$$

It is evident that, if u_z and w_z are known, the transverse components $\mathbf{u}_t$ and $\mathbf{w}_t$ are determined. This suggests that our strategy should be to first solve the wave equation (2.42) for just the longitudinal components u_z and w_z (with appropriate boundary conditions) and then determine the transverse components $\mathbf{u}_t$ and $\mathbf{w}_t$ from Eqs. (2.47) and (2.48).

Now we will consider the boundary conditions for the parallel components. On the cylindrical surface S (the walls of the cavity without the end surfaces), the boundary condition (2.20) gives

$$u_z|_S = 0. \tag{2.49}$$

The component of Eq. (2.48) parallel to the normal $\hat{\mathbf{n}}$ is

$$\frac{\partial}{\partial z}(\hat{\mathbf{n}} \cdot \mathbf{w}_t) + k^2(\hat{\mathbf{n}} \times \hat{\mathbf{z}}) \cdot \mathbf{u}_t = -\frac{\partial w_z}{\partial n}, \tag{2.50}$$

where $\partial/\partial n$ is the normal derivative at a point on S. The boundary conditions (2.20) and (2.21) imply that $(\hat{\mathbf{n}} \times \hat{\mathbf{z}}) \cdot \mathbf{u}_t|_S = 0$ and $\hat{\mathbf{n}} \cdot \mathbf{w}_t|_S = 0$, and so the boundary condition on w_z is

$$\left.\frac{\partial w_z}{\partial n}\right|_S = 0. \tag{2.51}$$

Since the boundary conditions on u_z and w_z are different, the fields naturally separate into two distinct categories: transverse magnetic (TM) modes with

$$w_z = 0 \quad u_z|_S = 0 \tag{2.52}$$

and transverse electric (TE) modes with

$$u_z = 0 \quad \left.\frac{\partial w_z}{\partial n}\right|_S = 0. \tag{2.53}$$

On the end surfaces, taken to be located at $z = 0$ and $z = d$, the boundary conditions (2.20) and (2.21) require that $\mathbf{u}_t$ and w_z vanish. For TM modes, the vanishing of $\mathbf{u}_t$ at the end surfaces requires

$$u_z = u_z(x, y)\cos(k_z z) \tag{2.54}$$

$$k_z = \frac{p\pi}{d}, \quad p = 0, 1, 2, \ldots. \tag{2.55}$$

For TE modes, the vanishing of w_z at the end surfaces requires

$$w_z = w_z(x, y)\sin(k_z z) \tag{2.56}$$

$$k_z = \frac{p\pi}{d}, \quad p = 1, 2, \ldots. \tag{2.57}$$

These boundary conditions plus the wave equation (2.42) completely specify the functions $u_z(x, y)$ and $w_z(x, y)$ defining the parallel components of the field.

Once the parallel components of the field are known, the transverse components of the field are completely specified by Eqs. (2.47) and (2.48). For TM modes, we have $w_z = 0$ and Eq. (2.48) becomes

$$\mathbf{w}_t = \frac{k^2}{k_z^2}\frac{\partial}{\partial z}(\hat{\mathbf{z}} \times \mathbf{u}_t). \tag{2.58}$$

Substituting this into Eq. (2.47) we obtain

$$\mathbf{u}_t = -\frac{1}{k_t^2}\frac{\partial}{\partial z}\nabla_t u_z. \tag{2.59}$$

Substituting Eq. (2.54) into these results gives

$$\mathbf{u}_t = \frac{k_z}{k_t^2}\sin(k_z z)\nabla_t u_z(x, y) \tag{2.60}$$

$$\mathbf{w}_t = \frac{k^2}{k_t^2}\cos(k_z z)\hat{\mathbf{z}} \times \nabla_t u_z(x, y). \tag{2.61}$$

Similarly for TE modes, we obtain

$$\mathbf{u}_t = \frac{1}{k_t^2}\sin(k_z z)\hat{\mathbf{z}} \times \nabla_t w_z(x, y) \tag{2.62}$$

$$\mathbf{w}_t = -\frac{k_z}{k_t^2}\cos(k_z z)\nabla_t w_z(x, y). \tag{2.63}$$

Now consider a right circular cylindrical cavity with inner radius R. Because of the circular symmetry, it is useful to transform to cylindrical coordinates. The wave equation (2.42) in cylindrical coordinates is

$$\left(\frac{\partial^2}{\partial r^2}+\frac{1}{r}\frac{\partial}{\partial r}+\frac{1}{r^2}\frac{\partial^2}{\partial \phi}+k_t^2\right)\left\{\begin{array}{c} u_z(r,\phi) \\ w_z(r,\phi) \end{array}\right\}=0, \tag{2.64}$$

with solutions given by

$$\left\{\begin{array}{c} u_z(r,\phi) \\ w_z(r,\phi) \end{array}\right\}=J_m(k_t r)e^{\pm im\phi}, \tag{2.65}$$

where $J_m(x)$ is a Bessel function of the first kind (so that the solutions are finite at $r=0$), and m is an integer taking on the values $m=0,1,2,\ldots$ (so that the solutions are single valued). For TM modes, the boundary condition $u_z=0$ at $r=R$ gives the condition

$$k_t=\frac{x_{mn}}{R}, \tag{2.66}$$

where x_{mn} is the nth root of the equation $J_m(x)=0$. For TE modes, the boundary condition $\partial w_z/\partial r=0$ at $r=R$ gives the condition

$$k_t=\frac{x'_{mn}}{R}, \tag{2.67}$$

where x'_{mn} is the nth root of the equation $J_m{}'(x)=0$. Using Eqs. (2.60) and (2.62) we obtain the mode function $\mathbf{u}$. For TM modes we have

$$\begin{aligned}\mathbf{u} &= \frac{k_z}{k_t}\left(J'_m(k_t r)\hat{\mathbf{r}}\pm im\frac{J_m(k_t r)}{k_t r}\hat{\phi}\right)e^{\pm im\phi}\sin(k_z z) \\ &\quad +J_m(k_t r)e^{\pm im\phi}\cos(k_z z)\hat{\mathbf{z}},\end{aligned} \tag{2.68}$$

and for TE modes we have

$$\mathbf{u} = \frac{1}{k_t}\left(\mp im\frac{J_m(k_t r)}{k_t r}\hat{\mathbf{r}}+J'_m(k_t r)\hat{\phi}\right)e^{\pm im\phi}\sin(k_z z). \tag{2.69}$$

If desired, the auxiliary mode functions $\mathbf{w}$ can be obtained by taking the curl of $\mathbf{u}$ or using Eqs. (2.61) and (2.63).

2.4 Thermal Equilibrium of a Cavity Field

Consider a cavity field with the Hamiltonian (2.33) in thermal equilibrium for which we know only the average energy $\langle \mathcal{H} \rangle$. The density operator $\rho^{\rm th}$ describing this time-independent state with maximum entropy is given by

$$\rho^{\rm th} = \frac{e^{-\beta \mathcal{H}}}{Z} \tag{2.70}$$

and is called the thermal state. The partition function Z is given by

$$Z = {\rm tr}\{e^{-\beta \mathcal{H}}\} \tag{2.71}$$

and $\beta = 1/k_{\rm B}T$ is the Boltzmann coefficient with the temperature T of the system defined by the relation

$$\langle \mathcal{H} \rangle = -\frac{\partial}{\partial \beta} \ln Z. \tag{2.72}$$

Substituting in Eq. (2.33), Z becomes

$$\begin{aligned} Z &= {\rm tr}\left\{ \exp\left(-\beta\hbar \sum_l \omega_l a_l^\dagger a_l \right) \right\} \\ &= \prod_l \sum_{n_l=0}^{\infty} e^{-\beta \hbar \omega_l n_l} \\ &= \prod_l \frac{1}{1 - e^{-\beta \hbar \omega_l}}, \end{aligned} \tag{2.73}$$

and the thermal state becomes

$$\rho^{\rm th} = \prod_l \left(1 - e^{-\beta \hbar \omega_l} \right) e^{-\beta \hbar \omega_l a_l^\dagger a_l}. \tag{2.74}$$

The average excitation level of the lth mode in thermal equilibrium is given by

$$\nu_l \equiv \langle a_l^\dagger a_l \rangle_{\rm th} = \frac{1}{e^{\beta \hbar \omega_l} - 1}, \tag{2.75}$$

in terms of which $\rho^{\rm th}$ is given by

$$\rho^{\rm th} = \prod_l \frac{1}{\nu_l + 1} \left(\frac{\nu_l}{\nu_l + 1} \right)^{a_l^\dagger a_l}, \tag{2.76}$$

and the average energy of the field is

$$\langle \mathcal{H} \rangle = \hbar \sum_l \omega_l \nu_l. \tag{2.77}$$

2.5 Thermal Damping of a Single-mode Field

The statistical treatment of system-reservoir interactions is treated rather nicely by a number of references on Quantum Optics. Of particular interest is the book by Scully [58]. Consider a single mode of the cavity field as a system which is being driven away from equilibrium by some external mechanism. The system remains weakly coupled to other environmental degrees of freedom (e.g. phonons in the cavity walls), which act as a reservoir of energy that the system can exchange with. We postulate that the reservoir is in thermal equilibrium at temperature T, and is much larger than the system in regards to number of degrees of freedom and total energy. Left alone, the system would exchange energy with the reservoir until it approaches thermal equilibrium. We wish to describe this damping of the system for times short compared to times for which there is a significant change in the system variables. Any driving mechanism for the system is therefore neglected.

The Hamiltonian for a single-mode field is

$$\mathcal{H}_{\mathrm{f}} = \hbar \omega a^\dagger a, \tag{2.78}$$

and the reservoir is modelled as being a large number of harmonic oscillators described by the Hamiltonian

$$\mathcal{H}_{\mathrm{r}} = \hbar \sum_l \omega_l b_l^\dagger b_l, \tag{2.79}$$

where b_l and $b_l^\dagger$ are the boson anihilation and creation operators for the lth mode of the reservoir. We model the weak coupling between the single-mode field and the reservoir with the interaction Hamiltonian

$$\mathcal{V} = i\hbar \sum_l (g_l^* a b_l^\dagger - g_l a^\dagger b_l). \tag{2.80}$$

The exchange of energy is thus modelled as consisting of the simultaneous creation of a quantum of excitation of the system with an anihilation of a

quantum in the lth mode of the reservoir, or the reverse process. The coupling coefficients g_l denote the strength of the coupling and depend on the actual interaction mechanism.

It is assumed that initially the system and reservoir do not exhibit any correlations. Thus the initial state of the combined system is described by the factorized density operator

$$\rho(0) = \rho_{\rm f}(0)\rho_{\rm r}, \tag{2.81}$$

where $\rho_{\rm f}(0)$ is the density operator describing the initial state of the single-mode field and

$$\rho_{\rm r} = \frac{e^{-\beta\mathcal{H}_{\rm r}}}{{\rm tr}\{e^{-\beta\mathcal{H}_{\rm r}}\}} \tag{2.82}$$

is the density operator describing the time-independent thermal state of the reservoir.

In the absence of a driving mechanism, the dynamics of the combined system is described by the master equation

$$(\dot{\rho})_{\rm damp} = -\frac{i}{\hbar}[\mathcal{H}, \rho], \tag{2.83}$$

where the total Hamiltonian is given by $\mathcal{H} = \mathcal{H}_{\rm f} + \mathcal{H}_{\rm r} + \mathcal{V}$. We transform to the interaction picture with the transformation Hamiltonian $\mathcal{H}_0 = \mathcal{H}_{\rm f} + \mathcal{H}_{\rm r}$. The interaction Hamiltonian becomes

$$\begin{aligned} \mathcal{V} &\rightarrow e^{i\mathcal{H}_0\tau/\hbar}\mathcal{V}e^{-i\mathcal{H}_0\tau/\hbar} \\ &= i\hbar(aF^\dagger - a^\dagger F), \end{aligned} \tag{2.84}$$

where we have used the identities

$$e^{xa^\dagger a}a^\dagger e^{-xa^\dagger a} = e^x a^\dagger \tag{2.85}$$

$$e^{xa^\dagger a}a e^{-xa^\dagger a} = e^{-x} a \tag{2.86}$$

and have defined

$$F \equiv \sum_l g_l e^{i(\omega-\omega_l)\tau} b_l, \tag{2.87}$$

which acts only on the reservoir states. The master equation becomes

$$(\dot{\rho})_{\rm damp} = -\frac{i}{\hbar}[\mathcal{V}, \rho]. \tag{2.88}$$

We use time-dependent perturbation theory to solve the master equation to second order. We start with the formal solution of the master equation

$$\rho(\tau) = \rho(0) - \frac{i}{\hbar}\int_0^\tau d\tau' \, [\mathcal{V}(\tau'), \rho(\tau')]. \tag{2.89}$$

We then take $\rho(\tau) \simeq \rho^{(0)}(\tau) = \rho(0)$ in the commutator to obtain a first order solution:

$$\rho^{(1)}(\tau) = \rho(0) - \frac{i}{\hbar}\int_0^\tau d\tau' \, [\mathcal{V}(\tau'), \rho(0)]. \tag{2.90}$$

Using the improved approximation $\rho(\tau') \simeq \rho^{(1)}(\tau')$ we obtain a second order solution:

$$\begin{aligned} \rho^{(2)}(\tau) &= \rho(0) - \frac{i}{\hbar}\int_0^\tau d\tau' \, [\mathcal{V}(\tau'), \rho(0)] \\ &\quad -\frac{1}{\hbar^2}\int_0^\tau d\tau' \int_0^{\tau'} d\tau'' \, [\mathcal{V}(\tau'), [\mathcal{V}(\tau''), \rho(0)]]. \end{aligned} \tag{2.91}$$

Combining this with $\rho^{(2)}(-\tau)$, we can define the course-grained equation of motion for ρ by

$$\begin{aligned} (\dot{\rho})_{\rm damp} &\simeq \frac{\rho^{(2)}(\tau) - \rho^{(2)}(-\tau)}{2\tau} \\ &= \frac{-i}{2\hbar\tau}\int_{-\tau}^\tau d\tau' \, [\mathcal{V}(\tau'), \rho] \\ &\quad -\frac{1}{2\hbar^2\tau}\int_{-\tau}^\tau d\tau' \int_0^{\tau'} d\tau'' \, [\mathcal{V}(\tau'), [\mathcal{V}(\tau''), \rho]]. \end{aligned} \tag{2.92}$$

We proceed by tracing over the reservoir states to obtain the equation of motion for the reduced density operator for the single-mode field $\rho_{\rm f} = {\rm tr}_{\rm r}\{\rho\}$. Using the explicit form of the interaction Hamiltonian (2.84), we encounter terms such as

$${\rm tr}_{\rm r}\{a^\dagger F \rho\} = a^\dagger \rho_{\rm f} {\rm tr}_{\rm r}\{F\rho_{\rm r}\}. \tag{2.93}$$

The final trace in this equation vanishes since $\rho_{\rm r}$ is diagonal. Eliminating all terms that vanish, we are left with

$$\begin{aligned}(\dot{\rho}_{\rm f})_{\rm damp} &= -\frac{1}{2\tau}\int_{-\tau}^{\tau}d\tau'\int_{0}^{\tau'}d\tau''\,[a^\dagger a\rho_{\rm f}\langle F(\tau')F^\dagger(\tau'')\rangle_{\rm r} - a\rho_{\rm f}a^\dagger\langle F(\tau'')F^\dagger(\tau')\rangle_{\rm r} \\ &\quad + aa^\dagger\rho_{\rm f}\langle F^\dagger(\tau')F(\tau'')\rangle_{\rm r} - a^\dagger\rho_{\rm f}a\langle F^\dagger(\tau'')F(\tau')\rangle_{\rm r}] + \text{adj.}, \qquad (2.94)\end{aligned}$$

where we have used the property of traces that allows us to cyclically permute the operators under the trace. The averages are first-order correlation functions of the reservoir. They depend only on the time difference $T = \tau' - \tau''$ since the reservoir is stationary. Hence, for example, $\langle F(\tau'')F^\dagger(\tau')\rangle_{\rm r} = \langle F(\tau')F^\dagger(\tau'')\rangle_{\rm r}^*$.

Consider the integral

$$\int_{-\tau}^{\tau}d\tau'\int_{0}^{\tau'}d\tau''\,\langle F^\dagger(\tau')F(\tau'')\rangle_{\rm r} = \int_{-\tau}^{\tau}d\tau'\,\sum_l |g_l|^2\langle b_l^\dagger b_l\rangle_{\rm r}\int_0^{\tau'}dT\,e^{-i(\omega-\omega_l)T}. \qquad (2.95)$$

We approximate the sum over reservoir modes with an integral:

$$\sum_l f_l \simeq \int d\omega'\,\mathcal{D}(\omega')f(\omega'), \qquad (2.96)$$

where $\mathcal{D}(\omega')$ is the density of reservoir modes. We also note that the integral over T is strongly peaked near $\omega' = \omega$. We thus make the Markoff approximation by assuming that the upper limit of the T-integration can be extended to infinity:

$$\lim_{\tau'\to\infty}\int_0^{\tau'}dT\,e^{-i(\omega-\omega')T} = \pi\delta(\omega-\omega') - \mathcal{P}\left(\frac{i}{\omega-\omega'}\right). \qquad (2.97)$$

This corresponds to assuming that the reservoir has sufficient bandwidth that the correlations decay away much faster than all times of interest for the system. The principal part in Eq. (2.97) produces a shift in frequency analogous to the Lamb shift of an atom undergoing thermal damping, which we will neglect. Equation (2.95) becomes

$$\int_{-\tau}^{\tau}d\tau'\int_{0}^{\tau'}d\tau''\,\langle F^\dagger(\tau')F(\tau'')\rangle_{\rm r} = \gamma_{\rm f}\tau\nu, \qquad (2.98)$$

where we have defined

$$\gamma_{\rm f} \equiv 2\pi\mathcal{D}(\omega)|g(\omega)|^2 \tag{2.99}$$

$$\nu \equiv \langle a^\dagger a\rangle_{\rm th} = \langle b^\dagger(\omega)b(\omega)\rangle_{\rm r}. \tag{2.100}$$

Deriving similar results for the other terms in Eq. (2.94), we obtain the master equation for the evolution of the system in the interaction picture

$$(\dot\rho_{\rm f})_{\rm damp} = \mathcal{L}_{\rm f}\rho_{\rm f}, \tag{2.101}$$

where we define the field damping operator $\mathcal{L}_{\rm f}$ by

$$\begin{aligned}\mathcal{L}_{\rm f}\rho &= -\frac{\gamma_{\rm f}}{2}(\nu+1)(a^\dagger a\rho - 2a\rho a^\dagger + \rho a^\dagger a)\\ &\quad -\frac{\gamma_{\rm f}}{2}\nu(aa^\dagger\rho - 2a^\dagger\rho a + \rho aa^\dagger).\end{aligned} \tag{2.102}$$

Note the identity

$$\mathrm{tr}\{\mathcal{L}_{\rm f}\rho\} = 0, \quad \text{for any } \rho. \tag{2.103}$$

Using Eq. (2.101), the average excitation level of a single-mode field $\langle a^\dagger a\rangle = \mathrm{tr}_{\rm f}\{a^\dagger a\rho_{\rm f}\}$ undergoing pure damping is found to obey the differential equation

$$\frac{d}{dt}\langle a^\dagger a\rangle = \gamma_{\rm f}\nu(\langle a^\dagger a\rangle + 1) - \gamma_{\rm f}(\nu+1)\langle a^\dagger a\rangle. \tag{2.104}$$

The rate of change of the mean excitation level of the system is seen to result from the balance between emission from the system into the reservoir and from the reservoir into the system. The solution to Eq. (2.104) is

$$\langle a^\dagger a\rangle(t) = \langle a^\dagger a\rangle(0)e^{-\gamma_{\rm f}t} + \nu(1-e^{-\gamma_{\rm f}t}), \tag{2.105}$$

which shows that the excitation level of the system decays to the thermal average. We recognize $\gamma_{\rm f}$ as the decay rate of free field oscillations and hence it is related to the quality factor Q by $\gamma_{\rm f} = \omega/Q$.

If the field is diagonal (such as when it is in a steady state), then the damping operator has the matrix elements

$$\begin{aligned}\langle n|\mathcal{L}_{\rm f}\rho|n\rangle &= \mathcal{L}_{{\rm f}_{n-1}}^{(+1)}\langle n-1|\rho|n-1\rangle - (\mathcal{L}_{{\rm f}_n}^{(+1)} + \mathcal{L}_{{\rm f}_{n-1}}^{(-1)})\langle n|\rho|n\rangle\\ &\quad +\mathcal{L}_{{\rm f}_n}^{(-1)}\langle n+1|\rho|n+1\rangle.\end{aligned} \tag{2.106}$$

The coefficients

$$\mathcal{L}_{\mathrm{f}_n}^{(+1)} = \gamma_{\mathrm{f}}\nu(n+1) \tag{2.107}$$
$$\mathcal{L}_{\mathrm{f}_n}^{(-1)} = \gamma_{\mathrm{f}}(\nu+1)(n+1) \tag{2.108}$$

give the rates at which $|n\rangle \to |n+1\rangle$ transitions and $|n+1\rangle \to |n\rangle$ transitions occur. In this notation the superscript indicates the gain $(+1)$ or loss (-1) of the excitation level of the field. The steady state of the field ρ^{ss} is established when the rates of $|n\rangle \to |n+1\rangle$ transitions and $|n+1\rangle \to |n\rangle$ transitions are equal and $\mathcal{L}_{\mathrm{f}}\rho^{\mathrm{ss}} = 0$. This establishes the recurrence relation

$$\langle n+1|\rho^{\mathrm{ss}}|n+1\rangle = \frac{\mathcal{L}_{\mathrm{f}_n}^{(+1)}}{\mathcal{L}_{\mathrm{f}_n}^{(-1)}}\langle n|\rho^{\mathrm{ss}}|n\rangle. \tag{2.109}$$

with the solution

$$\langle n|\rho^{\mathrm{ss}}|n\rangle = \langle 0|\rho^{\mathrm{ss}}|0\rangle \left(\frac{\nu}{\nu+1}\right)^n. \tag{2.110}$$

Normalizing this result with

$$\langle 0|\rho^{\mathrm{ss}}|0\rangle = \left[\sum_{n=0}^{\infty}\left(\frac{\nu}{\nu+1}\right)^n\right]^{-1} = \frac{1}{\nu+1} \tag{2.111}$$

gives

$$\rho^{\mathrm{ss}} = \frac{1}{\nu+1}\left(\frac{\nu}{\nu+1}\right)^{a^\dagger a}, \tag{2.112}$$

which is equivalent to Eq. (2.74) when restricted to a single mode. Thus the steady state of the master equation (2.101), is indeed a thermal state as it should be for a field undergoing pure damping.

2.6 Field Damping Eigenstates

The right and left eigenstates of the field damping operator (2.102) were derived in a paper by Briegel and Englert [4], though some typing errors need to be fixed and our treatment of the left eigenstates and the establishment of

orthonormality will be different. The right eigenstates ρ_λ and left eigenstates $\check{\rho}_\lambda$ of the field damping operator are defined by

$$\mathcal{L}_{\rm f}\rho_\lambda = \lambda\rho_\lambda \tag{2.113}$$
$$\check{\rho}_\lambda\mathcal{L}_{\rm f} = \lambda\check{\rho}_\lambda. \tag{2.114}$$

The left action $\rho\mathcal{L}_{\rm f}$ is defined by the requirement that

$$\mathrm{tr}\{(\rho_1\mathcal{L})\rho_2\} = \mathrm{tr}\{\rho_1(\mathcal{L}_{\rm f}\rho_2)\} \tag{2.115}$$

for all operators ρ_1 and ρ_2, and is given by

$$\begin{aligned}\rho\mathcal{L}_{\rm f} &= -\frac{\gamma_{\rm f}}{2}(\nu+1)(a^\dagger a\rho - 2a^\dagger\rho a + \rho a^\dagger a) \\ &\quad -\frac{\gamma_{\rm f}}{2}\nu(aa^\dagger\rho - 2a\rho a^\dagger + \rho aa^\dagger)].\end{aligned} \tag{2.116}$$

The eigenstates are normalized such that the duality relation

$$\mathrm{tr}\{\check{\rho}_\lambda\rho_{\lambda'}\} = \delta_{\lambda\lambda'} \tag{2.117}$$

holds. Then any state ρ and any observable $\mathcal{O}$ can be expanded in eigenstates of $\mathcal{L}_{\rm f}$ as

$$\rho = \sum_\lambda \mathrm{tr}\{\check{\rho}_\lambda\rho\}\rho_\lambda \tag{2.118}$$
$$\mathcal{O} = \sum_\lambda \mathrm{tr}\{\mathcal{O}\rho_\lambda\}\check{\rho}_\lambda. \tag{2.119}$$

We assume solutions of the form

$$\rho_\lambda = \begin{cases} a^{\dagger k}f_\lambda(a^\dagger a), & k \geq 0 \\ f_\lambda(a^\dagger a)a^{|k|}, & k \leq 0 \end{cases} \tag{2.120}$$
$$\check{\rho}_\lambda = \begin{cases} a^k\check{f}_\lambda(a^\dagger a), & k \geq 0 \\ \check{f}_\lambda(a^\dagger a)a^{\dagger|k|}, & k \leq 0 \end{cases}, \tag{2.121}$$

for $k = 0, \pm1, \pm2, \ldots$. Upon substitution into Eqs. (2.113) and (2.114), we could proceed by hitting the equations with $\langle m|$ and $|n\rangle$ and finding difference equations for the functions $f_\lambda(n) = \langle n|f_\lambda(a^\dagger a)|n\rangle$ and $\check{f}_\lambda(n) = \langle n|\check{f}_\lambda(a^\dagger a)|n\rangle$.

Instead, we will proceed in the manner of Ref. [4] that leads to differential equations.

We start by normal ordering the equation for the right eigenstates and antinormal ordering the equation for the left eigenstates, using the identities

$$[a, f(a, a^\dagger)] = \frac{\partial}{\partial a^\dagger} f(a, a^\dagger) \tag{2.122}$$

$$[f(a, a^\dagger), a^\dagger] = \frac{\partial}{\partial a} f(a, a^\dagger). \tag{2.123}$$

Our reason for deriving the antinormal form of the left eigenstates instead of the normal form of the left eigenstates (as was done in Ref. [4]) will become clear when we establish the orthonormality of the eigenstates. The same result is achieved for the two cases $k \geq 0$ and $k \leq 0$, and is given by

$$\begin{aligned} 0 &= (\nu+1)a^\dagger \frac{\partial^2 f_\lambda^{(\mathrm{n})}}{\partial z^2} a + a^\dagger \frac{\partial f_\lambda^{(\mathrm{n})}}{\partial z} a + (\nu+1)(|k|+1)\frac{\partial f_\lambda^{(\mathrm{n})}}{\partial z} \\ &\quad + \left(1 + \frac{|k|}{2} - \frac{\lambda}{\gamma_\mathrm{f}}\right) f_\lambda^{(\mathrm{n})} \end{aligned} \tag{2.124}$$

$$\begin{aligned} 0 &= (\nu+1)a \frac{\partial^2 \check{f}_\lambda^{(\mathrm{a})}}{\partial z^2} a^\dagger - a \frac{\partial \check{f}_\lambda^{(\mathrm{a})}}{\partial z} a^\dagger + (\nu+1)(|k|+1)\frac{\partial \check{f}_\lambda^{(\mathrm{a})}}{\partial z} \\ &\quad - \left(\frac{|k|}{2} + \frac{\lambda}{\gamma_\mathrm{f}}\right) \check{f}_\lambda^{(\mathrm{a})}, \end{aligned} \tag{2.125}$$

where $f_\lambda^{(\mathrm{n})}(a^\dagger, a)$ and $\check{f}_\lambda^{(\mathrm{a})}(a^\dagger, a)$ are the normal and antinormal forms of $f_\lambda(a^\dagger a)$ and $\check{f}_\lambda(a^\dagger a)$, respectively, and $\partial/\partial z$ is defined by

$$\frac{\partial}{\partial z} f^{(\mathrm{n})}(a^\dagger a) = \frac{1}{a^\dagger}\frac{\partial}{\partial a} f^{(\mathrm{n})}(a^\dagger a) = \frac{\partial}{\partial a^\dagger} f^{(\mathrm{n})}(a^\dagger a)\frac{1}{a} \tag{2.126}$$

$$\frac{\partial}{\partial z} f^{(\mathrm{a})}(a^\dagger a) = \frac{\partial}{\partial a} f^{(\mathrm{a})}(a^\dagger a)\frac{1}{a^\dagger} = \frac{1}{a}\frac{\partial}{\partial a^\dagger} f^{(\mathrm{a})}(a^\dagger a). \tag{2.127}$$

We can use the uniqueness of the normal and antinormal forms of a function to establish a one-to-one correspondence between either $f^{(\mathrm{n})}(a, a^\dagger)$ or $f^{(\mathrm{a})}(a, a^\dagger)$ and the ordinary functions $f^{(\mathrm{n})}(\alpha, \alpha^*)$ or $f^{(\mathrm{a})}(\alpha, \alpha^*)$ of the complex variable α. We do this by defining the operators $\mathcal{N}$ and $\mathcal{A}$:

$$f^{(\mathrm{n})}(a, a^\dagger) = \mathcal{N}\{f^{(\mathrm{n})}(\alpha, \alpha^*)\} \tag{2.128}$$

$$f^{(\mathrm{a})}(a, a^\dagger) = \mathcal{A}\{f^{(\mathrm{n})}(\alpha, \alpha^*)\}. \tag{2.129}$$

Here $\mathcal{N}$ denotes the process of replacing α by a and α^* by $a^\dagger$ in normal form with all of the a's to the right of the $a^\dagger$'s and $\mathcal{A}$ denotes the process of replacing α by a and α^* by $a^\dagger$ in antinormal form with all of the a's to the left of the $a^\dagger$'s. The reverse processes of replacing a by α and $a^\dagger$ by α^* are denoted by $\mathcal{N}^{-1}$ and $\mathcal{A}^{-1}$. The ordinary function $f^{(\mathrm{n})}(\alpha,\alpha^*)$ associated with the normal form of a function $f(a,a^\dagger)$ is equivalent to the diagonal matrix elements in the coherent state representation:

$$f^{(\mathrm{n})}(\alpha,\alpha^*) = \langle\alpha|f(a,a^\dagger)|\alpha\rangle. \tag{2.130}$$

On the other hand, the ordinary function $f^{(\mathrm{a})}(\alpha,\alpha^*)$ associated with the antinormal form of a function $f(a,a^\dagger)$ defines an integral representation:

$$f(a,a^\dagger) = \int \frac{d^2\alpha}{\pi}|\alpha\rangle\langle\alpha|f^{(\mathrm{a})}(\alpha,\alpha^*), \tag{2.131}$$

where the integration is over the entire complex plane.

By Applying $\mathcal{N}^{-1}$ and $\mathcal{A}^{-1}$ to Eqs. (2.124) and (2.125), respectively, and dropping the (n) and (a) superscripts, we obtain the second order differential equations

$$\begin{aligned} 0 &= (\nu+1)zf_\lambda''(z) + [z+(\nu+1)(1+|k|)]f_\lambda'(z) \\ &\quad + \left(1+\frac{|k|}{2}-\frac{\lambda}{\gamma_{\mathrm{f}}}\right)f_\lambda(z) \qquad (2.132) \\ 0 &= (\nu+1)z\check{f}_\lambda''(z) + [(\nu+1)(|k|+1)-z]\check{f}_\lambda'(z) \\ &\quad - \left(\frac{|k|}{2}+\frac{\lambda}{\gamma_{\mathrm{f}}}\right)\check{f}_\lambda(z), \qquad (2.133) \end{aligned}$$

where $z=\alpha^*\alpha$. Note that Ref. [4] does not mention the process of replacing a and $a^\dagger$ by the complex variables α and α^* to obtain real-valued differential equations. Note also that z does not equal $a^\dagger a$ as was misstated in Ref. [4], and $\mathcal{N}\{z^n\} = a^{\dagger n}a^n \neq (a^\dagger a)^n$. Equation (2.132) turns into Kummer's equation when $-z/(\nu+1)$ is regarded as the variable. Equation (2.133) turns into the associated Laguerre equation when $z/(\nu+1)$ is regarded as the variable. The solutions are given by

$$\begin{aligned} f_j^k(z) &= C_j^k \exp\left(-\frac{z}{\nu+1}\right) L_j^{|k|}\left(\frac{z}{\nu+1}\right) \qquad (2.134) \\ \check{f}_j^k(z) &= \check{C}_j^k L_j^{|k|}\left(\frac{z}{\nu+1}\right) \qquad (2.135) \end{aligned}$$

with the eigenvalues

$$\lambda_j^k = -\gamma_{\rm f}\left(j + \frac{|k|}{2}\right), \quad j = 0, 1, 2, \ldots. \tag{2.136}$$

Here the L_j^k are the associated Laguerre polynomials.

The constants C_j^k and $\check{C}_j^k$ are to be determined from the orthonormality condition $\mathrm{tr}\{\check{\rho}_j^k \rho_{j'}^{k'}\} = \delta_{jj'}\delta_{kk'}$. Insofar as the factor $\delta_{kk'}$ is obvious, it suffices to establish the orthonormality for $k' = k$. Here is where deriving the antinormal form of the left eigenstates becomes useful. We make use of the theorem:

$$\mathrm{tr}\{f_1(a, a^\dagger) f_2(a, a^\dagger)\} = \int \frac{d^2\alpha}{\pi} f_1^{(\rm a)}(\alpha, \alpha^*) f_2^{(\rm n)}(\alpha, \alpha^*). \tag{2.137}$$

Using this, we obtain

$$\begin{aligned} \mathrm{tr}\{\check{\rho}_j^k \rho_{j'}^k\} &= \check{C}_j^k C_{j'}^k (\nu+1)^{k+1} \int_0^\infty dx\, x^k e^{-x} L_j^k(x) L_{j'}^k(x) \\ &= \check{C}_j^k C_{j'}^k (\nu+1)^{k+1} \frac{(j+k)!}{j!} \delta_{jj'}, \end{aligned} \tag{2.138}$$

which establishes the normalization condition

$$\check{C}_j^k C_j^k = \frac{1}{(\nu+1)^{|k|+1}} \frac{j!}{(j+|k|)!}. \tag{2.139}$$

Transforming the eigenstates into functions of a and $a^\dagger$ by reversing the normal and antinormal processes can be done by expanding in powers of z and then using the identities

$$\mathcal{N}\{z^m\} = a^{\dagger m} a^m = m! \begin{pmatrix} a^\dagger a \\ m \end{pmatrix} \tag{2.140}$$

$$\mathcal{A}\{z^m\} = a^m a^{\dagger m} = m! \begin{pmatrix} a^\dagger a + m \\ m \end{pmatrix}. \tag{2.141}$$

Using the power series expansion

$$L_j^k(x) = \sum_{m=0}^{j} (-1)^m \begin{pmatrix} k+j \\ k+m \end{pmatrix} \frac{x^m}{m!}, \quad k \geq 0, \tag{2.142}$$

we obtain

$$\begin{aligned} f_j^k(a^\dagger a) &= C_j^k \mathcal{N}\left\{\sum_{s=0}^{\infty}\left(\frac{-1}{\nu+1}\right)^s z^s \sum_{m=0}^{j}\frac{1}{m!(s-m)!}\left(\begin{array}{c}|k|+j\\|k|+m\end{array}\right)\right\} \\ &= C_j^k \sum_{s=0}^{a^\dagger a}\left(\frac{-1}{\nu+1}\right)^s \left(\begin{array}{c}a^\dagger a\\ s\end{array}\right)\sum_{m=0}^{j,s}\left(\begin{array}{c}s\\ m\end{array}\right)\left(\begin{array}{c}|k|+j\\|k|+m\end{array}\right) \qquad (2.143) \\ \check{f}_j^k(a^\dagger a) &= \check{C}_j^k \mathcal{A}\left\{\sum_{m=0}^{j}\left(\frac{-1}{\nu+1}\right)^m \left(\begin{array}{c}|k|+j\\|k|+m\end{array}\right)\frac{z^m}{m!}\right\} \\ &= \check{C}_j^k \sum_{m=0}^{j}\left(\frac{-1}{\nu+1}\right)^m \left(\begin{array}{c}|k|+j\\|k|+m\end{array}\right)\left(\begin{array}{c}a^\dagger a+m\\ m\end{array}\right), \qquad (2.144) \end{aligned}$$

where the notation $\sum_{m=0}^{j,s}$ means "sum over m from 0 to the smallest of j or s".

It is evident that $\mathrm{tr}\{\rho_j^k\} = 0$ for $k \neq 0$. For $k = 0$, we can use the identity (2.137) with $f_1 = 1 = L_0^0(x)$ to establish

$$\mathrm{tr}\{\rho_j^k\} = C_0^0(\nu+1)\delta_{j0}\delta_{k0}. \qquad (2.145)$$

Thus ρ_0^0 is the only right eigenstate to have a non-zero trace and represents a valid state of the field if it is normalized with

$$C_0^0 = \frac{1}{\nu+1}. \qquad (2.146)$$

Since $\lambda_0^0 = 0$, ρ_0^0 is the time-independent steady state of a field undergoing pure damping. From Eq. (2.143) we have

$$\begin{aligned} \rho_0^0 &= \frac{1}{\nu+1}\sum_{s=0}^{a^\dagger a}\left(\frac{-1}{\nu+1}\right)^s \left(\begin{array}{c}a^\dagger a\\ s\end{array}\right) \\ &= \frac{1}{\nu+1}\left(\frac{\nu}{\nu+1}\right)^{a^\dagger a}, \qquad (2.147) \end{aligned}$$

which agrees with Eq. (2.112).

Chapter 3

Rydberg Atoms in Electromagnetic Fields

3.1 Rydberg Atoms

Consider an atom with one highly-excited valance electron—a so called Rydberg atom. The electron has mass $m_{\rm e}$, position operator $\mathbf{r}_{\rm e}$, and momentum operator $\mathbf{p}_{\rm e}$. The electron spin is neglected. The nucleus of the atom (along with any remaining electrons) has a total mass $m_{\rm n}$, center-of-mass position operator $\mathbf{r}_{\rm n}$, and total momentum operator $\mathbf{p}_{\rm n}$. The Hamiltonian describing the free atom is then

$$\mathcal{H} = \frac{\mathbf{p}_{\rm e}^2}{2m_{\rm e}} + \frac{\mathbf{p}_{\rm n}^2}{2m_{\rm n}} + V(|\mathbf{r}_{\rm e} - \mathbf{r}_{\rm n}|), \tag{3.1}$$

where V is the effective interaction Hamiltonian between the electron and the ground state of the nucleus and remaining electrons, suitably averaged over any thermal fluctuations. We assume that the result is spherically symmetric and V is a function of the magnitude of the relative position operator $\mathbf{r}_{\rm e} - \mathbf{r}_{\rm n}$ only. This corresponds to assuming that the atom has no permanent dipole moment. Introducing the total mass

$$M \equiv m_{\rm e} + m_{\rm n}, \tag{3.2}$$

center-of-mass operator

$$\mathbf{R} \equiv \frac{m_{\rm e}}{M}\mathbf{r}_{\rm e} + \frac{m_{\rm n}}{M}\mathbf{r}_{\rm n}, \tag{3.3}$$

and the relative position operator

$$\mathbf{r} \equiv \mathbf{r}_{\rm e} - \mathbf{r}_{\rm n}, \tag{3.4}$$

we can express the position operators of the electron and nucleus as

$$\mathbf{r}_{\mathrm{e}} = \mathbf{R} + \frac{m_{\mathrm{n}}}{M}\mathbf{r} \tag{3.5}$$

$$\mathbf{r}_{\mathrm{n}} = \mathbf{R} - \frac{m_{\mathrm{e}}}{M}\mathbf{r}. \tag{3.6}$$

Introducing the total momentum

$$\mathbf{P} \equiv \mathbf{p}_{\mathrm{e}} + \mathbf{p}_{\mathrm{n}} \tag{3.7}$$

and the relative momentum

$$\mathbf{p} \equiv \frac{m_{\mathrm{n}}}{M}\mathbf{p}_{\mathrm{e}} - \frac{m_{\mathrm{e}}}{M}\mathbf{p}_{\mathrm{n}}, \tag{3.8}$$

we can express the momentum operators of the electron and nucleus as

$$\mathbf{p}_{\mathrm{e}} = \frac{m_{\mathrm{e}}}{M}\mathbf{P} + \mathbf{p} \tag{3.9}$$

$$\mathbf{p}_{\mathrm{n}} = \frac{m_{\mathrm{n}}}{M}\mathbf{P} - \mathbf{p}. \tag{3.10}$$

The Hamiltonian becomes

$$\mathcal{H} = \frac{\mathbf{P}^2}{2M} + \frac{\mathbf{p}^2}{2\mu} + V(|\mathbf{r}|), \tag{3.11}$$

where

$$\mu \equiv \frac{m_{\mathrm{e}} m_{\mathrm{n}}}{m_{\mathrm{e}} + m_{\mathrm{n}}} \tag{3.12}$$

is the reduced mass of the relative motion.

Without specifying the form of V, we write the Hamiltonian as

$$\mathcal{H} = \mathcal{H}_{\mathrm{cm}} + \mathcal{H}_{\mathrm{int}}, \tag{3.13}$$

where

$$\mathcal{H}_{\mathrm{cm}} = \frac{\mathbf{P}^2}{2M} \tag{3.14}$$

is the kinetic energy operator of the center-of-mass motion of the atom, and

$$\mathcal{H}_{\mathrm{int}} = \frac{\mathbf{p}^2}{2\mu} + V(|\mathbf{r}|) = \hbar \sum_s \omega_s \sigma_{ss} \tag{3.15}$$

corresponds to the internal states of the atom, here expanded in terms of eigenenergy states. We have denoted the eigenenergies of the atom as $\hbar\omega_s$, where s labels the eigenstate, and we have found it useful to introduce the transition operators

$$\sigma_{ab} \equiv |a\rangle\langle b|. \tag{3.16}$$

Note the commutators

$$[\sigma_{ab}, \mathcal{H}_{\rm int}] = \hbar\omega_{ab}\sigma_{ab} \tag{3.17}$$
$$[\mathcal{H}_{\rm int}, \sigma_{ab}^\dagger] = \hbar\omega_{ab}\sigma_{ab}^\dagger, \tag{3.18}$$

where $\omega_{ab} \equiv \omega_b - \omega_a$, and the identities

$$e^{i\mathcal{H}_{\rm int}\tau/\hbar}\sigma_{ab}e^{-i\mathcal{H}_{\rm int}\tau/\hbar} = e^{-i\omega_{ab}\tau}\sigma_{ab} \tag{3.19}$$
$$e^{i\mathcal{H}_{\rm int}\tau/\hbar}\sigma_{ab}^\dagger e^{-i\mathcal{H}_{\rm int}\tau/\hbar} = e^{i\omega_{ab}\tau}\sigma_{ab}^\dagger. \tag{3.20}$$

3.2 Hamiltonian of a Rydberg Atom in an Electromagnetic Field

We will first consider the interaction of a single charged particle with an electromagnetic field. The standard approach of coupling a single charged particle to an electromagnetic field relies on the minimal coupling scheme, where the canonical momentum operator $\mathbf{p}$ of the particle is replaced by the kinetic momentum $\mathbf{p} + q\mathbf{A}(\mathbf{r})$. Here $\mathbf{A}(\mathbf{r})$ is the vector potential as a function of the position operator $\mathbf{r}$ of the particle, and q is the charge of the particle. In addition, we would add the potential energy $q\Phi(\mathbf{r})$ to the Hamiltonian, but in the absence of other charges and currents $\Phi = 0$ in the coulomb guage. H. Weyl in 1928 showed that assuming the minimal coupling assures that the Schrödinger equation is invariant under local transformations (in which the wave function is transformed by a phase that depends on position and time)—local transformations then being identical to electromagnetic guage transformations. The Hamiltonian of a charged particle in an electromagnetic field is then given by

$$\mathcal{H} = \frac{1}{2m}(\mathbf{p} + q\mathbf{A})^2 + \hbar\sum_l \omega_l a_l^\dagger a_l, \tag{3.21}$$

where m is the mass of the particle.

When we evaluate the square in the kinetic energy, we obtain the two cross-terms $\mathbf{p}\cdot\mathbf{A}$ and $\mathbf{A}\cdot\mathbf{p}$. Considering the action of $\mathbf{p}\cdot\mathbf{A}$ on an arbitrary position dependent function $\psi(\mathbf{r})$, we have

$$\begin{aligned}\mathbf{p}\cdot(\mathbf{A}\psi) &= -i\hbar\nabla\cdot(\mathbf{A}\psi)\\ &= -i\hbar(\psi\nabla\cdot\mathbf{A}+\mathbf{A}\cdot\nabla\psi).\end{aligned}\tag{3.22}$$

In the coulomb guage we have $\nabla\cdot\mathbf{A}=0$, and we find

$$\mathbf{p}\cdot\mathbf{A}=\mathbf{A}\cdot\mathbf{p}.\tag{3.23}$$

The Hamiltonian then becomes

$$\mathcal{H}=\frac{\mathbf{p}^2}{2m}+\frac{q}{m}\mathbf{A}\cdot\mathbf{p}+\frac{q^2}{2m}\mathbf{A}^2+\hbar\sum_l\omega_l a_l^\dagger a_l.\tag{3.24}$$

Dropping the terms describing the free evolution of the particle and field, we obtain the interaction Hamiltonain

$$\mathcal{V}=\frac{q}{m}\mathbf{A}\cdot\mathbf{p}+\frac{q^2}{2m}\mathbf{A}^2\tag{3.25}$$

that describes the interaction between a particle and a field.

Applying this result to the valence electron and nucleus of a Rydberg atom gives the interaction Hamiltonian of a Rydberg atom interacting with an electromagnetic field:

$$\begin{aligned}\mathcal{V} &= -\frac{e}{m_\mathrm{e}}\mathbf{A}(\mathbf{r}_\mathrm{e})\cdot\mathbf{p}_\mathrm{e}+\frac{e^2}{2m_\mathrm{e}}\mathbf{A}^2(\mathbf{r}_\mathrm{e})+\frac{e}{m_\mathrm{n}}\mathbf{A}(\mathbf{r}_\mathrm{n})\cdot\mathbf{p}_\mathrm{n}+\frac{e^2}{2m_\mathrm{n}}\mathbf{A}^2(\mathbf{r}_\mathrm{n})\\ &= -\frac{e}{M}\left[\mathbf{A}\Big(\mathbf{R}+\frac{m_\mathrm{n}}{M}\mathbf{r}\Big)-\mathbf{A}\Big(\mathbf{R}-\frac{m_\mathrm{e}}{M}\mathbf{r}\Big)\right]\cdot\mathbf{P}\\ &\quad -\frac{e}{\mu}\left[\frac{\mu}{m_\mathrm{e}}\mathbf{A}\Big(\mathbf{R}+\frac{m_\mathrm{n}}{M}\mathbf{r}\Big)+\frac{\mu}{m_\mathrm{n}}\mathbf{A}\Big(\mathbf{R}-\frac{m_\mathrm{e}}{M}\mathbf{r}\Big)\right]\cdot\mathbf{p}\\ &\quad +\frac{e^2}{2m_\mathrm{e}}\mathbf{A}^2\Big(\mathbf{R}+\frac{m_\mathrm{n}}{M}\mathbf{r}\Big)+\frac{e^2}{2m_\mathrm{n}}\mathbf{A}^2\Big(\mathbf{R}-\frac{m_\mathrm{e}}{M}\mathbf{r}\Big).\end{aligned}\tag{3.26}$$

This simplifies considerably when we apply the dipole approximation. The position dependence of $\mathbf{A}$ is of the form $\mathbf{A}(\mathbf{R}+\delta\mathbf{r})$, where $\delta\mathbf{r}$ is either $m_\mathrm{n}\mathbf{r}/M$ or $-m_\mathrm{e}\mathbf{r}/M$. Expanding $\mathbf{A}(\mathbf{R}+\delta\mathbf{r})$ in a Taylor series around $\mathbf{R}$, we have

$$\mathbf{A}(\mathbf{R}+\delta\mathbf{r})\simeq\mathbf{A}(\mathbf{R})+(\delta\mathbf{r}\cdot\nabla_\mathbf{R})\mathbf{A}(\mathbf{R})+\ldots.\tag{3.27}$$

The vector potential changes on a characteristic length determined by the wavelengths $\lambda_l = 2\pi/k_l$, which vanish at optical wavelengths less than about 10^{-5} m. The atomic wave functions $\langle \mathbf{r}|s\rangle$ vanish when $\mathbf{r}$ is greater than about 10^{-10} m, the approximate atomic diameter. We thus have

$$\frac{|(\delta\mathbf{r}\cdot\nabla_{\mathbf{R}})\mathbf{A}(\mathbf{R})|}{|\mathbf{A}(\mathbf{R})|} \simeq \frac{|\delta\mathbf{r}|}{\lambda_l} < \frac{|\mathbf{r}|}{\lambda_l} \ll 1. \tag{3.28}$$

Hence the vector potential does not change considerably over the size of the atom, and, in the dipole approximation, we can assume that the electron and nucleus of the atom interact with essentially the same electromagnetic field described by the vector potential $\mathbf{A}(\mathbf{R})$ as a function of the center-of-mass coordinate operator. The interaction Hamiltonian (3.26) becomes

$$\mathcal{V} = -\frac{e}{\mu}\mathbf{A}\cdot\mathbf{p} + \frac{e^2}{2\mu}\mathbf{A}^2. \tag{3.29}$$

The higher order terms in the Taylor series expansion (3.27) that we neglect correspond to effects of the inhomogenity of the field over the size of the atom and differences in the field as seen by an observer moving with the electron.

The first term of Eq. (3.29) is first order in the coupling constant e and describes the coupling of the relative momentum to the electromagnetic field. The second term is of order e^2 and describes the interaction between different modes of the radiation field through the coupling of the electron to the field. Neglecting the term of order e^2, we have

$$\mathcal{V} \simeq -\frac{e}{\mu}\mathbf{A}\cdot\mathbf{p}. \tag{3.30}$$

Substituting the vector potential (2.34) gives

$$\mathcal{V} = -\frac{e}{\mu}\sum_l \sqrt{\frac{\hbar}{2\omega_l\epsilon_0}}\mathbf{u}_l\cdot\mathbf{p}(a_l + a_l^\dagger). \tag{3.31}$$

The matrix element between the atomic states $|a\rangle$ and $|b\rangle$ is

$$\langle a|\mathcal{V}|b\rangle = -\frac{e}{\mu}\sum_l \sqrt{\frac{\hbar}{2\omega_l\epsilon_0}}\mathbf{u}_l\cdot\mathbf{p}_{ab}(a_l + a_l^\dagger). \tag{3.32}$$

We can put this into a different form if we consider the commutator

$$[\mathbf{r}, \mathcal{H}_{\rm int}] = [\mathbf{r}, \frac{\mathbf{p}^2}{2\mu}] = \frac{i\hbar}{\mu}\mathbf{p}, \tag{3.33}$$

where in the last step we used the identity $[x_i, p_j^2] = 2i\hbar p_j \delta_{ij}$. Finding the matrix element between $|a\rangle$ and $|b\rangle$ of both sides of this equation gives

$$\mathbf{p}_{ab} = -i\mu\omega_{ab}\mathbf{r}_{ab}. \tag{3.34}$$

We thus have

$$\langle a|\mathcal{V}|b\rangle = ie\omega_{ab}\sum_l \sqrt{\frac{\hbar}{2\omega_l\epsilon_0}}\mathbf{u}_l \cdot \mathbf{r}_{ab}(a_l + a_l^\dagger). \tag{3.35}$$

In terms of the transition operators, the interaction Hamiltonian can be written as

$$\mathcal{V} = i\hbar \sum_{l,a<b} (g_{lab}\sigma_{ab} - g_{lab}^*\sigma_{ab}^\dagger)(a_l + a_l^\dagger), \tag{3.36}$$

where the coupling strengths g_{lab} are given by

$$g_{lab} \equiv \frac{e\omega_{ab}}{\sqrt{2\hbar\omega_l\epsilon_0}}\mathbf{u}_l \cdot \mathbf{r}_{ab}. \tag{3.37}$$

The matrix element of the dipole operator between an atomic state and itself

$$e\mathbf{r}_{ss} = e\int d\mathbf{r}\, \mathbf{r}|\langle \mathbf{r}|s\rangle|^2, \tag{3.38}$$

vanishes as a consequence of the assumed spherical symmetry of the interaction Hamiltonian $V(\mathbf{r})$ and the atomic wave functions $\langle \mathbf{r}|s\rangle$. Hence, the sum in Eq. (3.36) includes only the terms with $a \neq b$.

Consider the time-dependence of the expectation values:

$$\langle \sigma_{ab}^\dagger a_l^\dagger(t)\rangle = e^{i(\omega_{ab}+\omega_l)t}\langle \sigma_{ab}^\dagger a_l^\dagger(0)\rangle \tag{3.39}$$

$$\langle \sigma_{ab} a_l^\dagger(t)\rangle = e^{-i(\omega_{ab}-\omega_l)t}\langle \sigma_{ab} a_l^\dagger(0)\rangle \tag{3.40}$$

$$\langle \sigma_{ab}^\dagger a_l(t)\rangle = e^{i(\omega_{ab}-\omega_l)t}\langle \sigma_{ab}^\dagger a_l(0)\rangle \tag{3.41}$$

$$\langle \sigma_{ab} a_l(t)\rangle = e^{-i(\omega_{ab}+\omega_l)t}\langle \sigma_{ab} a_l(0)\rangle. \tag{3.42}$$

The first and last combinations evolve at optical frequencies and tend to average to zero in a few optical periods. The second and third combinations, in contrast, vary slowly near resonance. Therefore, in the rotating-wave approximation, we assume that only field modes and atomic transitions that are near resonance contribute significantly to the interaction. We thus have

$$\mathcal{V} \simeq i\hbar \sum_{l,a<b} (g_{lab}\sigma_{ab}a_l^\dagger - g_{lab}^*\sigma_{ab}^\dagger a_l), \tag{3.43}$$

where the sum is now assumed to include only near resonant interactions.

3.3 Thermal Equilibrium of a Rydberg Atom

A Rydberg atom with the Hamiltonian (3.15) has a partition function given by

$$\begin{aligned} Z &= \mathrm{tr}\left\{\exp\left(-\beta\hbar\sum_s \omega_s\sigma_{ss}\right)\right\} \\ &= \mathrm{tr}\left\{\prod_s e^{-\beta\hbar\omega_s\sigma_{ss}}\right\} \\ &= \sum_s e^{-\beta\hbar\omega_s} \end{aligned} \tag{3.44}$$

and a thermal state given by

$$\rho^{\mathrm{th}} = \frac{\prod_s e^{-\beta\hbar\omega_s\sigma_{ss}}}{\sum_s e^{-\beta\hbar\omega_s}}. \tag{3.45}$$

The average population of the sth atomic state in thermal equilibrium is given by

$$\langle\sigma_{ss}\rangle_{\mathrm{th}} = \frac{e^{-\beta\hbar\omega_s}}{\sum_s e^{-\beta\hbar\omega_s}}, \tag{3.46}$$

and the average internal energy of the atom is

$$\langle\mathcal{H}_{\mathrm{int}}\rangle = \hbar\sum_s \omega_s\langle\sigma_{ss}\rangle_{\mathrm{th}}. \tag{3.47}$$

3.4 Thermal Damping of a Two-level Rydberg Atom

Consider a single pair of neighboring energy levels in a Rydberg atom as a system—an atom with only two levels $|a\rangle$ and $|b\rangle$, and transition frequency ω_{ab}. We assume that the atom is initially in a superposition of the two states $|a\rangle$ and $|b\rangle$ and that transitions between the two states are in near resonance with a particular electromagnetic mode of frequency ω, such that $\omega \simeq \omega_{ab}$. This particular mode acts as a driving mechanism for transitions between the two levels. The coupling between the two levels and the single mode must be very strong (stronger than any other interaction) such that the description of the atom as having only two levels and the field as having only one mode is valid. However, the two levels remain weakly coupled to the remaining modes of the field which act as a thermal reservoir and cause the atom to undergo damping. These other modes of the field include modes that are not normal-modes of the cavity (vacuum modes). As in Sec. (2.5), we wish to describe the damping for times short compared to times for which there is a significant change in the system variables, and we therefore neglect the driving interaction with the single mode of frequency ω. There are three damping mechanisms for the two-level atom that we will treat separately and then combine. The first damping mechanism is the exchange of energy between just the two levels due to their interaction with the reservoir, which causes the two-level atom to relax to the steady state inversion. This we shall call inversion damping. The second damping mechanism is the depletion of the population of the two levels caused by reservoir induced transitions to other atomic states, which we shall call depletion damping. This result is equivalent to the Wigner-Weisskopf theory of spontaneous emission, except that we are using a density operator approach and are relaxing the assumption of zero temperature. The third damping mechanism is radiationless damping.

3.4.1 Inversion Damping

The interaction between the two levels of the atom and the reservoir is a situation similar to what we have considered in Sec. (2.5), except that our system is now a two-level atom and our reservoir is now the remaining modes of the electromagnetic field. We will show that this interaction leads to the

relaxation of two-level atom to the steady state inversion. The Hamiltonian for the two-level atom is

$$\begin{aligned}\mathcal{H}_{\rm at} &= \hbar(\omega_a\sigma_{aa}+\omega_b\sigma_{bb}) \\ &= \frac{1}{2}\hbar\omega_{ab}\sigma_z, \end{aligned} \tag{3.48}$$

where we have lowered the zero-point energy by the constant $\hbar(\omega_a+\omega_b)/2$ and have defined the inversion operator

$$\sigma_z \equiv \sigma_{ab}^\dagger\sigma_{ab} - \sigma_{ab}\sigma_{ab}^\dagger. \tag{3.49}$$

Dropping the label "ab" on the transition operators, we recognize σ and $\sigma^\dagger$ as Pauli pseudo spin-flip operators. The Hamiltonian for the reservoir is given by

$$\mathcal{H}_{\rm r} = \hbar{\sum_l}' \omega_l a_l^\dagger a_l, \tag{3.50}$$

where the sum is over the remaining modes of the field. The interaction Hamiltonian is Eq. (3.43) restricted to the two levels and the remaining field modes:

$$\mathcal{V} = i\hbar{\sum_l}'(g_l\sigma a_l^\dagger - g_l^*\sigma^\dagger a_l). \tag{3.51}$$

Transforming to the interaction picture with the transformation Hamiltonian $\mathcal{H}_0 = \mathcal{H}_{\rm at}+\mathcal{H}_{\rm r}$, we have

$$\begin{aligned}\mathcal{V} &\rightarrow e^{i\mathcal{H}_0\tau/\hbar}\mathcal{V}e^{-i\mathcal{H}_0\tau/\hbar} \\ &= i\hbar(\sigma F^\dagger - \sigma^\dagger F), \end{aligned} \tag{3.52}$$

where

$$F \equiv {\sum_l}' g_l^* e^{i(\omega_{ab}-\omega_l)\tau}a_l. \tag{3.53}$$

Here we have used the identities (3.19) and (3.20). From here, we proceed as in Sec. (2.5) and obtain

$$\begin{aligned}(\dot\rho_{\rm at})_{\rm inv} &= \frac{\gamma_{\rm at}}{4\Gamma}(1-\Gamma)(\sigma^\dagger\sigma\rho_{\rm at} - 2\sigma\rho_{\rm at}\sigma^\dagger + \rho_{\rm at}\sigma^\dagger\sigma) \\ &\quad + \frac{\gamma_{\rm at}}{4\Gamma}(1+\Gamma)(\sigma\sigma^\dagger\rho_{\rm at} - 2\sigma^\dagger\rho_{\rm at}\sigma + \rho_{\rm at}\sigma\sigma^\dagger), \end{aligned} \tag{3.54}$$

where we have again neglected the principal part in the integration over the density of reservoir modes (corresponding to the Lamb shift in the frequency). Here, we have defined the inversion damping rate

$$\gamma_{\rm at} \equiv 2\pi \mathcal{D}(\omega_{ab})|g(\omega_{ab})|^2 \tag{3.55}$$

and the average inversion in thermal equilibrium

$$\Gamma \equiv \langle \sigma_z \rangle_{th} = \frac{1 - e^{\beta\hbar\omega_{ab}}}{1 + e^{\beta\hbar\omega_{ab}}} \tag{3.56}$$

If you were to describe the reservoir-induced transitions between the two levels of the two-level atom as spontaneous emission at zero temperature, you would conclude that the steady state inversion of the atom is -1. Our contribution here is therefore to relax this assumption by describing the relaxation of the atom to the exact steady state inversion given by Eq. (3.56).

3.4.2 Depletion damping

The results of this section are essentially identical to the usual Wigner-Weisskopff theory of spontaneous emission, but we will be using a density operator approach as in the previous sections. Transitions between the two levels $|a\rangle$ and $|b\rangle$ and the other atomic states are induced by the exchange of energy with the reservoir, causing a depletion in the population of the two levels. If the atom is left to undergo pure damping for a sufficient length of time, this exchange of energy with the reservoir will continues until the thermal state (3.45) is achieved. Our system now consists of the two-level atom combined with the set of states C other than $|a\rangle$ and $|b\rangle$. The Hamiltonian of the system is given by $\mathcal{H}_{\rm at} + \mathcal{H}_c$, with

$$\mathcal{H}_c = \hbar \sum_{s \in C} \omega_s \sigma_{ss}. \tag{3.57}$$

We will consider only transitions between the two levels and states in C while neglecting transitions between states in C with other states in C. The atom-reservoir interaction Hamiltonian given in the interaction picture is then

$$\mathcal{V} \;=\; i\hbar \sum_{s \in C} (\sigma_{sa} F_{sa}^\dagger - \sigma_{sa}^\dagger F_{sa} + \sigma_{sb} F_{sb}^\dagger - \sigma_{sb}^\dagger F_{sb}) \tag{3.58}$$

where

$$F_{\alpha\beta} = \sum_l{}' g^*_{l\alpha\beta} e^{i(\omega_{\alpha\beta}-\omega_l)\tau} b_l. \tag{3.59}$$

Proceeding as before, we obtain

$$\begin{aligned}
(\dot{\rho}_{\rm at})_{\rm dep} &= -\sum_{s\in C}\frac{\gamma_{sa}}{2}(\nu_{sa}+1)(\sigma^\dagger_{sa}\sigma_{sa}\rho_{\rm at} - 2\sigma_{sa}\rho_{\rm at}\sigma^\dagger_{sa} + \rho_{\rm at}\sigma^\dagger_{sa}\sigma_{sa}) \\
&\quad -\sum_{s\in C}\frac{\gamma_{sa}}{2}\nu_{sa}(\sigma_{sa}\sigma^\dagger_{sa}\rho_{\rm at} - 2\sigma^\dagger_{sa}\rho_{\rm at}\sigma_{sa} + \rho_{\rm at}\sigma_{sa}\sigma^\dagger_{sa}) \\
&\quad -\sum_{s\in C}\frac{\gamma_{sb}}{2}(\nu_{sb}+1)(\sigma^\dagger_{sb}\sigma_{sb}\rho_{\rm at} - 2\sigma_{sb}\rho_{\rm at}\sigma^\dagger_{sb} + \rho_{\rm at}\sigma^\dagger_{sb}\sigma_{sb}) \\
&\quad -\sum_{s\in C}\frac{\gamma_{sb}}{2}\nu_{sb}(\sigma_{sb}\sigma^\dagger_{sb}\rho_{\rm at} - 2\sigma^\dagger_{sb}\rho_{\rm at}\sigma_{sb} + \rho_{\rm at}\sigma_{sb}\sigma^\dagger_{sb})],
\end{aligned} \tag{3.60}$$

where

$$\gamma_{\alpha\beta} \equiv 2\pi\mathcal{D}(\omega_{\alpha\beta})|g_{\alpha\beta}(\omega_{\alpha\beta})|^2 \tag{3.61}$$

$$\nu_{\alpha\beta} \equiv \langle b^\dagger(\omega_{\alpha\beta})b(\omega_{\alpha\beta})\rangle_{\rm r}. \tag{3.62}$$

Here, we have eliminated cross-terms such as

$$\sum_{s,s'\in C}\sigma^\dagger_{sa}\sigma_{s'b}\rho_{\rm at}\langle F_{sa}(\tau')F^\dagger_{s'b}(\tau'')\rangle_{\rm r} \tag{3.63}$$

which vanish since

$$\int_{-\tau}^{\tau} d\tau' e^{i(\omega_{sa}-\omega')\tau'} \int_0^{\tau'} d\tau'' e^{-i(\omega_{s'b}-\omega')\tau''} \tag{3.64}$$

is appreciable only if $\omega_{sa} = \omega_{s'b}$, and we assume that that is not the case.

We now make the assumption that the temperature is sufficiently low that in thermal equilibrium the occupation level of the states $|a\rangle$, $|b\rangle$, and any states of higher energy is negligible. This approximation is valid as long as

$$\sum_{s\notin C} e^{-\beta\hbar\omega_a} \ll \sum_{s\in C} e^{-\beta\hbar\omega_s}, \tag{3.65}$$

where we now take the set C to contain only atomic states of lower energy than $|a\rangle$ and $|b\rangle$. In this limit, the atom never absorbs energy from the reservoir,

it only looses energy to the reservoir as it decays to atomic states of lower energy. The thermal state of the atom becomes

$$\rho_{\rm at}^{\rm th} \simeq |c\rangle\langle c| \tag{3.66}$$

where we use the superposition

$$|c\rangle \equiv \sum_{s\in C} \alpha_s |s\rangle \tag{3.67}$$

to represent all of the atomic states in C. Here, the coefficients α_s are arbitrary provided the normalization $\langle c|c\rangle = 1$ is satisfied, and any such superposition is considered identical to $|c\rangle$. Our atomic system is now considered to consist of just the three states $|a\rangle$, $|b\rangle$, and $|c\rangle$. The terms with the factors $\nu_{sa}+1$ and $\nu_{sb}+1$ in Eq. (3.60) describe the decay of the atom to $|c\rangle$ along with the associated decay of off-diagonal elements. On the other hand, the terms with the factors ν_{sa} and ν_{sb} describe the opposite effect of the atom making a transition from $|c\rangle$ to $|a\rangle$ or $|b\rangle$, a process that is negligible under our assumption. We therefore neglect those terms. The remaining terms can be written as

$$\begin{aligned}(\dot{\rho}_{\rm at})_{\rm dep} &= -\frac{\gamma_a}{2}(\sigma_{ca}^\dagger\sigma_{ca}\rho_{\rm at} - 2\sigma_{ca}\rho_{\rm at}\sigma_{ca}^\dagger + \rho_{\rm at}\sigma_{ca}^\dagger\sigma_{ca}) \\ &\quad -\frac{\gamma_b}{2}(\sigma_{cb}^\dagger\sigma_{cb}\rho_{\rm at} - 2\sigma_{cb}\rho_{\rm at}\sigma_{cb}^\dagger + \rho_{\rm at}\sigma_{cb}^\dagger\sigma_{cb}),\end{aligned} \tag{3.68}$$

where we have defined the decay rates

$$\gamma_a \equiv \sum_{s\in C} \gamma_{sa}(\nu_{sa}+1) \tag{3.69}$$

$$\gamma_b \equiv \sum_{s\in C} \gamma_{sb}(\nu_{sb}+1). \tag{3.70}$$

3.4.3 Radiationless Damping

In many cases of radiationless damping (e.g. collisions) there are processes which lead purely to an additional loss of coherence. Without specifying the particular mechanism, this loss of coherence can be described by

$$(\dot{\rho}_{\rm at})_{\rm rad-less} = -\frac{D}{2}(\rho_{\rm at} - \sigma_z\rho_{\rm at}\sigma_z), \tag{3.71}$$

where D is the decoherence rate.

Putting this together with the other two damping mechanisms, we have

$$(\dot{\rho_{\rm at}})_{\rm damp} = \mathcal{L}_{\rm at}\rho_{\rm at}, \tag{3.72}$$

where the two-level atom damping operator $\mathcal{L}_{\rm at}$ is given by

$$\begin{aligned}\mathcal{L}_{\rm at}\rho &= \frac{\gamma_{\rm at}}{4\Gamma}(1-\Gamma)(\sigma^\dagger\sigma\rho_{\rm at} - 2\sigma\rho_{\rm at}\sigma^\dagger + \rho_{\rm at}\sigma^\dagger\sigma) \\ &\quad + \frac{\gamma_{\rm at}}{4\Gamma}(1+\Gamma)(\sigma\sigma^\dagger\rho_{\rm at} - 2\sigma^\dagger\rho_{\rm at}\sigma + \rho_{\rm at}\sigma\sigma^\dagger) \\ &\quad - \frac{\gamma_a}{2}(\sigma_{ca}^\dagger\sigma_{ca}\rho_{\rm at} - 2\sigma_{ca}\rho_{\rm at}\sigma_{ca}^\dagger + \rho_{\rm at}\sigma_{ca}^\dagger\sigma_{ca}) \\ &\quad - \frac{\gamma_b}{2}(\sigma_{cb}^\dagger\sigma_{cb}\rho_{\rm at} - 2\sigma_{cb}\rho_{\rm at}\sigma_{cb}^\dagger + \rho_{\rm at}\sigma_{cb}^\dagger\sigma_{cb}) \\ &\quad - \frac{D}{2}(\rho_{\rm at} - \sigma_z\rho_{\rm at}\sigma_z).\end{aligned} \tag{3.73}$$

In order to keep the terms in the damping operator that do not correspond to depletion damping from giving rise to matrix elements involving the state $|c\rangle$, we must assume that the actions of the operators $\sigma^\dagger$, σ, and σ_z are independent of $|c\rangle$. That is, we assert the identities

$$\sigma^\dagger|c\rangle = \sigma|c\rangle = \sigma_z|c\rangle = |c\rangle. \tag{3.74}$$

3.5 A Two-level Atom Interacting With a Single-mode Electromagnetic Field

Combining results from the previous sections, we arrive at a model for a two-level atom interacting with a single-mode electromagnetic field in a cavity. Our master equation is given by

$$\dot{\rho} = -\frac{i}{\hbar}[\mathcal{H}_{\rm f} + \mathcal{H}_{\rm cm} + \mathcal{H}_{\rm at} + \mathcal{V}, \rho] + \check{\mathcal{L}}_{\rm f}\rho + \check{\mathcal{L}}_{\rm at}\rho, \tag{3.75}$$

where ρ is the density operator for the combined two-level atom and single-mode field, the Hamiltonian $\mathcal{H}_{\rm f}$ for the free single-mode field is given by Eq. (2.78), the Hamiltonian $\mathcal{H}_{\rm cm}$ for the center-of-mass motion of the atom is given by Eq. (3.14), and the Hamiltonian $\mathcal{H}_{\rm at}$ for the free two-level atom is

given by Eq. (3.48). The strong coupling of the two-level atom to the single-mode field is described by the interaction Hamiltonian $\mathcal{V}$ given by Eq. (3.43) restricted to just the two levels of the atom and the single mode of the field:

$$\mathcal{V} = i\hbar g(\sigma a^\dagger - \sigma^\dagger a), \tag{3.76}$$

where we have dropped the labels l, a, and b, and have chosen the quantization axis of the atom so that the coupling strength g is real. The weak coupling of the two-level atom and the single-mode field to the other states of the atom and field are described by the damping operators $\check{\mathcal{L}}_{\rm f}$ and $\check{\mathcal{L}}_{\rm at}$ which are the Schrödinger operators that have the form of Eqs. (2.102) and (3.73) when transformed to the interaction picture.

We proceed by assuming that the motion of the atom through the field is essentially classical, such that $\mathcal{H}_{\rm cm}$ can be neglected. We then transform to the interaction picture. If we transform to the interaction picture via

$$\mathcal{V} \to e^{i\mathcal{H}_0\tau/\hbar}\mathcal{V}e^{-i\mathcal{H}_0\tau/\hbar} \tag{3.77}$$

with the transformation Hamiltonian $\mathcal{H}_0 = \mathcal{H}_{\rm f} + \mathcal{H}_{\rm at}$, we arrive at the time-dependent interaction Hamiltonian

$$\mathcal{V}(\tau) = i\hbar g(\sigma a^\dagger e^{i\delta\tau} - \sigma^\dagger a e^{-i\delta\tau}), \tag{3.78}$$

where $\delta = \omega - \omega_{ab}$ is the detuning of the field. Instead, we will rewrite the Hamiltonian for the free atom as

$$\mathcal{H}_{\rm at} = \frac{1}{2}\hbar(\omega - \delta)\sigma_z, \tag{3.79}$$

and use $\mathcal{H}_0 = \mathcal{H}_{\rm f} + \frac{1}{2}\hbar\omega\sigma_z$ as our transition Hamiltonian. Using this the interaction Hamiltonian remains unchanged in the interaction picture and time-independent. The master equation in the interaction picture is then

$$\dot{\rho} = -\frac{i}{\hbar}\left[\mathcal{V} - \frac{1}{2}\hbar\sigma_z, \rho\right] + \mathcal{L}_{\rm f}\rho + \mathcal{L}_{\rm at}\rho, \tag{3.80}$$

where the interaction Hamiltonian $\mathcal{V}$ is given by Eq. (3.76). The damping operators $\mathcal{L}_{\rm f}$ and $\mathcal{L}_{\rm at}$ are again given by Eqs. (2.102) and (3.73). However, since we used ω instead of ω_{ab} in our transformation Hamiltonian, we must use ω instead of ω_{ab} in the definitions of Γ, $\gamma_{\rm at}$, γ_a, and γ_b.

3.5.1 The Jaynes-Cummings Model

The simplest model of a two-level atom interacting with a single-mode field is the Jaynes-Cummings Model first studied by Jaynes and Cummings in 1963 [29]. In this model the damping of the atom and field is neglected. In its original form, the spacial dependence of the atom-field coupling strength was also neglected—the coupling strength being averaged over the trajectory of the atom. The master equation is then given by

$$\dot{\rho} = -\frac{i}{\hbar}\left[\mathcal{V} - \frac{1}{2}\hbar\delta\sigma_z, \rho\right]. \tag{3.81}$$

Pure state solutions $\rho = |\psi\rangle\langle\psi|$ to this equation obey the Schrödinger equation

$$|\dot{\psi}\rangle = -\frac{i}{\hbar}\left(\mathcal{V} - \frac{1}{2}\hbar\delta\sigma_z\right)|\psi\rangle. \tag{3.82}$$

We proceed by expanding the state vector as

$$|\psi\rangle = \sum_n (\psi_{an}|an\rangle + \psi_{bn}|bn\rangle), \tag{3.83}$$

and we note that the interaction Hamiltonian $\mathcal{V}$ couples only the states $|a, n+1\rangle$ and $|bn\rangle$ for each n. Substituting this into the Schrödinger equation, we find that the coefficients satisfy the equation

$$\begin{bmatrix} \dot{\psi}_{a,n+1} \\ \dot{\psi}_{bn} \end{bmatrix} = \begin{bmatrix} -\frac{i\delta}{2} & g\sqrt{n+1} \\ -g\sqrt{n+1} & \frac{i\delta}{2} \end{bmatrix} \begin{bmatrix} \psi_{a,n+1} \\ \psi_{bn} \end{bmatrix}. \tag{3.84}$$

The eigenvalues are given by $\pm i\omega_n/2$ with

$$\omega_n \equiv \sqrt{4g^2(n+1) + \delta^2}, \tag{3.85}$$

and the solution is

$$\begin{aligned} \psi_{a,n+1}(t) &= \left[\cos\left(\frac{1}{2}\omega_n t\right) - \frac{i\delta}{\omega_n}\sin\left(\frac{1}{2}\omega_n t\right)\right]\psi_{a,n+1}(0) \\ &\quad + \frac{2g\sqrt{n+1}}{\omega_n}\sin\left(\frac{1}{2}\omega_n t\right)\psi_{bn}(0) \qquad (3.86) \\ \psi_{bn}(t) &= -\frac{2g\sqrt{n+1}}{\omega_n}\sin\left(\frac{1}{2}\omega_n t\right)\psi_{a,n+1}(0) \\ &\quad + \left[\cos\left(\frac{1}{2}\omega_n t\right) + \frac{i\delta}{\omega_n}\sin\left(\frac{1}{2}\omega_n t\right)\right]\psi_{bn}(0). \qquad (3.87) \end{aligned}$$

By using this result to form the matrix elements of a density operator, the solution to the master equation (3.81) can easily be found. It can be written in the form

$$\rho(t) = (1 + \mathcal{U}_1(t))(\rho_{\rm f}(0) \otimes \rho_{\rm at}(0)), \tag{3.88}$$

where the one-atom event operator $\mathcal{U}_1$ is defined by the matrix elements

$$\begin{aligned} \langle a, n+1|\mathcal{U}_1\rho|a, n+1\rangle &= -\mathcal{U}_{1_n}^{(-1)}\langle a, n+1|\rho|a, n+1\rangle \\ &\quad +\mathcal{U}_{1_n}^{(+1)}\langle bn|\rho|bn\rangle \qquad (3.89) \\ \langle bn|\mathcal{U}_1\rho|bn\rangle &= \mathcal{U}_{1_n}^{(-1)}\langle a, n+1|\rho|a, n+1\rangle \\ &\quad -\mathcal{U}_{1_n}^{(+1)}\langle bn|\rho|bn\rangle. \qquad (3.90) \end{aligned}$$

Here we have assumed that the field and atom are both initially diagonal (as when the field is in a steady state and the atom is in the upper or lower state but not in a superposition of both). We have also assumed that the atom will either be observed in the upper or lower state by a detector or deliberately ignored (as opposed to being manipulated further and then detected)—thus we neglect the terms that are off-diagonal in the atomic states. The coefficients

$$\mathcal{U}_{1_n}^{(+1)} = \mathcal{U}_{1_n}^{(-1)} = \frac{1}{2}\left(1 - \frac{\delta^2}{\omega_n^2}\right)(1 - \cos\omega_n t) \tag{3.91}$$

give the probabilities of $|bn\rangle \to |a, n+1\rangle$ and $|a, n+1\rangle \to |bn\rangle$ transitions. As before the superscripts indicate the gain or loss of field excitation, though it is superfluous here since the transition probabilities are equal. Note the identity

$$\mathrm{tr}\{\mathcal{U}_1\rho\} = 0, \quad \text{for any } \rho. \tag{3.92}$$

3.5.2 The Jaynes-Cummings Model with a Spacial-dependent Coupling Strength

Here we will extend the Jaynes-Cummings model to include a spacial-dependent atom-field coupling strength. We consider the case of an atom traversing the cylindrical axis of a right circular cylindrical cavity. We will assume that the field, as in the experiments of Walther *et al.* [41, 50, 52, 54, 67],

is in a TE mode with $p = 1$. The spacial-dependence of the coupling strength is then given by Eq. (2.69)

$$g(z) = g_0 \sin\left(\pi \frac{z}{d}\right). \tag{3.93}$$

We will treat the trajectory of the atom classically. The z-coordinate of the center-of-mass position of the atom is then given by $z(t) = d\,t/t_{\rm int}$, where $t_{\rm int}$ is the total interaction-time between the atom and field. The spacial-dependence of the coupling strength therefore gives rise to a time-dependent Schrödinger equation

$$\begin{bmatrix} \dot{\psi}_{a,n+1} \\ \dot{\psi}_{bn} \end{bmatrix} = g_0\sqrt{n+1} \begin{bmatrix} 0 & \sin\left(\pi \frac{t}{t_{\rm int}}\right) \\ -\sin\left(\pi \frac{t}{t_{\rm int}}\right) & 0 \end{bmatrix} \begin{bmatrix} \psi_{a,n+1} \\ \psi_{bn} \end{bmatrix}, \tag{3.94}$$

where we have assumed perfect resonance ($\delta = 0$). We Assume a solution of the form

$$\psi_{a,n+1}(t) = \cos\phi(t)\psi_{a,n+1}(0) + \sin\phi(t)\psi_{bn}(0) \tag{3.95}$$

$$\psi_{bn}(t) = -\sin\phi(t)\psi_{a,n+1}(0) + \cos\phi(t)\psi_{bn}(0), \tag{3.96}$$

where $\phi(t)$ is a function to be determined with the constraint $\phi(0) = 0$. Upon substitution, we find that ϕ is given by the equation

$$\dot{\phi} = g_0\sqrt{n+1}\sin\left(\pi \frac{t}{t_{\rm int}}\right), \tag{3.97}$$

with the solution

$$\phi = \frac{g_0}{\pi}\sqrt{n+1}t_{\rm int}\left[1 - \cos\left(\pi \frac{t}{t_{\rm int}}\right)\right]. \tag{3.98}$$

After the atom has traversed the cavity, the state of the combined atom-field system is given by evaluating the coefficients at $t = t_{\rm int}$, giving

$$\phi(t = t_{\rm int}) = \frac{2g_0}{\pi}\sqrt{n+1}t_{\rm int}. \tag{3.99}$$

This agrees with the result of the Jaynes-Cummings model if the coupling strength is taken to be $g = g_0/\pi$ which is identical to the average

$$g = \frac{g_0}{d}\int_o^d dz\, \sin\left(p\pi \frac{z}{d}\right) = \frac{g_0}{\pi}. \tag{3.100}$$

We thus conclude, that replacing the spacial-dependent coupling strength with the spacially-averaged coupling strength gives the exact result when determining the state of the atom-field system after the interaction. Though including other effects in the model such as atomic damping might affect this result, we have confidence that using a spacially-averaged coupling strength remains a good approximation.

3.5.3 The Jaynes-Cummings Model with Depletion Damping

Here we will extend the Jaynes-Cummings model to include the effect of depletion damping of the two-level atom. This model was developed by Zhu *et al.* [68] and independently by us. The master equation is given by

$$\dot{\rho} = -\frac{i}{\hbar}\left[\mathcal{V}, \rho\right] + (\dot{\rho}_{\rm at})_{\rm dep}, \tag{3.101}$$

where we have taken $\delta = 0$ and the depletion damping $(\dot{\rho}_{\rm at})_{\rm dep}$ is described by Eq. (3.68). If the atom is initially in a superposition of the upper and lower maser transition, then we can ignore the decay of off-diagonal elements involving superpositions of state $|c\rangle$. The depletion damping then factors into two processes. The non-unitary process

$$-\frac{\gamma_a}{2}(\sigma_{ca}^{\dagger}\sigma_{ca}\rho_{\rm at} + \rho_{\rm at}\sigma_{ca}^{\dagger}\sigma_{ca}) - \frac{\gamma_b}{2}(\sigma_{cb}^{\dagger}\sigma_{cb}\rho_{\rm at} + \rho_{\rm at}\sigma_{cb}^{\dagger}\sigma_{cb}) \tag{3.102}$$

which can be written in terms of the Pauli pseudo spin-flip operators as

$$-\frac{\gamma_a}{2}(\sigma\sigma^{\dagger}\rho_{\rm at} + \rho_{\rm at}\sigma\sigma^{\dagger}) - \frac{\gamma_b}{2}(\sigma^{\dagger}\sigma\rho_{\rm at} + \rho_{\rm at}\sigma^{\dagger}\sigma) \tag{3.103}$$

now concerns only the states $|a\rangle$ and $|b\rangle$ and describes the depletion of the population of these levels and the corresponding decoherence. The remaining process

$$\gamma_a\sigma_{ca}\rho_{\rm at}\sigma_{ca}^{\dagger} + \gamma_b\sigma_{cb}\rho_{\rm at}\sigma_{cb}^{\dagger} \tag{3.104}$$

describes the increase in the population of the state $|c\rangle$ representing all of the other levels in the decay channels of $|a\rangle$ and $|b\rangle$. We will proceed by first treating the non-unitary evolution of the combined two-level atom and

field system, where the non-unitary of the evolution comes about due to the depletion of the two levels undergoing damping. We can then later expand the system to include the state $|c\rangle$ and obtain a normalized density operator by integrating the equation

$$\frac{d}{dt}\langle cn|\rho|cn\rangle = \gamma_a\langle an|\rho|an\rangle + \gamma_b\langle bn|\rho|bn\rangle. \tag{3.105}$$

The non-unitary evolution of the two-level atom and field system is described by the equation

$$\dot{\rho} = -\frac{i}{\hbar}\left[\mathcal{V},\rho\right] - \frac{\gamma_a}{2}(\sigma\sigma^\dagger\rho_{\rm at} + \rho_{\rm at}\sigma\sigma^\dagger) - \frac{\gamma_b}{2}(\sigma^\dagger\sigma\rho_{\rm at} + \rho_{\rm at}\sigma^\dagger\sigma). \tag{3.106}$$

Pure state solutions $\rho = |\psi\rangle\langle\psi|$ to this equation satisfy the Schrödinger-like equation

$$|\dot{\psi}\rangle = -\frac{i}{\hbar}\left(\mathcal{V} - i\hbar\frac{\gamma_a}{2}\sigma\sigma^\dagger - i\hbar\frac{\gamma_b}{2}\sigma^\dagger\sigma\right)|\psi\rangle. \tag{3.107}$$

We again expand the state vector as in Eq. (3.83), and find that the coefficients satisfy the equation

$$\left[\begin{array}{c}\dot{\psi}_{a,n+1}\\ \dot{\psi}_{bn}\end{array}\right] = \left[\begin{array}{cc}-\frac{\gamma_a}{2} & g\sqrt{n+1}\\ -g\sqrt{n+1} & -\frac{\gamma_b}{2}\end{array}\right]\left[\begin{array}{c}\psi_{a,n+1}\\ \psi_{bn}\end{array}\right]. \tag{3.108}$$

The eigenvalues are given by $-\gamma_+/2 \pm i\omega_n/2$ with

$$\omega_n \equiv \sqrt{4g^2(n+1) - \gamma_-^2} \tag{3.109}$$

$$\gamma_\pm \equiv \frac{1}{2}(\gamma_a \pm \gamma_b), \tag{3.110}$$

and the solution is

$$\begin{aligned}\psi_{a,n+1}(t) &= e^{-\gamma_+ t/2}\left[\cos\left(\frac{1}{2}\omega_n t\right) - \frac{\gamma_-}{\omega_n}\sin\left(\frac{1}{2}\omega_n t\right)\right]\psi_{a,n+1}(0)\\ &\quad + \frac{2g\sqrt{n+1}}{\omega_n}e^{-\gamma_+ t/2}\sin\left(\frac{1}{2}\omega_n t\right)\psi_{bn}(0) \qquad (3.111)\\ \psi_{bn}(t) &= -\frac{2g\sqrt{n+1}}{\omega_n}e^{-\gamma_+ t/2}\sin\left(\frac{1}{2}\omega_n t\right)\psi_{a,n+1}(0)\\ &\quad + e^{-\gamma_+ t/2}\left[\cos\left(\frac{1}{2}\omega_n t\right) + \frac{\gamma_-}{\omega_n}\sin\left(\frac{1}{2}\omega_n t\right)\right]\psi_{bn}(0) \qquad (3.112)\end{aligned}$$

By forming the matrix elements of a density operator and integrating Eq. (3.105), the solution to the master equation (3.101) can be put in the form of Eq. (3.88). Again we assume that the field and atom are initially diagonal and that the atom will either be detected in the state $|a\rangle$ or $|b\rangle$ or deliberately ignored. Then the one-atom event operator $\mathcal{U}_1$ that includes the effect of depletion damping has the matrix elements

$$\begin{aligned}
\langle a,n+1|\mathcal{U}_1\rho|a,n+1\rangle &= -\left[{\mathcal{U}_1}_n^{(-1)}+\mathcal{A}_n^{(0)}+\mathcal{B}_n^{(-1)}\right]\langle a,n+1|\rho|a,n+1\rangle \\
&\quad +{\mathcal{U}_1}_n^{(+1)}\langle bn|\rho|bn\rangle \qquad (3.113)\\
\langle bn|\mathcal{U}_1\rho|bn\rangle &= {\mathcal{U}_1}_n^{(-1)}\langle a,n+1|\rho|a,n+1\rangle \\
&\quad -\left[{\mathcal{U}_1}_n^{(+1)}+\mathcal{A}_n^{(+1)}+\mathcal{B}_n^{(0)}\right]\langle bn|\rho|bn\rangle \qquad (3.114)\\
\langle cn|\mathcal{U}_1\rho|cn\rangle &= \mathcal{A}_{n-1}^{(0)}\langle an|\rho|an\rangle+\mathcal{A}_{n-1}^{(+1)}\langle b,n-1|\rho|b,n-1\rangle \\
&\quad +\mathcal{B}_n^{(-1)}\langle a,n+1|\rho|a,n+1\rangle \\
&\quad +\mathcal{B}_n^{(0)}\langle bn|\rho|bn\rangle. \qquad (3.115)
\end{aligned}$$

The coefficients are given by

$$\begin{aligned}
\mathcal{U}_n^{(+1)} &= \mathcal{U}_n^{(-1)}=\frac{1}{2}\left(1+\frac{\gamma_-^2}{\omega_n^2}\right)e^{-\gamma_+ t}(1-\cos\omega_n t) \qquad (3.116)\\
\mathcal{A}_n^{(+1)} &= \frac{\gamma_a}{2}\left(1+\frac{\gamma_-^2}{\omega_n^2}\right)(\eta_n-\zeta_n) \qquad (3.117)\\
\mathcal{A}_n^{(0)} &= \frac{\gamma_a}{2}\left[\left(1+\frac{\gamma_-^2}{\omega_n^2}\right)\eta_n+\left(1-\frac{\gamma_-^2}{\omega_n^2}\right)\zeta_n-\frac{2\gamma_-}{\omega_n}\xi_n\right] \qquad (3.118)\\
\mathcal{B}_n^{(0)} &= \frac{\gamma_b}{2}\left[\left(1+\frac{\gamma_-^2}{\omega_n^2}\right)\eta_n+\left(1-\frac{\gamma_-^2}{\omega_n^2}\right)\zeta_n+\frac{2\gamma_-}{\omega_n}\xi_n\right] \qquad (3.119)\\
\mathcal{B}_n^{(-1)} &= \frac{\gamma_b}{2}\left(1+\frac{\gamma_-^2}{\omega_n^2}\right)(\eta_n-\zeta_n), \qquad (3.120)
\end{aligned}$$

where we have defined

$$\begin{aligned}
\eta_n &\equiv \frac{1}{\gamma_+}\left(1-e^{-\gamma_+ t}\right) \qquad (3.121)\\
\zeta_n &\equiv \frac{1}{\omega_n^2+\gamma_+^2}\left[\gamma_+ + e^{-\gamma_+ t}(-\gamma_+\cos\omega_n t+\omega_n\sin\omega_n t)\right] \qquad (3.122)\\
\xi_n &\equiv \frac{1}{\omega_n^2+\gamma_+^2}\left[\omega_n + e^{-\gamma_+ t}(-\omega_n\cos\omega_n t-\gamma_+\sin\omega_n t)\right]. \qquad (3.123)
\end{aligned}$$

As before, the coefficients give the transition probabilities with the superscripts indicating the gain or loss of field excitation. Here we use the notation "$\mathcal{A}$" or "$\mathcal{B}$" to indicate that the atom decayed while in state $|a\rangle$ or $|b\rangle$, respectively. For example, the coefficient $\mathcal{A}_n^{(+1)}$ gives the probability of the transition $|bn\rangle \rightarrow |a, n+1\rangle \rightarrow |c, n+1\rangle$.

Chapter 4

The Micromaser

A one-atom maser or micromaser consists of a series of identically prepared two-level atoms interacting with a single-mode microwave field inside a high-Q cavity. The atoms are injected at a rate small enough so that it is rare for more than one atom to interact with the field at the same time and cooperative effects can be neglected. The micromaser therefore is a system that allows us to observe single atoms interacting with the field. The high-Q of the cavity is necessary for the operating mode of the cavity to have a sharply defined energy response function. The cavity can therefore be tuned to transitions between the two levels with no other atomic transition being coupled to the cavity with an appreciable strength. The high-Q also gives the cavity a long photon storage-time necessary to build up an appreciable field without requiring higher injection rates. The photon storage-time is usually taken to be much longer than the interaction time for an atom passing through the cavity so that field damping can be neglected during the passage of an atom. The atoms play the dual-purpose of both pumping the field and also probing the field via measurements made on the outgoing atoms. Any other means of probing the field has the harmful effect of lowering the quality of the cavity.

4.1 Micromaser Field Dynamics

The dynamics of the micromaser field consists of times of pure damping punctuated by interactions with single atoms passing through the cavity. The interaction times between the atoms and field are taken to be much shorter than the photon-storage time of the cavity, such that the damping of the field can be neglected during the atom-field interactions. This is the standard micromaser model that was first proposed by Filipowicz *et al.* [20]. Here, we will derive a master equation describing the continuous evolution of the

micromaser field averaged over the stochastic arrival times of the injected atoms.

When no atom is present, the pure damping of the field for a time t is described by the equation

$$\rho_{\rm f}(t) = e^{\mathcal{L}_{\rm f} t}\rho_{\rm f}(0), \tag{4.1}$$

where $\rho_{\rm f}$ is the density operator for the micromaser field and $\mathcal{L}_{\rm f}$ is the field damping operator given by Eq. (2.102). When an atom is injected into the cavity, the effect of the atom's passage is described by the equation

$$\rho_{\rm f}(t_{\rm int}) = (1 + \mathcal{U}_{1\rm f})\rho_{\rm f}(0). \tag{4.2}$$

Here we have introduced the reduced one-atom event operator for the field defined by

$$\mathcal{U}_{1\rm f}\rho = {\rm tr}_{\rm at}\{\mathcal{U}_1(t = t_{\rm int})(\rho \otimes \rho_{\rm at})\}, \tag{4.3}$$

where $\rho_{\rm at}$ is the initial state of the injected atom and $t_{\rm int}$ is the total time for the passing of the atom and it's interaction with the cavity. We will assume here that all atoms arrive with the same velocity and interact with the cavity for the same length of time. The interaction is described by the one-atom event operator $\mathcal{U}_1$ which acts on the combined atom-field system, and is the solution to the Jaynes-Cummings model or one of its more general extensions. Tracing over the atomic variables gives the reduced density operator for the field—giving the best description of the field without utilizing any information gained from measurements made on the atom.

We wish to describe the evolution of the micromaser field averaged over the arrival times of injected atoms. Assuming the atoms are injected at a Poissonian rate r, the spacings s between the arrival times of the atoms are random variables with the probability density

$$\rho_s(s) = re^{-rs}. \tag{4.4}$$

The probability that no atom arrives in the interval $(0, t)$ is $\exp(-rt)$, while the probability density that an atom arrives at time t is given by $r\,dt$. The validity of assuming that in the micromaser there is never more than one atom

in the cavity at a time hinges upon the approximation $\exp(-rt_{\rm int}) \simeq 1$ and the smallness of the parameter $rt_{\rm int}$.

We proceed by expanding the density operator of the field at time t in terms of the number of atomic events that have occurred in the interval $(0,t)$:

$$\rho_{\rm f}(t) = e^{-rt}\left\{\rho_0(t) + r\int_0^t dt_1\rho_1(t;t_1) + r^2\int_0^t dt_2\int_0^{t_2} dt_1\rho_2(t;t_1,t_2) + \cdots\right\}. \quad (4.5)$$

Here $\rho_n(t;t_1,\ldots,t_n)$ denotes the density operator for the field at time t conditioned by the passing of n-atoms arriving at the times $0 \leq t_1 \leq \cdots \leq t_n \leq t$. The probability density $r^n\,dt_1\cdots dt_n$ gives the distribution of arrival times of n atoms, while the factor e^{-rt} gives the exclusive probability of no atoms arriving at any other times. It is easy to verify that this expression satisfies the condition $\mathrm{tr}\{\rho(t)\} = 1$. The conditioned density operators are given by

$$\rho_n(t;t_1,\ldots,t_n) = e^{\mathcal{L}_{\rm f}(t-t_n)}(1+\mathcal{U}_{1\rm f})\cdots e^{\mathcal{L}_{\rm f}(t_2-t_1)}(1+\mathcal{U}_{1\rm f})e^{\mathcal{L}_{\rm f}t_1}\rho(0), \quad (4.6)$$

where we have assumed that the interaction time is much smaller than the photon storage-time ($\gamma_{\rm f}t_{\rm int} \ll 1$) such that the damping of the field can be neglected during atom-field interactions. The damping of the field was therefore neglected in the model used in deriving the one-atom event operator and we have here neglected factors of $\exp(\mathcal{L}_{\rm f}t_{\rm int})$. This has the effect of describing the one-atom events as if they were point-like events in time requiring no duration. Substituting the conditioned density operators into the expansion (4.5) we obtain

$$e^{(r-\mathcal{L}_{\rm f})t}\rho_{\rm f}(t) \;=\; \rho_{\rm f}(0) + r\int_0^t dt' e^{-\mathcal{L}_{\rm f}t'}(1+\mathcal{U}_{1\rm f})e^{\mathcal{L}_{\rm f}t'}e^{(r-\mathcal{L}_{\rm f})t'}\rho_{\rm f}(t'), \quad (4.7)$$

which is the formal solution to the differential equation

$$\frac{d}{dt}\left[e^{(r-\mathcal{L}_{\rm f})t}\rho_{\rm f}\right] = re^{(r-\mathcal{L}_{\rm f})t}(1+\mathcal{U}_{1\rm f})\rho_{\rm f}. \quad (4.8)$$

This establishes the master equation for the micromaser field:

$$\dot{\rho}_{\rm f} = \mathcal{X}\rho_{\rm f}, \quad (4.9)$$

where the evolution operator $\mathcal{X}$ for the micromaser field is defined by

$$\mathcal{X} = \mathcal{L}_{\rm f} + r\mathcal{U}_{1\rm f}. \quad (4.10)$$

The matrix elements of $\mathcal{X}$ are given by

$$\begin{aligned}\langle n|\mathcal{X}\rho|n\rangle &= \left[\mathcal{L}_{\mathrm{f}}{}_{n-1}^{(+1)} + r\langle b|\rho_{\mathrm{at}}|b\rangle\left(\mathcal{U}_1{}_{n-1}^{(+1)} + \mathcal{A}_{n-1}^{(+1)}\right)\right]\langle n-1|\rho|n-1\rangle \\ &+ \left[\mathcal{L}_{\mathrm{f}}{}_{n}^{(-1)} + r\langle a|\rho_{\mathrm{at}}|a\rangle\left(\mathcal{U}_1{}_{n}^{(-1)} + \mathcal{B}_{n}^{(-1)}\right)\right]\langle n+1|\rho|n+1\rangle \\ &- \left[\mathcal{L}_{\mathrm{f}}{}_{n}^{(+1)} + r\langle b|\rho_{\mathrm{at}}|b\rangle\left(\mathcal{U}_1{}_{n}^{(+1)} + \mathcal{A}_{n}^{(+1)}\right)\right]\langle n|\rho|n\rangle \\ &- \left[\mathcal{L}_{\mathrm{f}}{}_{n-1}^{(-1)} + r\langle a|\rho_{\mathrm{at}}|a\rangle\left(\mathcal{U}_1{}_{n-1}^{(-1)} + \mathcal{B}_{n-1}^{(-1)}\right)\right]\langle n|\rho|n\rangle, \qquad (4.11)\end{aligned}$$

where we have again assumed that the atom and field are initially diagonal.

Filipowicz, Javanaeinen, and Meystre [20] proved that the steady state of the micromaser field was given by $\mathcal{X}\rho_{\mathrm{f}}^{\mathrm{ss}} = 0$ (though their definition of $\mathcal{X}$ did not include depletion damping). Since then, $\mathcal{X}$ has been used as an operator describing the evolution of the micromaser field, though it has been lacking a formal derivation.

The steady state of the micromaser field $\rho_{\mathrm{f}}^{\mathrm{ss}}$ was first derived by Filipowicz *et al.* [20]. Here we will derive a more general form for the steady state that includes atomic decay. The steady state of the field is established when the rates of $|n\rangle \to |n+1\rangle$ transitions and $|n+1\rangle \to |n\rangle$ transitions are equal and $\mathcal{X}\rho_{\mathrm{f}}^{\mathrm{ss}} = 0$. This establishes the recurrence relation

$$\langle n+1|\rho_{\mathrm{f}}^{\mathrm{ss}}|n+1\rangle = \frac{\mathcal{L}_{\mathrm{f}}{}_{n}^{(+1)} + r\langle b|\rho_{\mathrm{at}}|b\rangle\left(\mathcal{U}_1{}_{n}^{(+1)} + \mathcal{A}_{n}^{(+1)}\right)}{\mathcal{L}_{\mathrm{f}}{}_{n}^{(-1)} + r\langle a|\rho_{\mathrm{at}}|a\rangle\left(\mathcal{U}_1{}_{n}^{(-1)} + \mathcal{B}_{n}^{(-1)}\right)}\langle n|\rho_{\mathrm{f}}^{\mathrm{ss}}|n\rangle, \qquad (4.12)$$

with the solution

$$\langle n|\rho_{\mathrm{f}}^{\mathrm{ss}}|n\rangle = \langle 0|\rho_{\mathrm{f}}^{\mathrm{ss}}|0\rangle \prod_{m=0}^{n-1} \frac{\mathcal{L}_{\mathrm{f}}{}_{n}^{(+1)} + r\langle b|\rho_{\mathrm{at}}|b\rangle\left(\mathcal{U}_1{}_{n}^{(+1)} + \mathcal{A}_{n}^{(+1)}\right)}{\mathcal{L}_{\mathrm{f}}{}_{n}^{(-1)} + r\langle a|\rho_{\mathrm{at}}|a\rangle\left(\mathcal{U}_1{}_{n}^{(-1)} + \mathcal{B}_{n}^{(-1)}\right)}, \qquad (4.13)$$

where $\langle 0|\rho_{\mathrm{f}}^{\mathrm{ss}}|0\rangle$ is determined by the normalization condition $\mathrm{tr}\{\rho_{\mathrm{f}}^{\mathrm{ss}}\} = 1$. There are other ways to derive this result (see for example the steps leading up to Eq. (2.13) of Ref. [20]).

The master equation (4.9) and the steady state (4.13) rely heavily on the assumption that the atomic events are point-like events in time requiring durations much smaller than the photon storage-time of the cavity. Without this assumption, no continuous dynamical equation for the micromaser exists.

Instead, the dynamics of the micromaser field would need to be described by a return map such as:

$$\rho_{\rm f}(t_{i+1}) = e^{\mathcal{L}_{\rm f}(t_{i+1}-t_{\rm int}-t_i)}(1+\mathcal{U}_{1\rm f})\rho_{\rm f}(t_i), \tag{4.14}$$

giving the density operator of the micromaser field at successive atomic injections.

4.2 The Micromaser with Velocity Averaging

The atoms arriving at the micromaser cavity have a distribution of velocities and hence a distribution of interaction times. For simplicity we assume that the distribution of the interaction times is a highly peaked Gaussian with a mean $\bar{t}_{\rm int}$ and rms spread $\sigma_t \ll \bar{t}_{\rm int}$:

$$\rho_{t_{\rm int}}(t) = \frac{1}{\sqrt{2\pi}\sigma_t}\exp\left[-\frac{(t-\bar{t}_{\rm int})^2}{2\sigma_t^2}\right]. \tag{4.15}$$

As argued by Filipowicz *et al.* [20], as long as the interaction times of successive atoms are statistically independent, the correct way to introduce a distribution of interaction times is to average the one-atom event operator $U_{1\rm f}$ over the distribution. This method also relies on the assumptions of the model: that the interaction times are much less than the photon-storage time of the cavity. The average of $U_{1\rm f}$ can be obtained by replacing the time-dependent factors with the averages

$$\int_{-\infty}^{\infty} dt\, \rho_{t_{\rm int}}(t)e^{-\gamma_+ t} = \exp\left[\frac{1}{2}(\gamma_+\sigma_t)^2 - \gamma_+\bar{t}_{\rm int}\right] \tag{4.16}$$

$$\int_{-\infty}^{\infty} dt\, \rho_{t_{\rm int}}(t)e^{-\gamma_+ t}\cos\omega_n t = \exp\left[\frac{1}{2}(\gamma_+\sigma_t)^2 - \gamma_+\bar{t}_{\rm int}\right]\exp\left[-\frac{1}{2}(\omega_n\sigma_t)^2\right] \times\cos[\omega_n(\bar{t}_{\rm int}-\gamma_+\sigma_t^2)] \tag{4.17}$$

$$\int_{-\infty}^{\infty} dt\, \rho_{t_{\rm int}}(t)e^{-\gamma_+ t}\sin\omega_n t = \exp\left[\frac{1}{2}(\gamma_+\sigma_t)^2 - \gamma_+\bar{t}_{\rm int}\right]\exp\left[-\frac{1}{2}(\omega_n\sigma_t)^2\right] \times\sin[\omega_n(\bar{t}_{\rm int}-\gamma_+\sigma_t^2)]. \tag{4.18}$$

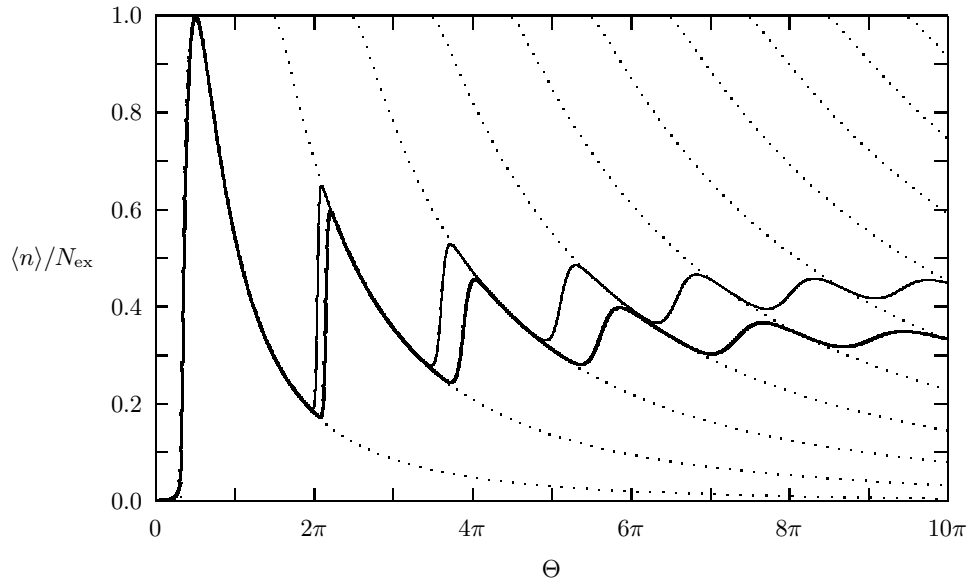

Figure 4.1: The average photon number $\langle n\rangle$ normalized by $N_{\rm ex}$ for a micromaser in which all of the atoms arrive in the upper maser level. The parameters used here are $N_{\rm ex} = 200$, $\nu = 0.054$, and $g = 39$ kHz. The thick curve is without atomic damping, and the thin curve is with the parameters $\gamma_a = (244\ \mu s)^{-1}$ and $\gamma_b = (488\ \mu s)^{-1}$. The dotted curves are the stable stationary solutions to a semiclassical rate equation.

4.3 The Micromaser Field Statistics

The photon statistics of the micromaser field were discussed rather nicely in Ref. [20]. Our discussion here will include the effect of atomic damping on the cavity photon distribution. The effect of atomic decay was also considered in Ref. [68], though the authors considered only the case when the decay rate of the upper and lower atomic states were equal. Figure 4.1 shows the average number of cavity photons

$$\langle n\rangle = \sum_{k=1}^{\infty} k\rho_k^{\rm ss}, \tag{4.19}$$

for a micromaser in which all of the atoms arrive in the upper maser level. The result is normalized by $N_{\rm ex} = r/\gamma_{\rm f}$ and plotted as a function of the

dimensionless pump parameter

$$\Theta \equiv \sqrt{N_{\rm ex}} g t_{\rm int}. \tag{4.20}$$

The parameters used were $N_{\rm ex} = r/\gamma_{\rm f} = 200$, $\nu = 0.054$, and $g = 39$ kHz. The thick curve is without atomic damping, and the thin curve is with the parameters $\gamma_a = (244\ \mu s)^{-1}$ and $\gamma_b = (488\ \mu s)^{-1}$.

A semiclassical rate-equation analysis for the average number of cavity photons similar to that in Refs. [20, 43] gives

$$\begin{aligned} \frac{d}{dt}\langle n\rangle &= \mathcal{L}_{\rm f}{}^{(+1)}_{\langle n\rangle} + r\langle b|\rho_{\rm at}|b\rangle \left(\mathcal{U}_1{}^{(+1)}_{\langle n\rangle} + \mathcal{A}^{(+1)}_{\langle n\rangle}\right) \\ &\quad -\mathcal{L}_{\rm f}{}^{(-1)}_{\langle n\rangle} - r\langle a|\rho_{\rm at}|a\rangle \left(\mathcal{U}_1{}^{(-1)}_{\langle n\rangle} + \mathcal{B}^{(-1)}_{\langle n\rangle}\right). \end{aligned} \tag{4.21}$$

The terms in Eq. (4.21) with $(+1)$ superscript describe the gain in field excitation due to interaction with the atom and reservoir, while the terms with (-1) superscripts describe the losses. For large $N_{\rm ex}$, the possible mean photon numbers in steady state are approximately given by the stable stationary solutions of this equation. The dotted curves in Fig. 4.1 show the stable stationary solutions of Eq. (4.21) for no atomic damping. The quantum mechanical calculation is given approximately by these solutions separated by first-order phase transitions as described in Refs. [20, 43]. The micromaser field in the vicinity of these phase transition regions has been shown to exhibit quantum jumps, and hysteresis [3, 20].

For small damping, the stable stationary solutions of Eq. (4.21) for no damping remain approximately valid, and the effect of atomic damping is to cause the phase transitions to shift. Since the atom is more likely to decay while in the lower state, the cavity is more likely to gain excitation levels. This causes the phase transition to larger $\langle n\rangle$ to occur at a smaller $t_{\rm int}$. Atomic damping also has the effect of changing the asymptotic limit of $\langle n\rangle$ as $t_{\rm int} \to \infty$.

Figure 4.2 shows the normalized standard deviation

$$\sigma = \frac{(\langle n^2\rangle - \langle n\rangle^2)^{1/2}}{\langle n\rangle^{1/2}} \tag{4.22}$$

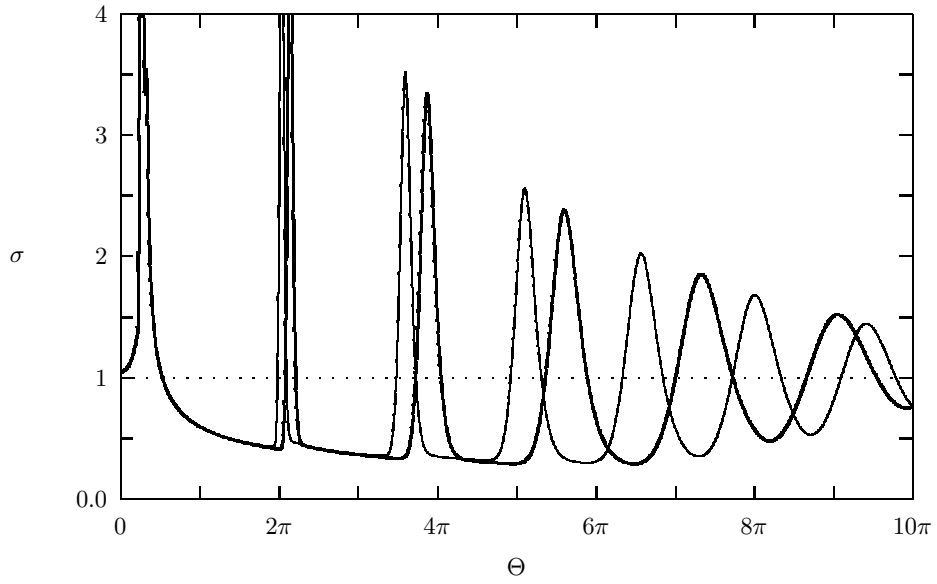

Figure 4.2: The normalized standard deviation σ for a micromaser in which all of the atoms arrive in the upper maser level. The parameters used here are $N_{\rm ex} = 200$, $\nu = 0.054$, and $g = 39$ kHz. The thick curve is without atomic damping, and the thin curve is with the parameters $\gamma_a = (244\ \mu s)^{-1}$ and $\gamma_b = (488\ \mu s)^{-1}$. A Poissonian photon distribution corresponds to $\sigma = 1$.

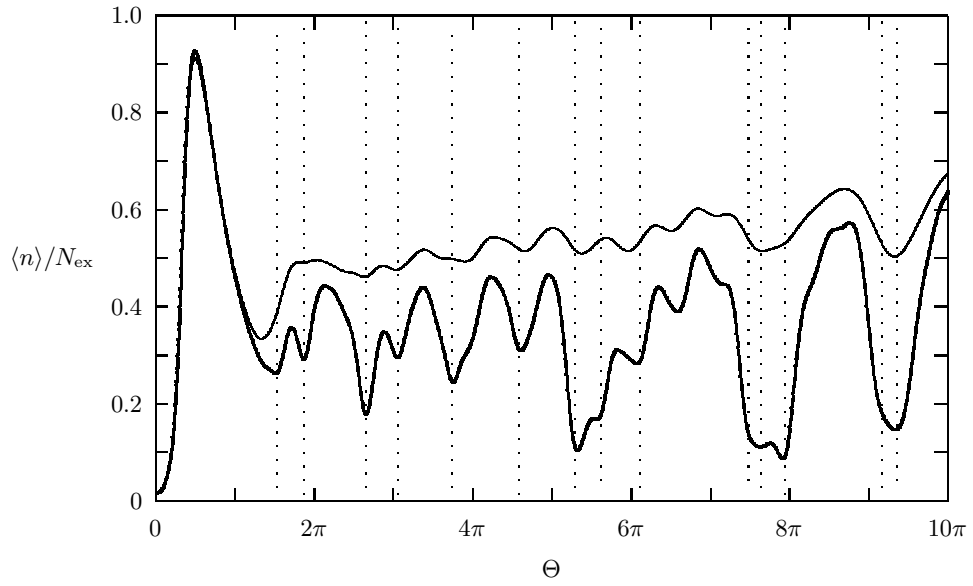

Figure 4.3: The average photon number $\langle n\rangle$ normalized by $N_{\rm ex}$ for a micromaser in which all of the atoms arrive in the upper maser level. The parameters used here are $N_{\rm ex} = 7$, $\nu = 0.054$, and $g = 39$ kHz. The thick curve is without atomic damping, and the thin curve is with the parameters $\gamma_a = (244\ \mu s)^{-1}$ and $\gamma_b = (488\ \mu s)^{-1}$. The vertical dotted lines indicate the trapping states for $n_q = 0, 1, 2$.

of the photon distribution for a micromaser in which all of the atoms arrive in the upper state. The parameters used here are the same for those of Fig. 4.1. The figure shows the sub-Poissonian nature of the field (Poissonian photon statistics correspond to $\sigma = 1$) with super-Poissonian peaks centered at the values of Θ where the phase transitions occur. The inclusion of a small amount of atomic damping as before shifts the location of the phase transitions and hence shifts the locations of the super-Poissonian peaks and the sub-Poissonian regions. The sub-Poissonian regions are indicative of the quantized nature of the field and its sources and the lack of sufficient stochasticity and noise, which when added to the model lead to the recovery of the ordinary Poissonian statistics of a macroscopic maser [20].

Figure 4.3 shows the normalized average number of cavity photons for

the small value of $N_{\rm ex} = 7$. All other parameters are the same. There is no longer any evidence of isolated phase transitions. The vertical dotted lines indicate the trapping states

$$t_{\rm int} = \frac{q\pi}{g\sqrt{n_q + 1}}, \tag{4.23}$$

for $n_q = 0, 1, 2$, which are visible for small $N_{\rm ex}$. As was described by Meystre *et al.* [20, 44], these are specific interaction times for which an atom will undergo an integer number q of Rabi cycles when interacting with a cavity field of n_q photons. Each atom leaves the cavity photon number unchanged, and the photon number is "trapped" with n_q being the maximum number of cavity photons allowed (except for thermal noise). As seen, they have the effect of suppressing the average number of cavity photons. The presence of atomic decay greatly reduces the effect of trapping states.

Figure 4.4 shows the normalized standard deviation of the cavity photon distribution for $N_{\rm ex} = 7$. All other parameters are the same. The statistics of the micromaser field is no longer neatly separated into sub-Poissonian regions with super-Poissonian peaks centered on the location of phase transitions. There still is a significant amount of sub-Poissonian behavior and the largest peaks in σ appear to still indicate locations where $\langle n \rangle$ undergoes abrupt changes as a function of $Theta$. The inclusion of atomic damping for this small value of $N_{\rm ex}$ is seen to greatly suppress the deviation from Poissonian statistics, though the first sub-Poissonian region near $\Theta = \pi$ appears to be mostly unaffected.

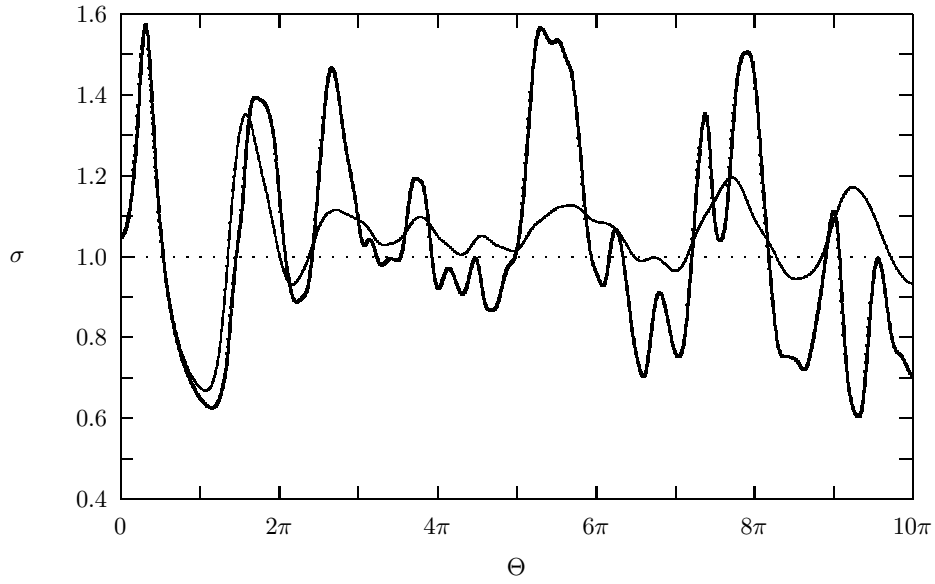

Figure 4.4: The normalized standard deviation σ for a micromaser in which all of the atoms arrive in the upper maser level. The parameters used here are $N_{\rm ex} = 7$, $\nu = 0.054$, and $g = 39$ kHz. The thick curve is without atomic damping, and the thin curve is with the parameters $\gamma_a = (244\ \mu s)^{-1}$ and $\gamma_b = (488\ \mu s)^{-1}$. A Poissonian photon distribution corresponds to $\sigma = 1$.

Chapter 5

The Micromaser with Two-atom Events

An extension of the standard micromaser theory that is of interest is the inclusion of two-atom events. Even when two-atom events are rare, two-atom events are expected to make the effect of trapping states less visible [47, 66]. It has been shown for the trapping states that, after a single two-atom event, the micromaser field relaxes slow enough that another two-atom event is likely to occur before the field returns to the steady-state (as calculated using single atom events only) [66]. Also, we would like to generalize the micromaser theory to larger pump rates where the one-atom approximation becomes invalid.

5.1 Two Atoms Interacting with the Micromaser Field

When two atoms are interacting with the micromaser field, we will neglect any direct interactions between the two atoms. Correlations between the atoms will develop solely due to their interaction with the same field. As with the Jaynes-Cummings Model, we will neglect damping during the interaction and neglect the spacial dependence of the atom-field coupling strength. We will also assume that the atoms are in resonance with the field and take $\delta = 0$. The Schrödinger equation is then given by

$$|\dot{\psi}\rangle = -\frac{i}{\hbar}\mathcal{V}|\psi\rangle, \tag{5.1}$$

with the interaction Hamiltonian

$$\mathcal{V} = i\hbar g[(\sigma_1 + \sigma_2)a^\dagger - (\sigma_1 + \sigma_2)^\dagger a]. \tag{5.2}$$

Here the subscripts "1" and "2" indicate the first or second atom to arrive at the micromaser cavity. We proceed by expanding the state vector as

$$|\psi\rangle = \sum_n (\psi_{aan}|aan\rangle + \psi_{abn}|abn\rangle + \psi_{ban}|ban\rangle + \psi_{bbn}|bbn\rangle) \tag{5.3}$$

and note that the interaction Hamiltonian $\mathcal{V}$ only couples the states $|aa, n+2\rangle$, $|ab, n+1\rangle$, $|ba, n+1\rangle$, and $|bbn\rangle$ for each n. Here the first and second ket labels refer to the state of the first and second atoms, respectively. Substituting this into the Schrödinger equation, we find that the coefficients satisfy the equation

$$\begin{bmatrix} \dot{\psi}_{aa,n+2} \\ \dot{\psi}_{ab,n+1} \\ \dot{\psi}_{ba,n+1} \\ \dot{\psi}_{bbn} \end{bmatrix} = g \begin{bmatrix} 0 & \sqrt{n+2} & \sqrt{n+2} & 0 \\ -\sqrt{n+2} & 0 & 0 & \sqrt{n+1} \\ -\sqrt{n+2} & 0 & 0 & \sqrt{n+1} \\ 0 & -\sqrt{n+1} & -\sqrt{n+1} & 0 \end{bmatrix} \begin{bmatrix} \psi_{aa,n+2} \\ \psi_{ab,n+1} \\ \psi_{ba,n+1} \\ \psi_{bbn} \end{bmatrix} \quad (5.4)$$

Defining the useful combinations

$$\psi_{0n} = \sqrt{\frac{\alpha_n}{2}}\psi_{aa,n+2} + \sqrt{\frac{\beta_n}{2}}\psi_{bbn} \quad (5.5)$$

$$\psi_{1n} = \sqrt{\frac{\beta_n}{2}}\psi_{aa,n+2} - \sqrt{\frac{\alpha_n}{2}}\psi_{bbn} \quad (5.6)$$

$$\psi_{2n} = \frac{1}{\sqrt{2}}(\psi_{ab,n+1} + \psi_{ba,n+1}) \quad (5.7)$$

$$\psi_{3n} = \frac{1}{\sqrt{2}}(\psi_{ab,n+1} - \psi_{ba,n+1}), \quad (5.8)$$

where we have defined

$$\alpha_n \equiv \frac{2n+2}{2n+3} \quad \beta_n \equiv \frac{2n+4}{2n+3}, \quad (5.9)$$

we obtain the differential equations

$$\dot{\psi}_{0n} = \dot{\psi}_{3n} = 0 \quad (5.10)$$

$$\dot{\psi}_{1n} = g\sqrt{4n+6}\psi_{2n} \quad (5.11)$$

$$\dot{\psi}_{2n} = -g\sqrt{4n+6}\psi_{1n}. \quad (5.12)$$

These equations are solved by

$$\psi_{0n}(t) = \psi_{0n}(0) \quad (5.13)$$

$$\psi_{1n}(t) = \psi_{1n}(0)c_{2n}(t) + \psi_{2n}(0)s_{2n}(t) \quad (5.14)$$

$$\psi_{2n}(t) = \psi_{2n}(0)c_{2n}(t) - \psi_{1n}(0)s_{2n}(t) \quad (5.15)$$

$$\psi_{3n}(t) = \psi_{3n}(0), \quad (5.16)$$

where we have defined

$$c_{2n} \equiv \cos(g\sqrt{4n+6}t) \quad s_{2n} \equiv \sin(g\sqrt{4n+6}t). \tag{5.17}$$

In terms of the original variables, we have

$$\begin{aligned}
\psi_{aa,n+2}(t) &= \frac{1}{2}(\alpha_n + \beta_n c_{2n})\psi_{aa,n+2}(0) + \frac{1}{2}\sqrt{\alpha_n\beta_n}(1-c_{2n})\psi_{bbn}(0) \\
&\quad + \frac{1}{2}\sqrt{\beta_n}s_{2n}(\psi_{ab,n+1}(0) + \psi_{ba,n+1}(0)) \qquad (5.18) \\
\psi_{ab,n+1}(t) &= \frac{1}{2}(c_{2n}+1)\psi_{ab,n+1}(0) + \frac{1}{2}(c_{2n}-1)\psi_{ba,n+1}(0) \\
&\quad - \frac{1}{2}\sqrt{\beta_n}s_{2n}\psi_{aa,n+2}(0) + \frac{1}{2}\sqrt{\alpha_n}s_{2n}\psi_{bbn}(0) \qquad (5.19) \\
\psi_{ba,n+1}(t) &= \frac{1}{2}(c_{2n}-1)\psi_{ab,n+1}(0) + \frac{1}{2}(c_{2n}+1)\psi_{ba,n+1}(0) \\
&\quad - \frac{1}{2}\sqrt{\beta_n}s_{2n}\psi_{aa,n+2}(0) + \frac{1}{2}\sqrt{\alpha_n}s_{2n}\psi_{bbn}(0) \qquad (5.20) \\
\psi_{bbn}(t) &= \frac{1}{2}\sqrt{\alpha_n\beta_n}(1-c_{2n})\psi_{aa,n+2}(0) + \frac{1}{2}(\beta_n + \alpha_n c_{2n})\psi_{bbn}(0) \\
&\quad - \frac{1}{2}\sqrt{\alpha_n}s_{2n}(\psi_{ab,n+1}(0) + \psi_{ba,n+1}(0)). \qquad (5.21)
\end{aligned}$$

This result is identitcal to Eq. (3.11) of Ref. [33] if we correct for notational differences and set $\psi_{aa,n+2}(0) = \psi_{ba,n+1}(0) = 0$ (which corresponds to having the second atom arrive in the upper state). Note that the one instance of $C_{ab,n+1}$ in Eq. (3.11) of Ref. [33] is a typing error, and needs to be replaced with $C_{ba,n+1}$.

5.2 Two-atom Events

A two-atom event consists of two atoms entering the microamser cavity such that the second atom arrives before the first atom has left. Here we will assume that both atoms arrive in the upper maser level and with the same velocity—interacting with the cavity for the same time $t_{\rm int}$. When the first atom arrives at the cavity we have

$$\begin{aligned}
\psi_{bbn}(0) &= \psi_n(0) \qquad (5.22) \\
\psi_{aa,n+2}(0) &= \psi_{ab,n+1}(0) = \psi_{ba,n+1}(0) = 0, \qquad (5.23)
\end{aligned}$$

where $|\psi_{\rm f}(0)\rangle = \sum_n \psi_n(0)|n\rangle$ is the initial state of the field. The first atom interacts with the field for a time s before the second atom arrives. This is described by the solution to the Jaynes-Cummings Model where only the first atom and the field interact. This gives

$$\begin{aligned}
\psi_{ab,n+1}(s) &= s_{1n}\psi_n(0) && (5.24)\\
\psi_{bbn}(s) &= c_{1n}\psi_n(0) && (5.25)\\
\psi_{aa,n+2}(s) &= \psi_{ba,n+1}(s) = 0, && (5.26)
\end{aligned}$$

where

$$\begin{aligned}
c_{1n} &\equiv \cos\left(\frac{1}{2}\omega_n s\right) && (5.27)\\
s_{1n} &\equiv \sin\left(\frac{1}{2}\omega_n s\right). && (5.28)
\end{aligned}$$

The second atom then arrives and both atoms interact with the field for a time $t_{\rm int} - s$ before the first atom leaves. This is described by the results from the previous section giving

$$\begin{aligned}
\psi_{aa,n+2}(t_{\rm int}) &= \frac{1}{2}[\sqrt{\alpha_n\beta_n}(1-c_{2n})c_{1n} + \sqrt{\beta_n}s_{2n}s_{1n}]\psi_n(0) && (5.29)\\
\psi_{ab,n+1}(t_{\rm int}) &= \frac{1}{2}[(c_{2n}+1)s_{1n} + \sqrt{\alpha_n}s_{2n}c_{1n}]\psi_n(0) && (5.30)\\
\psi_{ba,n+1}(t_{\rm int}) &= \frac{1}{2}[(c_{2n}-1)s_{1n} + \sqrt{\alpha_n}s_{2n}c_{1n}]\psi_n(0) && (5.31)\\
\psi_{bbn}(t_{\rm int}) &= \frac{1}{2}[(\beta_n + \alpha_n c_{2n})c_{1n} - \sqrt{\alpha_n}s_{2n}s_{1n}]\psi_n(0), && (5.32)
\end{aligned}$$

where c_{2n} and s_{2n} are evaluated at $t = t_{\rm int} - s$. The first atom then leaves the cavity while the second atom continues to interact with the field for a time s. This is described by the solution to the Jaynes-Cummings Model where only the second atom and the field interact. This gives

$$\begin{aligned}
\psi_{aa,n+2}(t_{\rm int}+s) &= \frac{1}{2}\{c_{1n+1}[\sqrt{\alpha_n\beta_n}(1-c_{2n})c_{1n} + \sqrt{\beta_n}s_{2n}s_{1n}]\\
&\quad + s_{1n+1}[(c_{2n}+1)s_{1n} + \sqrt{\alpha_n}s_{2n}c_{1n}]\}\psi_n(0) && (5.33)\\
\psi_{ab,n+1}(t_{\rm int}+s) &= \frac{1}{2}\{-s_{1n+1}[\sqrt{\alpha_n\beta_n}(1-c_{2n})c_{1n} + \sqrt{\beta_n}s_{2n}s_{1n}]
\end{aligned}$$

$$+c_{1n+1}[(c_{2n}+1)s_{1n}+\sqrt{\alpha_n}s_{2n}c_{1n}]\}\psi_n(0) \quad (5.34)$$

$$\psi_{ba,n+1}(t_{\rm int}+s) = \frac{1}{2}\{[\beta_n-1+(1+\alpha_n)c_{2n}]s_{1n}c_{1n} + \sqrt{\alpha_n}s_{2n}(c_{1n}^2-s_{1n}^2)\}\psi_n(0) \quad (5.35)$$

$$\psi_{bbn}(t_{\rm int}+s) = \frac{1}{2}\{(1-c_{2n})s_{1n}^2 - 2\sqrt{\alpha_n}s_{2n}s_{1n}c_{1n} + (\beta_n+\alpha_n c_{2n})c_{1n}^2\}\psi_n(0). \quad (5.36)$$

The second atom then leaves marking the end of the two-atom event. Note that the coefficients $\psi_{aa,n+2}$ and $\psi_{ab,n+1}$ have factors of c_{1n+1} and s_{1n+1}. This is because there is an extra photon in the cavity due to the first atom being in the lower state upon leaving the cavity.

Using this result to form the matrix elements of a density operator for the combined atom-atom-field system, we obtain the two-atom event operator $\mathcal{U}_2$ defined by

$$\rho(t_{\rm int}+s) = (1+\mathcal{U}_2(t_{\rm int},s))(\rho_{\rm f}(0)\otimes|bb\rangle\langle bb|). \quad (5.37)$$

It has the matrix elements

$$\langle aa,n+2|\mathcal{U}_2\rho|aa,n+2\rangle = \mathcal{U}_{2_n}^{(+1,+1)}\langle bbn|\rho|bbn\rangle \quad (5.38)$$

$$\langle ab,n+1|\mathcal{U}_2\rho|ab,n+1\rangle = \mathcal{U}_{2_n}^{(+1,0)}\langle bbn|\rho|bbn\rangle \quad (5.39)$$

$$\langle ba,n+1|\mathcal{U}_2\rho|ba,n+1\rangle = \mathcal{U}_{2_n}^{(0,+1)}\langle bbn|\rho|bbn\rangle \quad (5.40)$$

$$\langle bbn|\mathcal{U}_2\rho|bbn\rangle = -(\mathcal{U}_{2_n}^{(+1,+1)}+\mathcal{U}_{2_n}^{(+1,0)} + \mathcal{U}_{2_n}^{(0,+1)})\langle bbn|\rho|bbn\rangle, \quad (5.41)$$

where the coefficients

$$\mathcal{U}_{2_n}^{(+1,+1)}(t_{\rm int},s) = \frac{1}{4}\{c_{1n+1}[\sqrt{\alpha_n\beta_n}(1-c_{2n})c_{1n}+\sqrt{\beta_n}s_{2n}s_{1n}] + s_{1n+1}[(1+c_{2n})s_{1n}+\sqrt{\alpha_n}s_{2n}c_{1n}]\}^2 \quad (5.42)$$

$$\mathcal{U}_{2_n}^{(+1,0)}(t_{\rm int},s) = \frac{1}{4}\{-s_{1n+1}[\sqrt{\alpha_n\beta_n}(1-c_{2n})c_{1n}+\sqrt{\beta_n}s_{2n}s_{1n}] + c_{1n+1}[(1+c_{2n})s_{1n}+\sqrt{\alpha_n}s_{2n}c_{1n}]\}^2 \quad (5.43)$$

$$\mathcal{U}_{2_n}^{(0,+1)}(t_{\rm int},s) = \frac{1}{4}\{[\beta_n-1+(1+\alpha_n)c_{2n}]s_{1n}c_{1n} + \sqrt{\alpha_n}s_{2n}(c_{1n}^2-s_{1n}^2)\}^2 \quad (5.44)$$

give the probabilities of $|bbn\rangle \to |aa, n+2\rangle$, $|bbn\rangle \to |ab, n+1\rangle$, and $|bbn\rangle \to |ba, n+1\rangle$ transitions. Here the superscripts indicates the emission of the first atom $(+1, 0)$, the second atom $(0, +1)$, or both atoms $(+1, +1)$, and the gain of the excitation level of the field.

5.3 The Micromaser Field Dynamics Including Two-atom Events

When an atom arrives at the micromaser cavity, we wish to determine the probability that the atom belongs to a one-atom event and the probability that the atom is the first atom of a two-atom event. Given that an atom has arrived while the cavity was empty, the probability that the atom will leave before the next atom arrives is

$$\int_{t_{\rm int}}^{\infty} ds\, \rho_s(s) = e^{-rt_{\rm int}}, \tag{5.45}$$

where we have used the Poissonian distribution (4.4). The probability that the second atom arrives before the first atom has left, such that there is an overlapping time for which both atoms are interacting with the field, is given by

$$\int_{0}^{t_{\rm int}} ds\, \rho_s(s) = 1 - e^{-rt_{\rm int}}. \tag{5.46}$$

Putting these together, we determine that the probability that the atom is the first atom of an n-atom event is

$$P_n = e^{-rt_{\rm int}}(1 - e^{-rt_{\rm int}})^{n-1}. \tag{5.47}$$

They are normalized as

$$\sum_{n=1}^{\infty} P_n = 1. \tag{5.48}$$

Here we are only interested in one-atom and two-atom events, so we will use the modified probabilities

$$\tilde{P}_1 \equiv \frac{P_1}{P_1 + P_2} \quad \tilde{P}_2 \equiv \frac{P_2}{P_1 + P_2}. \tag{5.49}$$

In order to determine the dynamics of the micromaser field including the effect of two-atom events, we must also average over the spacing between the two atoms participating in two-atom events. Given that a two-atom event has occurred, the spacing s between the two atoms is given by the probability density

$$w(s) = \frac{re^{-rs}}{1 - e^{-rt_{\rm int}}}, \quad 0 < s < t_{\rm int}. \tag{5.50}$$

Putting everything together, we obtain the evolution operator for the micromaser field including the effect of two-atom events

$$\mathcal{X} = \mathcal{L}_{\rm f} + r(\tilde{P}_1 \mathcal{U}_{1\rm f} + \tilde{P}_2 \mathcal{U}_{2\rm f}), \tag{5.51}$$

where we have introduced the reduced two-atom event operator averaged over the spacing between the two atoms, defined by

$$\mathcal{U}_{2\rm f}\rho = \int_0^{t_{\rm int}} ds\, w(s) {\rm tr}_{{\rm at}_1,{\rm at}_2}\{\mathcal{U}_2(t_{\rm int}, s)(\rho \otimes |bb\rangle\langle bb|)\}. \tag{5.52}$$

The matrix exlements of $\mathcal{X}$ are now given by

$$\begin{aligned}
\langle n|\mathcal{X}\rho|n\rangle &= r\tilde{P}_2 \tilde{\mathcal{U}_2}_{n-2}^{(+2)} \langle n-2|\rho|n-2\rangle \\
&\quad + \left(\mathcal{L}_{{\rm f}n-1}^{(+1)} + r\tilde{P}_1 {\mathcal{U}_1}_{n-1}^{(+1)} + r\tilde{P}_2 \tilde{\mathcal{U}_2}_{n-1}^{(+1)}\right) \langle n-1|\rho|n-1\rangle \\
&\quad - \Big(r\tilde{P}_2 \tilde{\mathcal{U}_2}_{n}^{(+2)} + \mathcal{L}_{{\rm f}n}^{(+1)} + r\tilde{P}_1 {\mathcal{U}_1}_{n}^{(+1)} \\
&\quad + r\tilde{P}_2 \tilde{\mathcal{U}_2}_{n}^{(+1)} + \mathcal{L}_{{\rm f}n-1}^{(-1)}\Big) \langle n|\rho|n\rangle \\
&\quad + \mathcal{L}_{{\rm f}n}^{(-1)} \langle n+1|\rho|n+1\rangle,
\end{aligned} \tag{5.53}$$

where

$$\begin{aligned}
\tilde{\mathcal{U}_2}_{n}^{(+2)} &\equiv \int_0^{t_{\rm int}} ds\, w(s) {\mathcal{U}_2}_{n}^{(+1,+1)}(t_{\rm int}, s) \\
\tilde{\mathcal{U}_2}_{n}^{(+1)} &\equiv \int_0^{t_{\rm int}} ds\, w(s) [{\mathcal{U}_2}_{n}^{(+1,0)}(t_{\rm int}, s) + {\mathcal{U}_2}_{n}^{(0,+1)}(t_{\rm int}, s)].
\end{aligned} \tag{5.54}$$

The steady state of the micromaser field $\rho_{\rm f}^{\rm ss}$ is given by $\mathcal{X}\rho_{\rm f}^{\rm ss} = 0$. This equation can be solved using the method in Ref. [33]. First we solve Eq. (5.53)

recursively starting with $n = 0$ to establish the third-order recurrence relation

$$\begin{aligned}\mathcal{L}_{\mathrm{f}_n}^{(-1)}\langle n+1|\rho_{\mathrm{f}}^{\mathrm{ss}}|n+1\rangle &= \Big(r\tilde{P}_2\tilde{\mathcal{U}_2}_n^{(+2)} + \mathcal{L}_{\mathrm{f}_n}^{(+1)} \\ &\quad + r\tilde{P}_1{\mathcal{U}_1}_n^{(+1)} + r\tilde{P}_2\tilde{\mathcal{U}_2}_n^{(+1)}\Big)\langle n|\rho_{\mathrm{f}}^{\mathrm{ss}}|n\rangle \\ &\quad + r\tilde{P}_2\tilde{\mathcal{U}_2}_{n-1}^{(+2)}\langle n-1|\rho_{\mathrm{f}}^{\mathrm{ss}}|n-1\rangle. \end{aligned} \tag{5.55}$$

We then simplify this to a second-order recurrence relation by dividing by $\langle n|\rho_{\mathrm{f}}^{\mathrm{ss}}|n\rangle$ and introducing the ration

$$S_n \equiv \frac{\langle n+1|\rho_{\mathrm{f}}^{\mathrm{ss}}|n+1\rangle}{\langle n|\rho_{\mathrm{f}}^{\mathrm{ss}}|n\rangle}. \tag{5.56}$$

This results in the first-order recurrence relation

$$S_n = a_n + \frac{b_n}{S_{n-1}}, \tag{5.57}$$

with the coefficients

$$a_n \equiv \frac{r\tilde{P}_2\tilde{\mathcal{U}_2}_n^{(+2)} + \mathcal{L}_{\mathrm{f}_n}^{(+1)} + r\tilde{P}_1{\mathcal{U}_1}_n^{(+1)} + r\tilde{P}_2\tilde{\mathcal{U}_2}_n^{(+1)}}{\mathcal{L}_{\mathrm{f}_n}^{(-1)}} \tag{5.58}$$

$$b_n \equiv \frac{r\tilde{P}_2\tilde{\mathcal{U}_2}_{n-1}^{(+2)}}{\mathcal{L}_{\mathrm{f}_n}^{(-1)}}. \tag{5.59}$$

Starting with $S_0 = a_0$, we obtain S_n as the continued fraction

$$S_n = a_n + \frac{b_n}{a_{n-1}+}\frac{b_{n-1}}{a_{n-2}+}\cdots\frac{b_1}{a_0}, \tag{5.60}$$

and the steady state of the micromaser field is given by the product

$$\langle n|\rho_{\mathrm{f}}^{\mathrm{ss}}|n\rangle = \langle 0|\rho_{\mathrm{f}}^{\mathrm{ss}}|0\rangle \prod_{m=0}^{n-1} S_m, \tag{5.61}$$

where $\langle 0|\rho_{\mathrm{f}}^{\mathrm{ss}}|0\rangle$ is determined by the normalization condition $\mathrm{tr}\{\rho_{\mathrm{f}}^{\mathrm{ss}}\} = 1$.

5.4 The Micromaser Field Statistics Including Two-atom Events

If we ignore the integration and weighting function in Eq. (5.52) and use a fixed value of s, then we have an analytic formula for the photon statistics in steady state for a micromaser in which all two-atom events occur with atoms arriving a time s apart. Other than the exact solution, in which the integration is performed numerically to determine the average effect, we can consider two extreme cases. If there is minimum overlap with $s = t_{\rm int}$, then the two atoms arrive consecutively. Our formula for the two-atom event operator then reduces trivially to two applications of the one-atom event operator and gives results similar to those for the one-atom maser. If there is maximum overlap with $s = 0$, then the two atoms arrive in simultaneous pairs. Our formula for the two-atom event operator then reduces to the result for the atom-pair approximation [66]. This gives us confidence that are formula for the two-atom event operator is correct for intermediate values of s.

In Fig. 5.1, the average photon number $\langle n \rangle$ and the scaled variance $\sigma^2 = (\langle n^2 \rangle - \langle n \rangle^2)/\langle n \rangle$ in steady state are ploted versus the pump parameter $\Theta = \sqrt{N_{\rm ex}} g t_{\rm int}$, for comparison with Fig. 2 of Ref. [9]. The parameters used are $N_{\rm ex} = 25$, $g/\gamma_{\rm f} = 7020$, and $\nu = 0$. The calculations are made near the trapping state at $g t_{\rm int} = \pi/2$. The thick curve is the one-atom maser result in which two-atom events are excluded, which, for these parameters is indistinguishable from the result when including two-atom events with minimum overlap. The thin curve is the result when including two-atom events with maximum overlap—the atoms arriving in pairs. The trapping behavior for this result is suppressed due to the time the two atoms are present in the cavity giving rise to the oscillating factors c_{2n} and s_{2n} (5.17) which do not oscillate at the Rabi frequency. The results for these two extreme cases agree with the results of Ref. [9]. We repeated the calculation for intermediate values of s, and obtained results with intermediate levels of trapping suppression—the suppression increasing from none at $s = t_{\rm int}$ to its maximum amount at $s = 0$. We then obtained the average result by performing the integration in Eq. (5.52) numerically. This result is given as the dotted curve in Fig. 5.1, which necessarily exhibits an intermediate amount of trapping suppression.

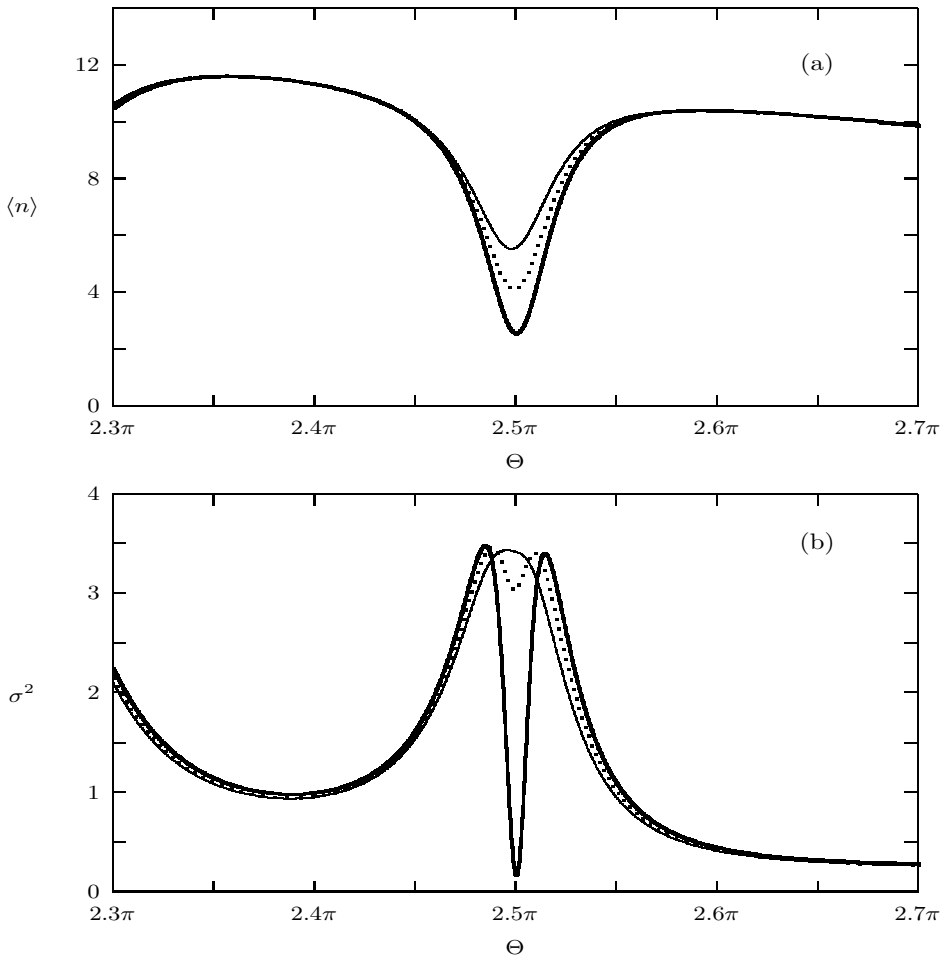

Figure 5.1: Two atom effects. (a) Average photon number $\langle n \rangle$ and (b) scaled variance σ^2 as a function of the pump parameter Θ. The parameters are $N_{\rm ex} = 25$, $g/\gamma_{\rm c} = 7020$, and $\nu = 0$. The thick curve is without two-atom events, the thin curve is with the atom-pair approximation, and the dotted curve is with two-atom events.

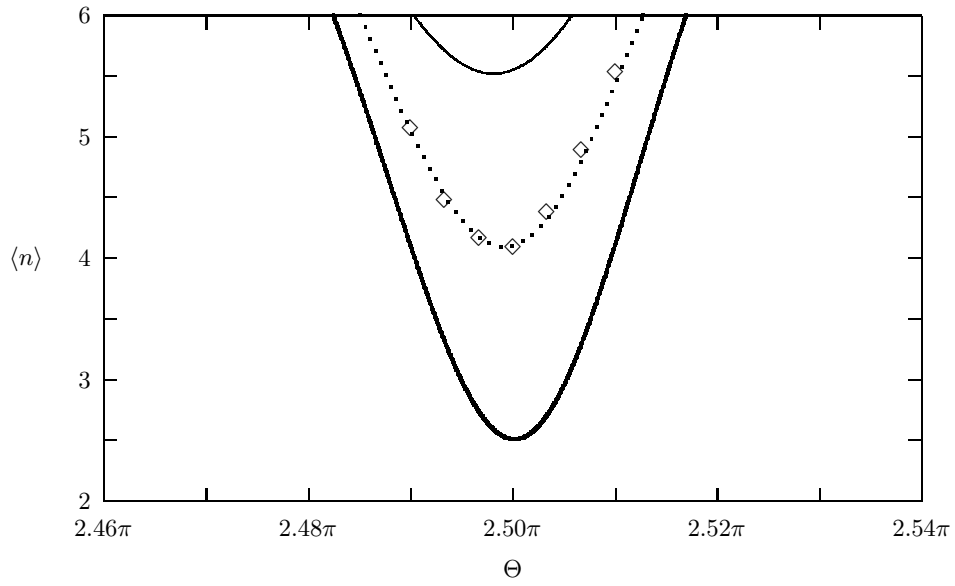

Figure 5.2: Average photon number $\langle n \rangle$ as a function of the pump paremter Θ. The parameters are $N_{\rm ex} = 25$, $g/\gamma_{\rm c} = 7020$, and $\nu = 0$. The thick curve is without two-atom events, the thin curve is with the atom-pair approximation, and the dotted curve is with two-atom events. The diamond points are the result of a Monte Carlo simulation including two-atom events as described in the text.

The corresponding results of Ref. [9], however, fall outside of the two extremes and show almost a complete suppression of the trapping behavior.

As a further test, we performed a Monte Carlo simulation. The results are shown in Fig. 5.2. Here, the curves are as in Fig. 5.1 with the diamond points indicating the results of our simulation. Each simulation started initially with a field in a Fock state $\rho_{\rm f} = |n\rangle\langle n|$, where n was taken randomly from the photon distribution of the one-atom maser in steady state excluding the effect of two-atom events. Three random variables were then used to determine the time until the next event of each type. The three possible types of events were the absorption of a quantum of energy from the reservoir (occurring at the rate $\mathcal{L}_{{\rm f}_n^+}$), the emission of a quantum of energy into the reservoir (occurring at the rate $\mathcal{L}_{{\rm f}_{n-1}^-}$), and the arrival of an atom (occurring

at the rate r). Whichever event occurred first was processed and then the times were recalculated. If the event processed was the arrival of an atom, a random variable was used to determine if the event was a one-atom event (with probability $\tilde{P}_1$) or a two-atom event (with probability $\tilde{P}_2$). If a one-atom event occurred, a random variable was used to determine if the event resulted in the emission of a quantum of energy into the cavity. If a two-atom event occurred, the spacing in arrival times s of the two atoms was determined randomly (with probability density $w(s)$). A random variable was then used to determine whether the event resulted in the emission of zero, one, or two quantum of energy into the cavity. Each simulation span a time of 5000 s to achieve a steady state that includes two-atom events. Each point in Fig. 5.2 is the average of 10000 to 100000 simulations to achieve adequate convergence. The results of the simulation agree with our calculation, and not with the calculation of Ref. [9].

Chapter 6

Detection Statistics

Here we are interested in the statistics of detection events where the detectors do not have 100% efficiency and the evolution of the micromaser field between detection events must include the effect of undetected atoms. The conditioned evolution of the micromaser field between detection events was derived by Briegel *et al.* [6]. They showed that conditioned evolution of the field is described by a nonlinear master equation. However, we will show that the use of a linear master equation and a non-normalized conditioned density operator, as used by Herzog [25], can be used in place of the nonlinear equation and the normalized conditioned density operator.

We will assume that all of the atoms arrive in the upper maser level and the detectors are set up to detect the state of the atoms ($|a\rangle$ and $|b\rangle$) as the atoms leave the micromaser cavity. We will also neglect the effect of two-atom events in our discussion. For a particular detection event of interest, it is convenient to define the operator $\mathcal{X}^+$ corresponding to the occurrence of that detection event, and the operator $\mathcal{X}^- \equiv \mathcal{X} - \mathcal{X}^+$ corresponding to the evolution of the cavity field in the absence of detection events of that type. Here $\mathcal{X}$ is the evolution operator for the micromaser field given by Eq. (4.10). If we are interested in the detection of outgoing atoms in state $|a\rangle$, then we use the operator $\mathcal{X}_a^+$ whose matrix elements are given by the amplitude $\langle a|\rho|a\rangle$ of the combined atom-field density operator ρ after the atom has passed through the cavity:

$$\begin{aligned} \langle n+1|\mathcal{X}_a^+\rho_{\rm f}|n+1\rangle &= \eta_a\langle a|[1+\mathcal{U}_1](\rho_{\rm f}\otimes|b\rangle\langle b|)|a\rangle \\ &= \eta_a\mathcal{U}_1{}_n^{(+1)}\langle n|\rho_{\rm f}|n\rangle. \end{aligned} \tag{6.1}$$

Here η_a is the detector efficiency for detecting atoms in state $|a\rangle$. Similarly, if we are interested in the detection of outgoing atoms in state $|b\rangle$, we use the

operator $\mathcal{X}_b^+$ whose matrix elements are given by

$$\begin{aligned}\langle n|\mathcal{X}_b^+\rho_{\rm f}|n\rangle &= \eta_b\langle b|[1+\mathcal{U}_1](\rho_{\rm f}\otimes|b\rangle\langle b|)|b\rangle \\ &= \eta_b[1-\mathcal{U}_{1_n}^{(+1)}-\mathcal{A}_n^{(+1)}-\mathcal{B}_n^{(0)}]\langle n|\rho_{\rm f}|n\rangle, \end{aligned} \tag{6.2}$$

where η_b is the detector efficiency for detecting atoms in state $|b\rangle$. If we are interested in detection events of either type, then we use the operator $\mathcal{X}_{ab}^+ = \mathcal{X}_a^+ + \mathcal{X}_b^+$.

A detection event at time t leads to the nonlocal state reduction

$$\rho_{\rm f}(t) \to \frac{\mathcal{X}^+\rho_{\rm f}(t)}{{\rm tr}\{\mathcal{X}^+\rho_{\rm f}(t)\}}, \tag{6.3}$$

and occurs with a probability density

$$r\,{\rm tr}\{\mathcal{X}^+\rho_{\rm f}(t)\}. \tag{6.4}$$

For times between detections, the passing of an atom at time t, undetected due to detector inefficiency, leads to the nonlocal state reduction

$$\rho_{\rm f}(t) \to \frac{[r(1+\mathcal{U}_{1{\rm f}})-\mathcal{X}^+]\rho_{\rm f}(t)}{{\rm tr}\{[r(1+\mathcal{U}_{1{\rm f}})-\mathcal{X}^+]\rho_{\rm f}(t)\}}, \tag{6.5}$$

and occurs with a probability density

$$r\,{\rm tr}\{[r(1+\mathcal{U}_{1{\rm f}})-\mathcal{X}^+]\,\rho_{\rm f}(t)\}\ . \tag{6.6}$$

This, along with the continuous effect of thermal damping, leads to the master equation for the evolution of the density operator between detections conditioned by the absence of detections

$$\begin{aligned}\dot{\rho}_{\rm f}^{\rm c} &= \mathcal{L}_{\rm f}\rho_{\rm f}^{\rm c} + {\rm tr}\{[r(1+\mathcal{U}_{1{\rm f}})-\mathcal{X}^+]\rho_{\rm f}^{\rm c}\}\left(\frac{[r(1+\mathcal{U}_{1{\rm f}})-\mathcal{X}^+]\rho_{\rm f}^{\rm c}}{{\rm tr}\{[r(1+\mathcal{U}_{1{\rm f}})-\mathcal{X}^+]\rho_{\rm f}^{\rm c}\}}-\rho_{\rm f}^{\rm c}\right) \\ &= \mathcal{X}^-\rho_{\rm f}^{\rm c} - {\rm tr}\{\mathcal{X}^-\rho_{\rm f}^{\rm c}\}\rho_{\rm f}^{\rm c}, \end{aligned} \tag{6.7}$$

where we have used the identities $\mathcal{X}^+ = \mathcal{X} - \mathcal{X}^-$, and, for any ρ, ${\rm tr}\{\mathcal{U}_{1{\rm f}}\rho\} = {\rm tr}\{\mathcal{X}\rho\} = 0$. This agrees with Eq. (2.25) of Ref. [6]. This equation is nonlinear, and has the formal solution given by Eq. (2.26) of Ref. [6]

$$\rho_{\rm f}^{\rm c}(t) = \frac{e^{\mathcal{X}^- rt}\rho_{\rm f}(0)}{{\rm tr}\{e^{\mathcal{X}^- rt}\rho_{\rm f}(0)\}}. \tag{6.8}$$

The nonlinearity in Eq. (6.7) is what leads to the normalization of the conditioned density operator (6.8). The conditional probability density for a detection event occurring at time t given that no detections events have occurred between times 0 and t is given by

$$r\,\mathrm{tr}\{\mathcal{X}^+\rho_{\mathrm{f}}^{\mathrm{c}}(t)\}. \tag{6.9}$$

The *exclusion probability*, or the probability that a detection does not occur between times 0 and t is

$$\exp\left(-r\int_0^t dt\,\mathrm{tr}\{\mathcal{X}^+\rho_{\mathrm{f}}^{\mathrm{c}}(t)\}\right) = \exp\left(-r\int_0^t dt\,\frac{\mathrm{tr}\{\mathcal{X}^+e^{\mathcal{X}^-rt}\rho_{\mathrm{f}}(0)\}}{\mathrm{tr}\{e^{\mathcal{X}^-rt}\rho_{\mathrm{f}}(0)\}}\right). \tag{6.10}$$

If we define

$$u(t) \equiv \mathrm{tr}\{e^{\mathcal{X}^-rt}\rho_{\mathrm{f}}(0)\}, \tag{6.11}$$

We find that

$$\begin{aligned}\dot{u}(t) &= r\,\mathrm{tr}\{\mathcal{X}^-e^{\mathcal{X}^-rt}\rho_{\mathrm{f}}(0)\} \\ &= -r\,\mathrm{tr}\{\mathcal{X}^+e^{\mathcal{X}^-rt}\rho_{\mathrm{f}}(0)\},\end{aligned} \tag{6.12}$$

where we have used the identities $\mathcal{X}^- = \mathcal{X} - \mathcal{X}^+$ and, for any ρ, $\mathrm{tr}\{\mathcal{X}\rho\} = 0$. So the expression (6.10) becomes

$$\exp\left(\int_0^t dt\,\frac{\dot{u}(t)}{u(t)}\right) = u(t). \tag{6.13}$$

Thus the exclusion probability is $u(t)$ given by Eq. (6.11) and is equivalent to the denominator of Eq. (6.8).

The probability density for the next detection occurring at time t is the conditional probability density (6.9) for a detection occurring at time t multiplied by the probability $u(t)$ that the condition is satisfied, or

$$r\,u(t)\mathrm{tr}\{\mathcal{X}^+\rho_{\mathrm{f}}^{\mathrm{c}}(t)\} = r\,\mathrm{tr}\{\mathcal{X}^+\tilde{\rho}_{\mathrm{f}}^{\mathrm{c}}(t)\}. \tag{6.14}$$

Here we have defined the non-normalized conditioned density operator

$$\tilde{\rho}_{\mathrm{f}}^{\mathrm{c}}(t) \equiv u(t)\rho_{\mathrm{f}}^{\mathrm{c}}(t) = e^{\mathcal{X}^-rt}\rho_{\mathrm{f}}(0), \tag{6.15}$$

where the decay in the norm of the operator is due solely to the exclusion of detections between times 0 and t. This is the solution to the linear master equation

$$\dot{\tilde{\rho}}_{\rm f}^{\rm c} = \mathcal{X}^{-}\tilde{\rho}_{\rm f}^{\rm c}. \tag{6.16}$$

This has been used by Herzog [25]. The two approaches to Eq. (6.14) are identical, but the linear equation (6.16), as opposed to the nonlinear equation (6.7), is simpler to numerically integrate.

Ignoring prior observations, detections of atoms in state $|\mathrm{a}\rangle$ and $|\mathrm{b}\rangle$ will occur at the uncorrelated rates

$$r_a = r\,\mathrm{tr}\{\mathcal{X}_a^{+}\rho_{\rm f}^{\rm ss}\}, \quad r_b = r\,\mathrm{tr}\{\mathcal{X}_b^{+}\rho_{\rm f}^{\rm ss}\}. \tag{6.17}$$

For any statistical variable x, it is interesting to calculate the average normalized to the uncorrelated value

$$\langle x\rangle_{\rm norm} \equiv \frac{\langle x\rangle}{\langle x\rangle_{\rm uncor}}, \tag{6.18}$$

where $\langle x\rangle$ is the average of x, and $\langle x\rangle_{\rm uncor}$ is the average performed in the absence of correlations with the detection rates (6.17). This ratio is equal to unity for Poissonian statistics, and otherwise tells us whether the correlations are positive or negative, and, for the case of successive detections, whether the detection events are bunched or anti-bunched. As the detectors become less efficient, the times between detections grow larger (with an increasing number of atoms passing undetected between detections). The detected atoms thus become less correlated and we have the general result

$$\text{for any } x, \quad \langle x\rangle_{\rm norm} \to 1, \quad \text{as } \eta_a, \eta_b \to 0. \tag{6.19}$$

6.1 Counting statistics

The counting statistics and the Fano-Mandel function were treated rather nicely by Briegel *et al.* [6] and will be discussed here only briefly. By counting statistics, we mean the statical properties of the detection events

counted for a certain observation period. They are fundamentally characterized by the joint probabilities for detecting n atoms in state $|a\rangle$ and m atoms in state $|b\rangle$ in an observation time $t_{\rm obs}$. Of particular interest is the Fano-Mandel function Q which measures the deviation of the variance of the counts from that for Poissonian statistics [19, 38]. It is defined by convention as

$$\begin{aligned} Q(t_{\rm obs}) &\equiv \left\langle (N(t_{\rm obs}) - \langle N(t_{\rm obs})\rangle)^2 \right\rangle_{\rm norm} - 1, \\ &= \frac{\langle N(t_{\rm obs})^2\rangle}{\langle N(t_{\rm obs})\rangle} - \langle N(t_{\rm obs})\rangle - 1, \end{aligned} \tag{6.20}$$

where $N(t_{\rm obs})$ is the number of counts observed. The Fano-Mandel function is of interest since for a micromaser in which all of the atoms arrive in the upper state, the counting statistics of the atoms observed to be in the lower state should be closely related to the photon number statistics of the micromaser field (since every atom observed to be in the lower state corresponds to the photon number of the field increasing by one). It was therefore hoped that the sub-Poissonian variance of the micromaser photon statistics would give rise to a sub-Poissonian variance of the counting statistics of atoms observed in the lower state. Measurements of the Fano-Mandel function have indeed shown the pressence of sub-Poissonian variance in the counting statistics [52], which can be viewed as an indirect observation of the pressence of sub-Poissonian variance in the photon statistics of the micromaser field.

An approximate expression for calculating the Fano-Mandel function was developed by Rempe and Walther [53], who achieved results that agreed well with a simulation, and later with experimental results [52]. An exact expression was derived by Briegel [6], and was shown to agree well with the previous approximation in the regime for which it is valid. For counting atoms in the lower state $|a\rangle$, the Fano-Mandel function can be expressed as [6]

$$Q_a(t_{\rm obs}) = \quad 2r\int_0^{t_{\rm obs}} dt' \left(1 - \frac{t'}{t_{\rm obs}}\right) {\rm tr}\left\{\mathcal{X}_a^+ e^{\mathcal{X}rt'} \mathcal{M}_a \rho_{\rm f}^{\rm ss}\right\}, \tag{6.21}$$

where

$$\mathcal{M}_a\rho \equiv \frac{\mathcal{X}_a^+\rho}{{\rm tr}\{\mathcal{X}_a^+\rho\}} - \rho. \tag{6.22}$$

Q_a is related to the two-time correlation function for the detection of atoms in state $|a\rangle$ [6]. The normalized standard deviation of the field σ can be related to the short-time limit of the same atomic correlation function [18], providing the connection between Q_a and σ.

6.2 Sequence statistics

Here we ask a different question: "given n successive detections, what is the probability that the detections are of atoms in a particular sequence of the states $|a\rangle$ and $|b\rangle$?" We use the notation $P[abba\ldots(n \text{ terms})]$ to denote the probability of n-detection events being comprised of atoms detected in the sequence of states "$abba\ldots$." They are normalized such that, for each n, the sum of all $P[x]$, where x is a sequence of "a" and "b" of length n, is unity. The simplest of these probabilities are the probabilities that a single atom is detected in state $|a\rangle$ or $|b\rangle$, given by

$$P[a] = \frac{\mathrm{tr}\{\mathcal{X}_a^+ \rho_{\mathrm{f}}^{\mathrm{ss}}\}}{\mathrm{tr}\{\mathcal{X}_{ab}^+ \rho_{\mathrm{f}}^{\mathrm{ss}}\}}, \quad P[b] = \frac{\mathrm{tr}\{\mathcal{X}_b^+ \rho_{\mathrm{f}}^{\mathrm{ss}}\}}{\mathrm{tr}\{\mathcal{X}_{ab}^+ \rho_{\mathrm{f}}^{\mathrm{ss}}\}}. \tag{6.23}$$

At the next level of complexity are the probabilities $P[aa]$, $P[ab]$, $P[ba]$, and $P[bb]$ for $n = 2$. Rather than calculate them directly, it is convenient to first consider the conditional probabilities $P[\underline{a}a]$, $P[\underline{a}b]$, $P[\underline{b}a]$, and $P[\underline{b}b]$, where the underline indicates the given condition. For example, $P[\underline{a}b]$ denotes the probability that the second detection of a two-detection event is of an atom in state $|b\rangle$, given that the first detection is of an atom in state $|a\rangle$. The joint probability $P[ab]$ is then given by the conditional probability $P[\underline{a}b]$ multiplied by the probability $P[a]$ that the condition is true:

$$P[ab] = P[a]\, P[\underline{a}b]\ . \tag{6.24}$$

We will now derive an expression for $P[\underline{a}a]$. Expressions for the other conditional probabilities can be generated in an analogous manner. Given that an atom in state $|a\rangle$ was detected at time 0 we have $\rho_{\mathrm{f}}(0) = \mathcal{X}_a^+ \rho_{\mathrm{f}}^{\mathrm{ss}} / \mathrm{tr}\{\mathcal{X}_a^+ \rho_{\mathrm{f}}^{\mathrm{ss}}\}$. Until a later time t, when a second atom in state $|a\rangle$ is detected, we wish to exclude detections of atoms in either state, so we use the non-normalized

conditioned density operator $\tilde{\rho}_{\rm f}^{\rm c}(t) = e^{\mathcal{X}_{ab}^{-}rt}\rho_{\rm f}(0)$. Then the probability density for the time t when the second atom is detected is $r\,{\rm tr}\{\mathcal{X}_a^+\tilde{\rho}_{\rm f}^{\rm c}(t)\}$, so that

$$\begin{aligned} P[\underline{a}a] &= r\int_0^\infty dt\,{\rm tr}\{\mathcal{X}_a^+\tilde{\rho}_{\rm f}^{\rm c}(t)\} \\ &= \frac{1}{{\rm tr}\{\mathcal{X}_a^+\rho_{\rm f}^{\rm ss}\}}{\rm tr}\left\{\mathcal{X}_a^+\frac{-1}{\mathcal{X}_{ab}^-}\mathcal{X}_a^+\rho_{\rm f}^{\rm ss}\right\}. \end{aligned} \tag{6.25}$$

The identities

$$\begin{aligned} \mathcal{X}\rho_{\rm f}^{\rm ss} &= 0 \\ {\rm tr}\{\mathcal{X}\rho\} &= 0, \quad \text{for any } \rho \end{aligned} \tag{6.26}$$

are especially useful. Using $\mathcal{X}_a^+ = \mathcal{X} - \mathcal{X}_{ab}^- - \mathcal{X}_b^+$ and the identities (6.26), we have

$${\rm tr}\left\{\mathcal{X}_a^+\frac{-1}{\mathcal{X}_{ab}^-}\mathcal{X}_a^+\rho_{\rm f}^{\rm ss}\right\} = {\rm tr}\{\mathcal{X}_a^+\} - \Gamma \tag{6.27}$$

and

$$P[\underline{a}a] = 1 - \frac{\Gamma}{{\rm tr}\{\mathcal{X}_a^+\rho_{\rm f}^{\rm ss}\}}, \tag{6.28}$$

where we have defined

$$\Gamma \equiv {\rm tr}\left\{\mathcal{X}_a^+\frac{-1}{\mathcal{X}_{ab}^-}\mathcal{X}_b^+\rho_{\rm f}^{\rm ss}\right\} = {\rm tr}\left\{\mathcal{X}_b^+\frac{-1}{\mathcal{X}_{ab}^-}\mathcal{X}_a^+\rho_{\rm f}^{\rm ss}\right\}. \tag{6.29}$$

The sequence probability P[aa] and the other sequence probabilities for $n = 2$ are given by

$$P[aa] = P[a] - \frac{\Gamma}{{\rm tr}\{\mathcal{X}_{ab}^+\rho_{\rm f}^{\rm ss}\}} \tag{6.30}$$

$$P[bb] = P[b] - \frac{\Gamma}{{\rm tr}\{\mathcal{X}_{ab}^+\rho_{\rm f}^{\rm ss}\}} \tag{6.31}$$

$$P[ab] = P[ba] = \frac{\Gamma}{{\rm tr}\{\mathcal{X}_{ab}^+\rho_{\rm f}^{\rm ss}\}}. \tag{6.32}$$

Eq. (6.32) provides us with an interpretation of Γ as relating to the probability that a switch occurs in the type of detection event, given by

$$P[ab] + P[ba] = \frac{2\Gamma}{\mathrm{tr}\{\mathcal{X}^{+}_{ab}\rho^{\mathrm{ss}}_{\mathrm{f}}\}}. \tag{6.33}$$

Note also that these probabilities obey a useful "distributive property". For example,

$$P[aa] + P[ab] = P[a(a+b)] = P[a], \tag{6.34}$$

which is a way of stating that the detection of an atom in state $|a\rangle$ will necessarily be followed by the detection of an atom in either state $|a\rangle$ or $|b\rangle$ with unit probability. This distributive property holds for all sequence probabilities.

Expressions for sequence probabilities for $n = 3$ and greater can be formed by a sequence of the operators $\mathcal{X}^{+}_{a}$ and $\mathcal{X}^{+}_{b}$ in right to left order, separated by the operator $-1/\mathcal{X}^{-}_{ab}$. For example,

$$P[abb] \;=\; \frac{1}{\mathrm{tr}\{\mathcal{X}^{+}_{ab}\rho^{\mathrm{ss}}_{\mathrm{f}}\}}\mathrm{tr}\left\{\mathcal{X}^{+}_{b}\frac{-1}{\mathcal{X}^{-}_{ab}}\mathcal{X}^{+}_{b}\frac{-1}{\mathcal{X}^{-}_{ab}}\mathcal{X}^{+}_{a}\rho^{\mathrm{ss}}_{\mathrm{f}}\right\}, \tag{6.35}$$

stated without proof.

6.2.1 Successive detections

The mean number of successive detections of atoms in the same state, $\langle n\rangle$, was first calculated by Wagner *et al.* [63–65] using Monte Carlo techniques for the phase-sensitive micromaser experiment described in those papers. They had surmised that this mean number would contain information about the phase dynamics of the micromaser field. Later, Englert *et al.* [17] derived an expression for $\langle n\rangle$ and $\langle n\rangle_{\mathrm{norm}}$. Using an eigenvalue method, they reproduced the results of Wagner *et al.* with good agreement and calculated $\langle n\rangle_{\mathrm{norm}}$ for the standard micromaser experiment. Though this was a good test of micromaser theory, it was shown that the mean number of successive detections of atoms in the same state did not contain the sought information about the phase dynamics. Here we will derive the mean number $\langle n_a\rangle$ of successive detections of atoms in state $|a\rangle$ and the mean number $\langle n_b\rangle$ of successive detections of

atoms in state $|b\rangle$. The derivation of $\langle n\rangle = \frac{1}{2}(\langle n_a\rangle + \langle n_b\rangle)$ in Ref. [17] needs to be modified only slightly in order to obtain $\langle n_a\rangle$ and $\langle n_b\rangle$. We will later show that these quantities are greatly influenced by the trapping states, providing a means of observing trapping states in measurements of the mean number of successive detections.

Given that the detection of an atom in state $|b\rangle$ has occurred, we denote the probability of detecting n atoms in state $|a\rangle$ prior to the next detection of an atom in state $|b\rangle$ by $p_n^a = P[\underline{b}a^n b]$, where "$a^n$" is short for n terms of "a" in the sequence. (similarly for p_n^b). They obey the normalization

$$\sum_{n=0}^{\infty} p_n^a = \sum_{n=0}^{\infty} p_n^b = 1. \tag{6.36}$$

Note that the probability of having n detections of atoms in one state between two detections of atoms in the other state, p_n, used in the derivation of $\langle n\rangle$ in Ref. [17] is related to p_n^a and p_n^b by

$$\begin{aligned} p_n &= P[b]p_n^a + P[a]p_n^b \\ &= P[ba^n b] + P[ab^n a]. \end{aligned} \tag{6.37}$$

We then consider the probability $p_0^a = P[\underline{b}b]$ of detecting an atom in state $|b\rangle$ after a previous atom detected in state $|b\rangle$, and the possible ways in which the two events can occur between the detection of two atoms in state $|a\rangle$:

$$\begin{aligned} p_0^a &= P[\underline{b}b] \\ &= P[a\underline{b}ba] + (P[a\underline{b}bba] + P[ab\underline{b}ba]) + \cdots. \end{aligned} \tag{6.38}$$

Noting that, for example,

$$P[abba] = P[a]P[\underline{a}bba] = P[b]P[a\underline{b}ba], \tag{6.39}$$

Eq. (6.38) becomes

$$\begin{aligned} p_0^a &= \frac{P[a]}{P[b]}(P[\underline{a}bba] + 2P[\underline{a}bbba] + \cdots) \\ &= \frac{P[a]}{P[b]}\sum_{n=2}^{\infty}(n-1)p_n^b. \end{aligned} \tag{6.40}$$

A similar expression is obtained for p_0^b. Using this expression with Eqs. (6.36), we can establish

$$\sum_{n=1}^{\infty} n p_n^a = \frac{P[a]}{P[b]}, \tag{6.41}$$

and a similar expression for p_n^b.

We now consider the probability P_n^a of detecting n atoms in state $|a\rangle$ in succession (similarly for P_n^b). They are normalized as

$$\sum_{n=1}^{\infty} P_n^a = \sum_{n=1}^{\infty} P_n^b = 1 \ . \tag{6.42}$$

P_n^a differs from p_n^a only by the exclusion of $n = 0$, so that

$$P_n^a = \frac{p_n^a}{1 - p_0^a} = \frac{P[b]}{P[ab]} p_n^a \ . \tag{6.43}$$

For the mean number of successive detections of atoms in state $|a\rangle$ we obtain

$$\langle n_a \rangle \equiv \sum_{n=1}^{\infty} n P_n^a = \frac{P[a]}{P[ab]}, \tag{6.44}$$

and similarly

$$\langle n_b \rangle = \frac{P[b]}{P[ab]}. \tag{6.45}$$

The average of the two expressions gives

$$\langle n \rangle = \frac{1}{2P[ab]}, \tag{6.46}$$

which is the inverse of the switch probability (6.33) and is equivalent to Eq. (3.24) of Ref. [17]. The uncorrelated values are

$$\begin{aligned} (p_0^a)_{\rm uncor} &= r_b \int_0^{\infty} dt \, e^{-(r_a + r_b)t} = P[b] \\ (P_n^a)_{\rm uncor} &= \frac{(p_n^a)_{\rm uncor}}{P[a]} \\ \langle n_a \rangle_{\rm uncor} &= \frac{1}{P[b]}, \end{aligned} \tag{6.47}$$

and similarly for $(p_0^b)_{\rm uncor}$, $(P_n^b)_{\rm uncor}$, and $\langle n_b\rangle_{\rm uncor}$. The average of $\langle n_a\rangle_{\rm uncor}$ and $\langle n_b\rangle_{\rm uncor}$ gives Eq. (3.10) of Ref. [17]

$$\langle n\rangle_{\rm uncor} = \frac{1}{2P[a]P[b]}. \tag{6.48}$$

Thus

$$\langle n_a\rangle_{\rm norm} \;=\; \langle n_b\rangle_{\rm norm} = \langle n\rangle_{\rm norm} = \frac{P[a]P[b]}{P[ab]}. \tag{6.49}$$

6.3 Waiting time statistics

Waiting time distributions have been calculated previously for particular trapping states [6, 25]. Here we will calculate the mean waiting times between various detection events. We begin by deriving an expression for the mean time $\langle t_{a\to a}\rangle$ between detections of atoms in state $|a\rangle$. Given that an atom in state $|a\rangle$ was detected at time 0 we start with $\rho_{\rm f}(0) = \mathcal{X}_a^+\rho_{\rm f}^{\rm ss}/{\rm tr}\{\mathcal{X}_a^+\rho_{\rm f}^{\rm ss}\}$. At a later time t, the next atom in state $|a\rangle$ is detected. Until then, we wish to exclude detections of atoms in state $|a\rangle$, but we do not care how many atoms are detected in state $|b\rangle$. So we use the non-normalized conditioned density operator $\tilde\rho_{\rm f}^{\rm c}(t) = e^{\mathcal{X}_a^- rt}\rho_{\rm f}(0)$. Then the probability density for the time t when the next atom is detected in state $|a\rangle$ is $r\,{\rm tr}\{\mathcal{X}_a^+\tilde\rho_{\rm f}^{\rm c}(t)\}$. The mean time between detections of atoms in state $|a\rangle$ is then

$$\begin{aligned}\langle t_{a\to a}\rangle &= r\int_0^\infty dt\, t\,{\rm tr}\{\mathcal{X}_a^+\tilde\rho_{\rm f}^{\rm c}(t)\}\\ &= \frac{1}{r_a}{\rm tr}\left\{\mathcal{X}_a^+\frac{1}{\mathcal{X}_a^{-2}}\mathcal{X}_a^+\rho_{\rm f}^{\rm ss}\right\}.\end{aligned} \tag{6.50}$$

Using $\mathcal{X}_a^+ = \mathcal{X} - \mathcal{X}_a^-$ and the identities (6.26) we have

$${\rm tr}\left\{\mathcal{X}_a^+\frac{1}{\mathcal{X}_a^{-2}}\mathcal{X}_a^+\rho_{\rm f}^{\rm ss}\right\} = 1, \tag{6.51}$$

and we conclude that the mean time between detections of atoms in state $|a\rangle$ is equal to the uncorrelated value

$$\langle t_{a\to a}\rangle_{\rm uncor} = r_a\int_0^\infty dt\, te^{-r_a t} = \frac{1}{r_a}. \tag{6.52}$$

Likewise, for atoms in state $|b\rangle$ we have $\langle t_{b\to b}\rangle = \langle t_{b\to b}\rangle_{\rm uncor} = 1/r_b$.

These results do not prove that there are no correlations between atoms in the same state—only that we have to go to higher powers in the waiting time in order to see those correlations. For example, the mean squared time between detections of atoms in state $|a\rangle$ is

$$\begin{aligned}\langle t^2_{a\to a}\rangle &= r\int_0^\infty dt\, t^2 {\rm tr}\{\mathcal{X}_a^+ \tilde{\rho}_{\rm f}^{\rm c}(t)\} \\ &= \frac{2}{r r_a}{\rm tr}\left\{\mathcal{X}_a^+ \frac{-1}{\mathcal{X}_a^{-3}}\mathcal{X}_a^+\rho_{\rm f}^{\rm ss}\right\} \\ &= \frac{2}{r r_a}{\rm tr}\left\{\frac{-1}{\mathcal{X}_a^-}\rho_{\rm f}^{\rm ss}\right\}, \end{aligned} \tag{6.53}$$

where, in the last step, we have again substituted $\mathcal{X}_a^+ = \mathcal{X} - \mathcal{X}_a^-$ and used the identities (6.26). This does not reduce to the uncorrelated value

$$\langle t^2_{a\to a}\rangle_{\rm uncor} = \frac{2}{r_a^2}. \tag{6.54}$$

If we want a more interesting mean waiting time (one that exhibits correlations without needing to go to higher powers), we have to compute $\langle t_{a\to b}\rangle$ or $\langle t_{b\to a}\rangle$. Starting with the same initial condition $\rho_{\rm f}(0) = \mathcal{X}_a^+\rho_{\rm f}^{\rm ss}/{\rm tr}\{\mathcal{X}_a^+\rho_{\rm f}^{\rm ss}\}$, and using the non-normalized conditioned density operator $\tilde{\rho}_{\rm f}^{\rm c}(t) = e^{\mathcal{X}_b^- rt}\rho_{\rm f}(0)$ for the absence of detections of atoms in state $|b\rangle$, the probability density for the time t until the next detection of an atom in state $|b\rangle$ is $r\,{\rm tr}\{\mathcal{X}_b^+\tilde{\rho}_{\rm f}^{\rm c}(t)\}$. The mean time until the next detection of an atom in state $|b\rangle$ is

$$\begin{aligned}\langle t_{a\to b}\rangle &= r\int_0^\infty dt\, t\,{\rm tr}\{\mathcal{X}_a^+ \tilde{\rho}_{\rm f}^{\rm c}(t)\} \\ &= \frac{1}{r_a}{\rm tr}\left\{\mathcal{X}_b^+ \frac{1}{\mathcal{X}_b^{-2}}\mathcal{X}_a^+\rho_{\rm f}^{\rm ss}\right\}. \end{aligned} \tag{6.55}$$

Using $\mathcal{X}_b^+ = \mathcal{X} - \mathcal{X}_b^-$ and the identities (6.26), we have

$${\rm tr}\left\{\mathcal{X}_b^+ \frac{1}{\mathcal{X}_b^{-2}}\mathcal{X}_a^+\rho_{\rm f}^{\rm ss}\right\} = {\rm tr}\{\frac{-1}{\mathcal{X}_b^-}\mathcal{X}_a^+\rho_{\rm f}^{\rm ss}\}, \tag{6.56}$$

so that

$$\langle t_{a\to b}\rangle = \frac{1}{r_a}\,\mathrm{tr}\{\frac{-1}{\mathcal{X}_b^-}\mathcal{X}_a^+\rho_{\mathrm{f}}^{\mathrm{ss}}\}. \tag{6.57}$$

The uncorrelated value is

$$\langle t_{a\to b}\rangle_{\mathrm{uncor}} = r_b\int_0^\infty dt\, te^{-r_b t} = \frac{1}{r_b}, \tag{6.58}$$

so that

$$\langle t_{a\to b}\rangle_{\mathrm{norm}} = \frac{r_b}{r_a}\,\mathrm{tr}\{\frac{-1}{\mathcal{X}_b^-}\mathcal{X}_a^+\rho_{\mathrm{f}}^{\mathrm{ss}}\}. \tag{6.59}$$

Similar results can be obtained for $\langle t_{b\to a}\rangle$ and $\langle t_{b\to a}\rangle_{\mathrm{norm}}$.

Chapter 7

Results

7.1 Atomic Inversion

The atomic inversion is defined as the difference in the probabilities of a given outgoing atom being in the ground state and the excited state. A more practical definition is the difference in the probabilities of a given *detected* atom being in the ground state and the excited state

$$I \equiv P[a] - P[b]. \tag{7.1}$$

This formula reduces to the difference in the number of outgoing atoms in the ground state and excited state if the detector efficiencies are equal ($\eta_a = \eta_b$), which we will assume.

A recent paper by Weidinger *et al.* [67] gives results of experimental observations of the atomic inversion and shows the first evidence for the existence of trapping states. Figure 7.1 shows I calculated for $N_{\rm ex} = 7$ and $N_{\rm ex} = 10$ for comparison to Fig. 3 of Ref. [67]. Here $\nu = 0.054$ and $g = 39$ kHz. The thick curves are the result of the micromaser theory with atomic decay or velocity averaging, while the thin curve includes depletion damping with the parameters $\gamma_a = (244\ \mu s)^{-1}$ and $\gamma_b = (488\ \mu s)^{-1}$, and also velocity averaging with $\sigma_t/\bar{t}_{\rm int} = 3\%$. The inclusion of two-atom events was found to have a negligible effect for these parameters and is not included here. The vertical dotted lines indicate the same trapping states as in Fig. 3 of Ref. [67]. The trapping states are seen to have the effect of creating dips in the atomic inversion.

The experimental results show a linear trend due to the difference in the decay rates of the two atomic levels and the flight time to the state selective

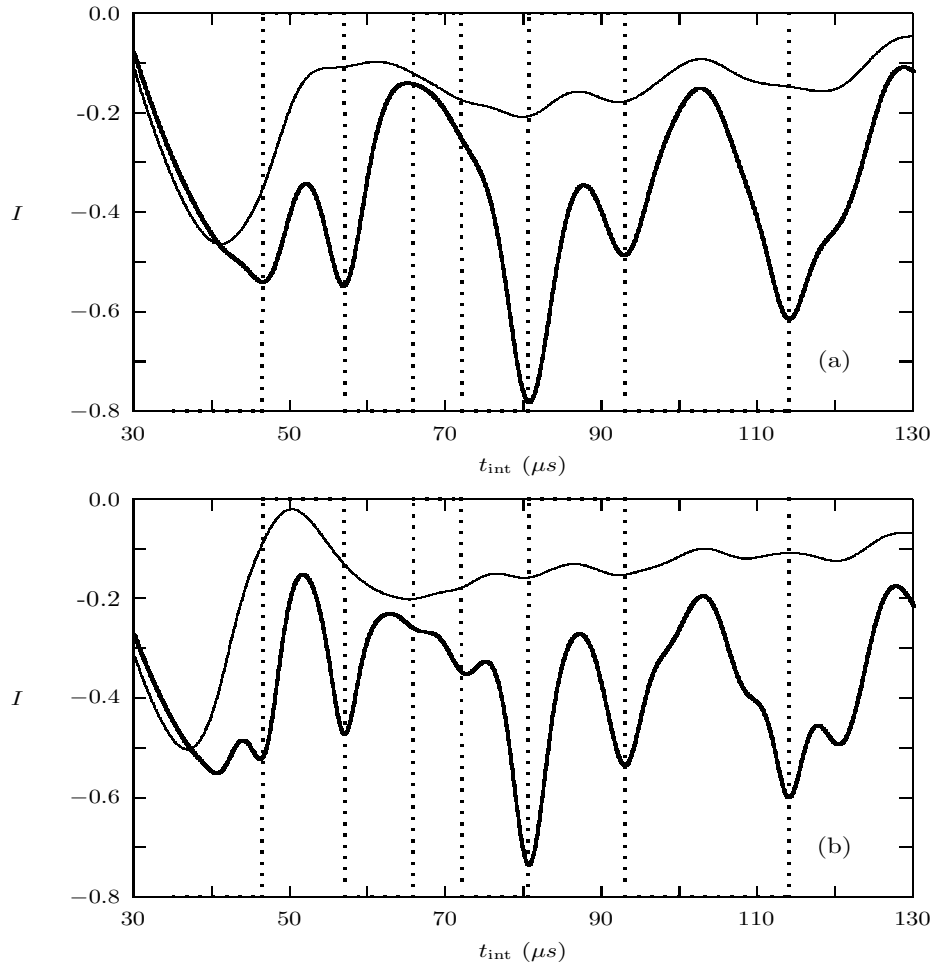

Figure 7.1: The inversion I for $N_{\rm ex} = 7$ (a) and $N_{\rm ex} = 10$ (b). The atoms are assumed to all arrive in the upper state. The parameters used here are $\nu = 0.054$ and $g = 39$ kHz. The thick curves are the results of the micromaser theory without atomic decay or velocity averaging. The thin curves are the results of including depletion damping with $\gamma_a = (244\,\mu s)^{-1}$ and $\gamma_b = (488\,\mu s)^{-1}$, and velocity averaging with $\sigma_t/\bar{t}_{\rm int} = 3\%$. The vertical dotted lines indicate trapping states.

field ionisation detectors. Because of this, the detector efficiencies effectively become

$$\eta_a \rightarrow \eta_a e^{-\gamma_a f_a t_{\rm int}} \tag{7.2}$$

$$\eta_b \rightarrow \eta_b e^{-\gamma_b f_b t_{\rm int}}, \tag{7.3}$$

where f_a and f_b are the distances to the detectors in units of the cavity length d. Figure 7.2 shows the effect of having chosen the detector distances $f_a = 4$ and $f_b = 2$. These choices were made without knowledge of the detector geometry used in Ref. [67], but produce an effect that is comparable. Here we also including the results of a Monte Carlo simulation that includes the effect of quantum fluxuations due to exchanges of energy with the reservoir. The diamond points in Fig. 7.2 are the result of averaging over 2×10^4 detector events, where the detectors were taken to have an efficiency of $\eta_a = \eta_b = 40\%$.

Figure 7.3 shows the results of having applied a first order correction by subtracting the linear trend. The linear trend was determined by considering only points with $t_{\rm int} \geq 60\ \mu s$.

In comparing our theoretical results with the experimental results of Ref. [67], we first note the glaring discrepancy for interaction times less than 60 μs. In this region, the predicted features of the inversion are invisible in the experimental results. In addition, before subtracting the linear trend, the predicted inversion is never positive, unlike the experimental results for interaction times less than 60 μs. Also, the effect of the trapping states at $t_{\rm int} = 46.5\ \mu s,\ 57.0\ \mu s,\ 65.8\ \mu s$, and $72.0\ \mu s$ are predicted to be suppressed by the amount of atomic decay and atomic velocity spread present in the experiment. The experimental results, however, show dips in the inversion at those locations. The authors of Ref. [67] note that for interaction times below 40 μs the Doppler distributions of the upper atomic state (the $63P_{3/2}$ state of Rubidium) and a neighboring level (the $63P_{1/2}$ state of Rubidium) overlap, leading to the excitation of atoms that don't interact with the micromaser field. This effectively lowers the injection rate r of interacting atoms and will disturb the maser statistics, but cannot explain the discrepancy between the theory and experiment for interaction times up to 60 μs.

The shape of the inversion is hardly affected by the detector geometry. Changing the detector geometry by increasing the distance between the

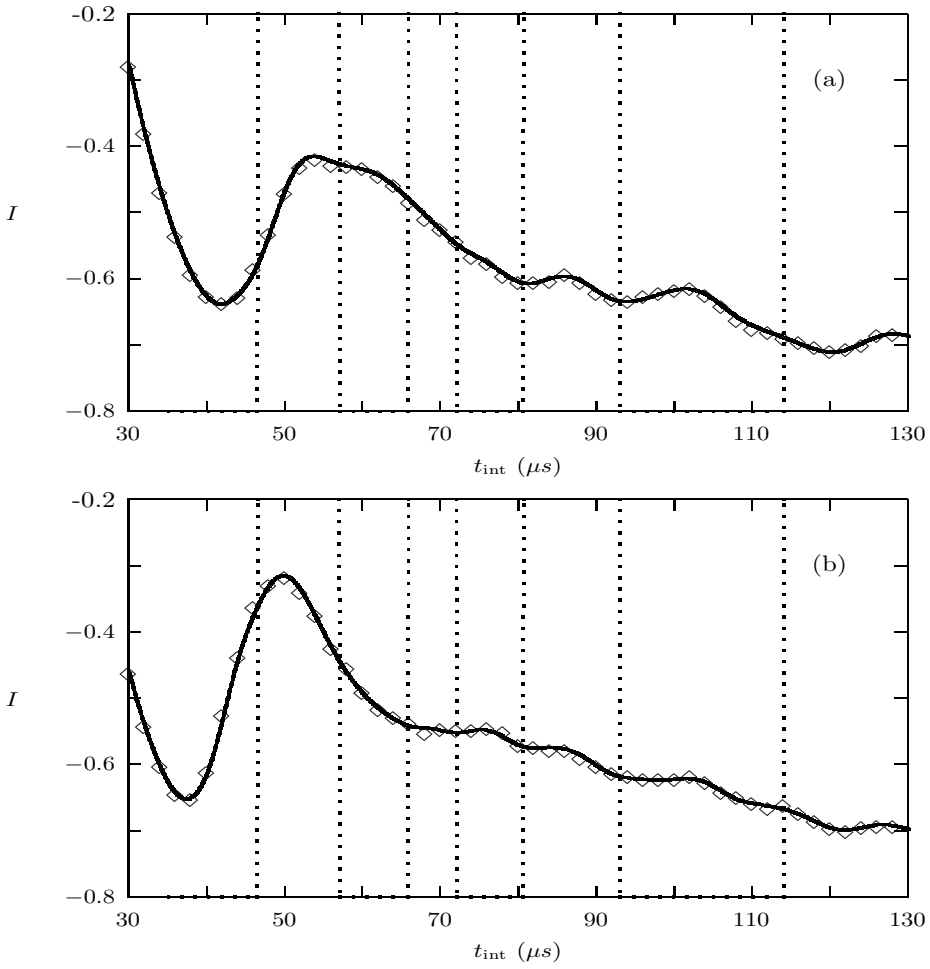

Figure 7.2: The inversion I for $N_{\rm ex} = 7$ (a) and $N_{\rm ex} = 10$ (b). The atoms are assumed to all arrive in the upper state. The parameters used here are $\nu = 0.054$ and $g = 39$ kHz, $\gamma_a = (244\ \mu s)^{-1}$, $\gamma_b = (488\ \mu s)^{-1}$, and $\sigma_t/\bar{t}_{\rm int} = 3\%$. The detectors are treated as being at distances of $f_a = 4$ and $f_b = 2$ in units of the cavity length. The vertical dotted lines indicate trapping states. The diamond points are the results of a Monte Carlo simulation that includes quantum fluxuations due to exchanges of energy with the reservoir. The detectors were taken to have an efficiency of $\eta_a = \eta_b = 40\%$ Each diamond point is the average of a 2×10^4 detection events.

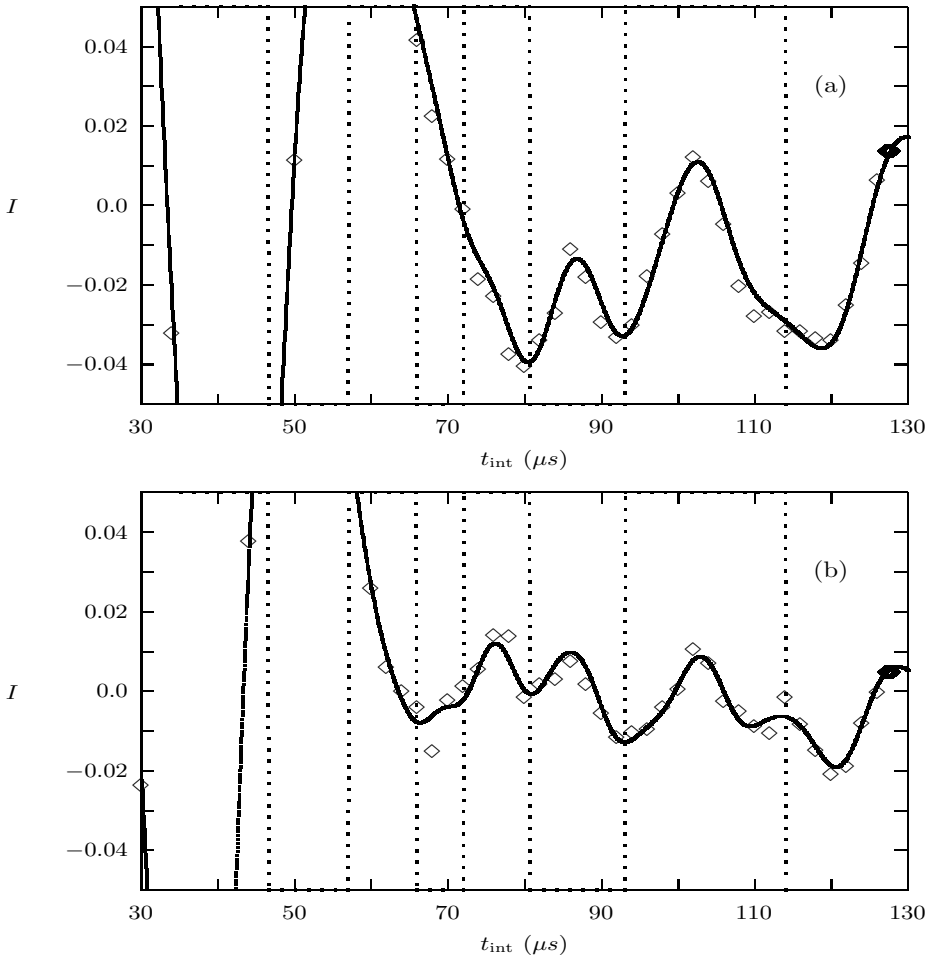

Figure 7.3: The inversion I for $N_{\rm ex} = 7$ (a) and $N_{\rm ex} = 10$ (b). The atoms are assumed to all arrive in the upper state. The parameters used here are $\nu = 0.054$ and $g = 39$ kHz, $\gamma_a = (244\,\mu s)^{-1}$, $\gamma_b = (488\,\mu s)^{-1}$, and $\sigma_t/\bar{t}_{\rm int} = 3\%$. The detectors are treated as being at distances of $f_a = 4$ and $f_b = 2$ in units of the cavity length. The linear trend for points with $t_{\rm int} \geq 60\ \mu s$ has been subtracted. The vertical dotted lines indicate trapping states. The diamond points are the results of a Monte Carlo simulation that includes quantum fluxuations due to exchanges of energy with the reservoir. Each diamond point is the average of a 2×10^4 detection events.

detectors and the cavity increases the linear trend (which eventually is seen as an exponential trend), but does not otherwise affect the shape of the inversion after the trend is removed. The degree of signal suppression in our model is due solely to atomic decay and the distribution of atomic velocities. The amount of atomic damping and velocity spread included in our model is based on the experimental parameters of Ref. [67], and is seen to produce a comparable amount of amplitude suppression. The Monte Carlo simulation shows the effect of including quantum fluxuations, where each diamond point is the result of averaging over 2×10^4 detection events as was done in earlier experiments [52]. We see that this is enough to reduce the fluxuations and achieve a good signal.

Although the experimental results show dips occurring in the inversion at the locations of the trapping states, the results disagree with the theoretical shape of the inversion everywhere else. We can only conclude that either the theory needs to be extended further to include some effect that is present in this experiment (but did not affect the earlier experiments of Walther *et al.* [52, 54], where agreement with the theory was good) or there was some difficulty with the experiment that led to too much noise in the data.

7.2 The Fano-Mandel Function

Figure 7.4 shows the Fano-Mandel function Q_a for the detection of lower state atoms for a micromaser in which all of the atoms arrive in the upper state. The observation time was chosen to be one cavity decay time for comparison to Fig. 4 of Ref. [67] in which the results were averaged over observation times between one and four cavity decay times. The parameters used here are $N_{\rm ex} = 7$, $\nu = 0.054$, $g = 39$ kHz. The vertical dotted lines indicate the same trapping states as in Fig. 4 of Ref. [67]. Increasing the observation time of the Fano-Mandel function has the effect of increasing the amplitude of the super-Poissonian peaks. The sub-Poissonian regions are barely affected by the increase in the observation time, since in these regions the steady state Fano-Mandel function is reached in less than one cavity decay time [6]. In super-Poissonian regions, the Fano-Mandel function reaches its steady state at a much slower rate.

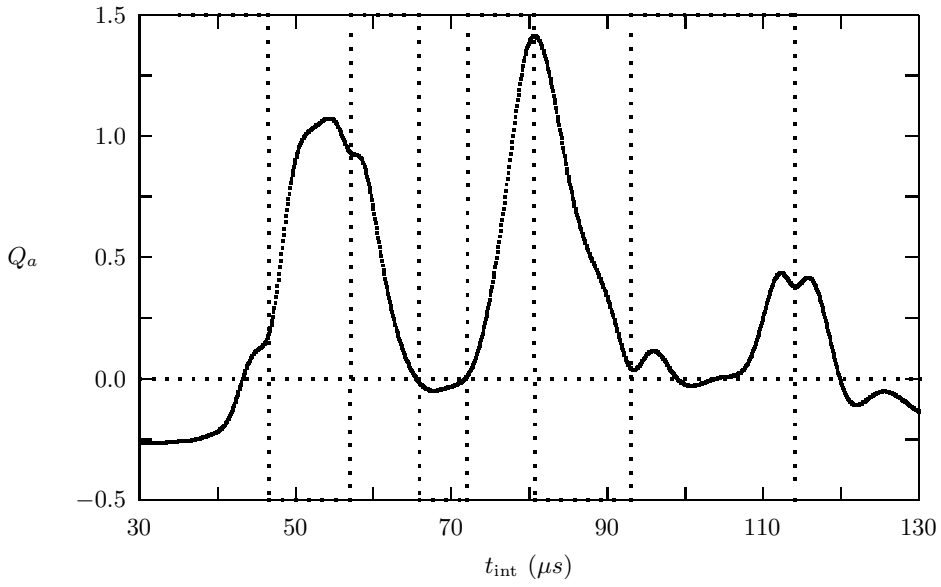

Figure 7.4: The Fano-Mandel Function Q_a for the detection of atoms in the lower state. The atoms are assumed to all arrive in the upper state and atomic damping and velocity averaging are neglected. The parameters used here are $N_{\rm ex} = 7$, $\nu = 0.054$, $g = 39$ kHz, and $t_{\rm obs} = 1/\gamma_f$. The vertical dotted lines indicate trapping states. Poissonian statistics corresponds to $Q_a = 0$.

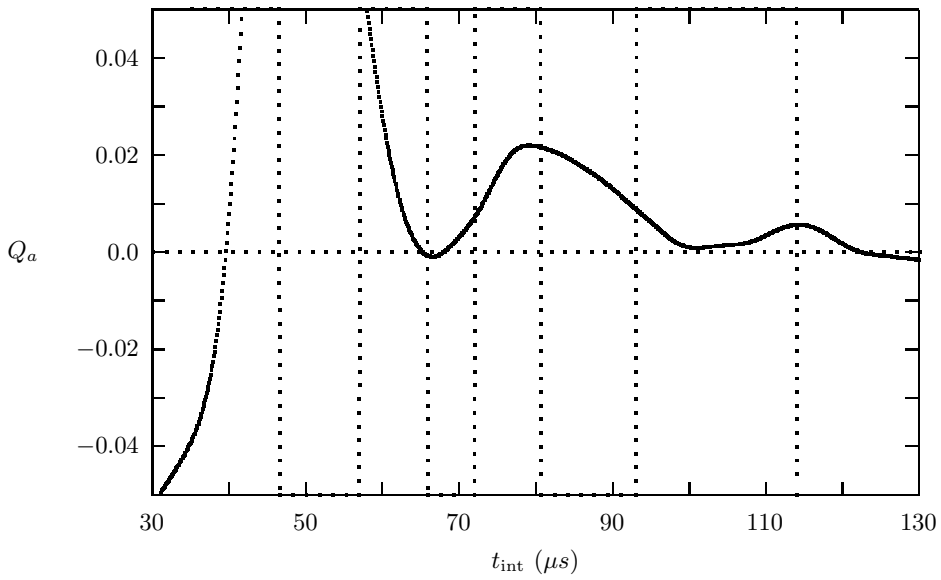

Figure 7.5: The Fano-Mandel Function Q_a for the detection of atoms in the lower state. The atoms are assumed to all arrive in the upper state. The parameters used here are $N_{\rm ex} = 7$, $\nu = 0.054$, $g = 39$ kHz, $t_{\rm obs} = 1/\gamma_f$, $\gamma_a = (244\ \mu s)^{-1}$, $\gamma_b = (488\ \mu s)^{-1}$, $\sigma_t/\bar{t}_{\rm int} = 3\%$, $f_a = 4$, and $\eta_a = 40\%$. The vertical dotted lines indicate trapping states. Poissonian statistics corresponds to $Q_a = 0$.

Though the trapping states do have some affect on the shape of Q_a, the effect is not as striking as the effect on the ...

Figure 7.5 shows the effect of including atomic decay and velocity averaging with the parameters $\gamma_a = (244\ \mu s)^{-1}$, $\gamma_b = (488\ \mu s)^{-1}$, and $\sigma_t/\bar{t}_{\rm int} = 3\%$. We also assumed a detection efficiency for lower state atoms of $\eta_a = 40\%$ and a distance to the detector of $f_a = 4$. The inclusion of velocity averaging and atomic damping has has destroyed any effect the trapping states have on Q_a except perhaps at the trapping state $t_{\rm int} = 65.8\ \mu s$. Another effect is that the sub-Poissonian regions are greatly reduced except for the region $t_{\rm int} \leq 40\ \mu s$.

Compared to the experimental results of Ref. [67], we again note the glaring discrepancy for interaction times less than 60 μs. The theoretical results show a decrease in amplitude for larger interaction times due to the

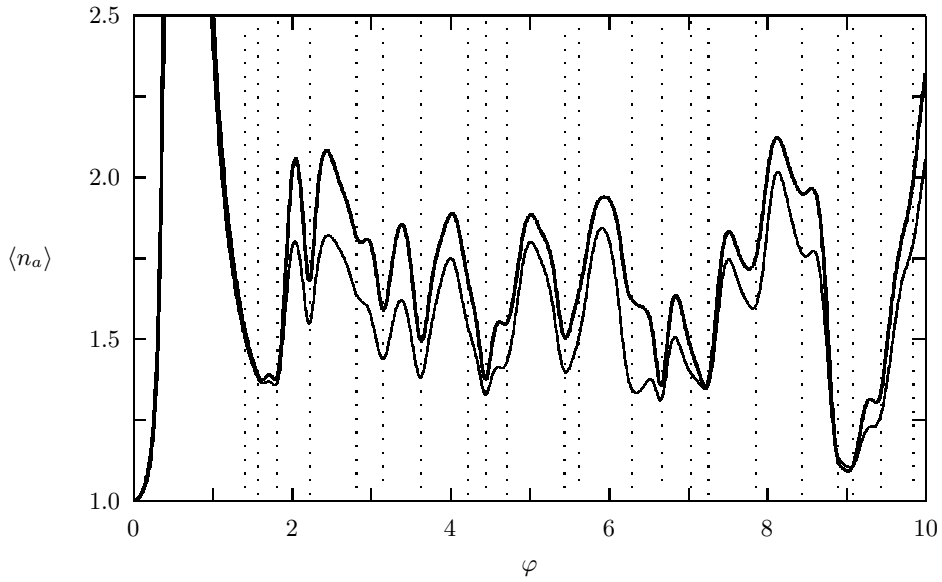

Figure 7.6: Mean number $\langle n_a \rangle$ of successive detections of lower state atoms for $N_{\rm ex} = 7$ and $\nu = 0.054$. The curves are for $\eta = 100\%$ (thick line) and $\eta = 10\%$ (thin line). The vertical dotted lines indicate the trapping states for $n_q = 0, \ldots, 4$.

distance between the cavity and the detector for lower state atoms. Either the use of $f_a = 4$ is much too large, or the experimental results include a corrective factor of $exp(\gamma_a f_a t_{\rm int})$ (though the authors did not mention any correction). The experimental results show variations in Q_a on a scale much shorter in $t_{\rm int}$ than the theoretical results predict (even before the inclusion of velocity averaging and atomic decay smooth the results further). This is even more convincing than the atomic inversion that the results of Ref. [67] is excessively noisy, and not a good indicator that anything is wrong with the theory.

7.3 Successive detections

Figure 7.6 shows the mean number of successive detections of atoms in the lower maser level $|a\rangle$, $\langle n_a \rangle$, for detector efficiencies of $\eta = 100\%$ and 10%. The vertical dotted lines in the figure indicate the trapping states for

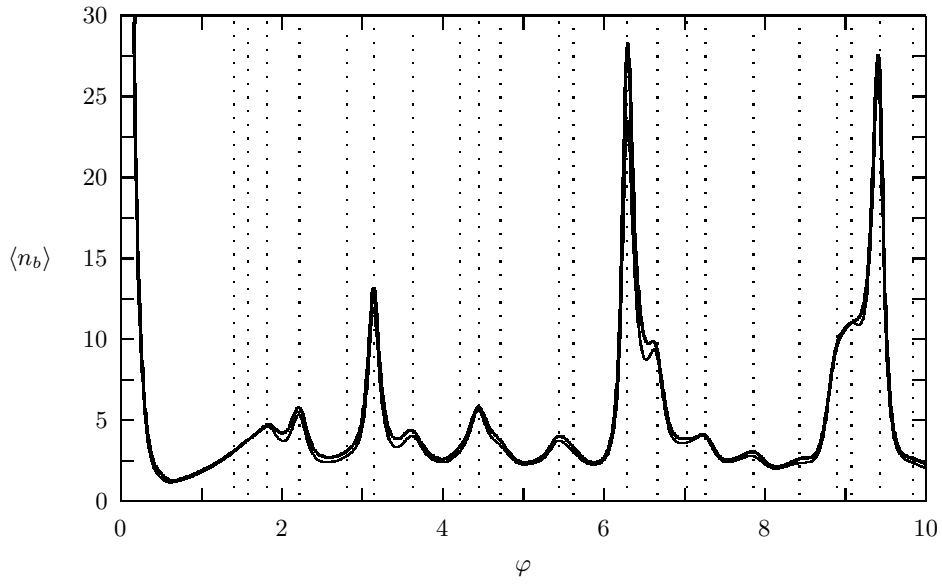

Figure 7.7: Mean number $\langle n_b \rangle$ of successive detections of upper state atoms for $N_{\rm ex} = 7$ and $\nu = 0.054$. The curves are for $\eta = 100\%$ (thick line) and $\eta = 10\%$ (thin line). The vertical dotted lines indicate the trapping states for $n_q = 0, \ldots, 4$.

$n_q = 0, \ldots, 4$. At a trapping state, if it were not for the effect of thermal damping, we would expect all of the atoms to emerge in the upper maser level, having undergone an integer multiple of Rabi cycles. This has the effect of giving rise to a dip in the average number of successive detections of atoms in the lower maser level. Figure 7.7 shows the mean number of successive detections of atoms in the upper maser level $|b\rangle$, $\langle n_b \rangle$. In this figure, we see that trapping states give rise to peaks indicating an increase in the number of successive detections of excited atoms as expected, though some trapping states have only a small effect on the shape of nearby peaks. Both Figs. 7.6 and 7.7 show a decrease in the mean number of successive detections as the detectors become less efficient. The uncorrelated values are unaffected by the detector efficiencies (for equal detector efficiencies), and this decrease in the mean number of successive detections is just an indication of the decrease in correlations for decreasing detector efficiencies. Trapping states are seen to greatly affect

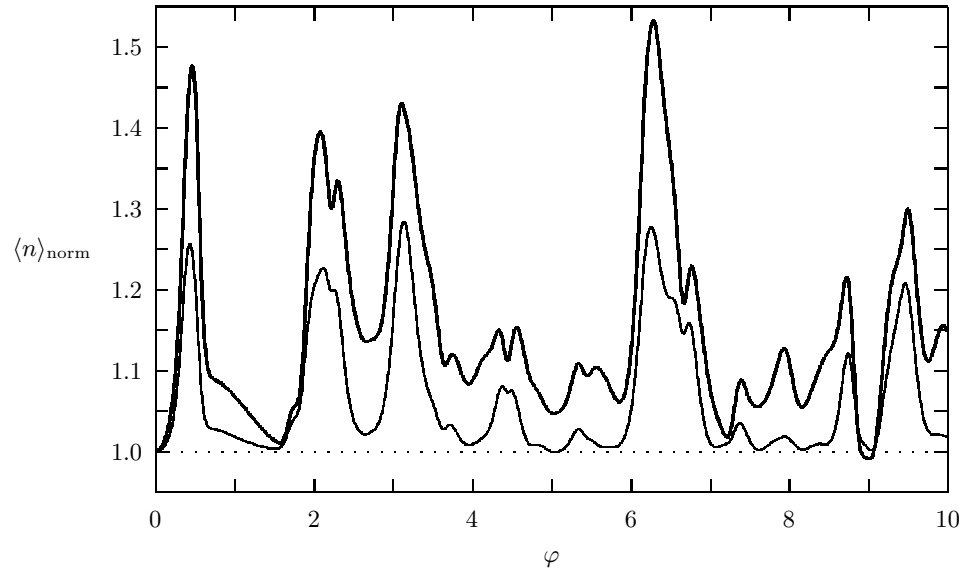

Figure 7.8: Mean number of successive detections (of any type) normalized to the uncorrelated value for $N_{\rm ex} = 7$ and $\nu = 0.054$. The curves are for $\eta = 100\%$ (thick line) and $\eta = 10\%$ (thin line).

these mean numbers, providing a means of observing trapping states alternative to measurements of the atomic inversion. Figure. 7.8 shows the mean number of successive detections (of any type) normalized to the uncorrelated value, $\langle n \rangle_{\rm norm}$. For decreasing detector efficiency, $\langle n \rangle_{\rm norm}$ approaches unity as expected. Antibunching occurs in a narrow interval of $\varphi = 9$.

7.4 Waiting times

Figure 7.9 shows the average time until the next detection of an atom in the upper state after an initial detection of an atom in the lower state, $\langle t_{a\to b} \rangle$, scaled by $r\eta_b$. The scaling compensates for the increase in mean waiting time as the detectors become less efficient and the probability of the final detection occurring decreases. Again, the vertical dotted lines indicate the trapping states for $n_q = 0, \ldots, 4$. The trapping states have the effect of giving rise to dips in the average waiting time for the next detection of an atom in the

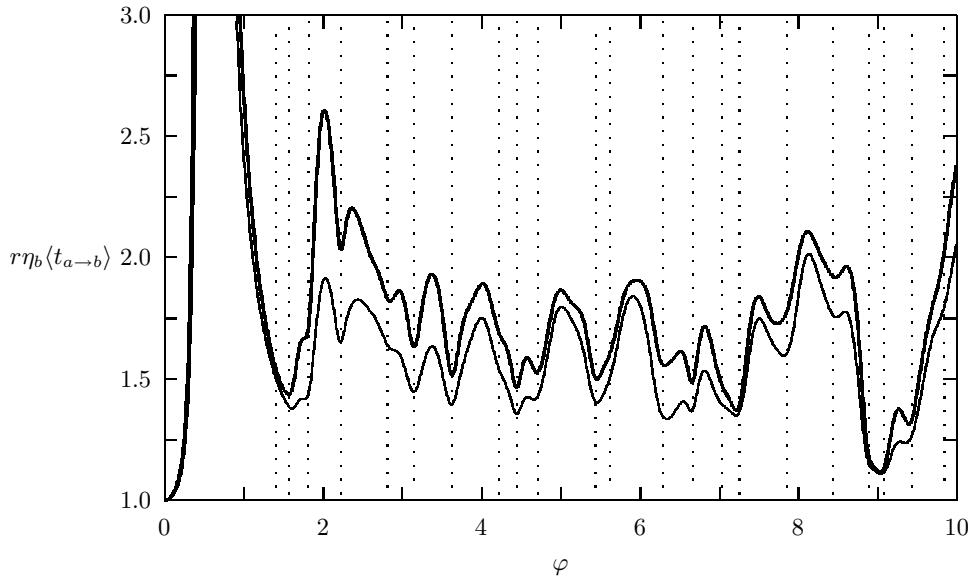

Figure 7.9: Mean waiting time $\langle t_{a\to b}\rangle$ until the next detection of an upper state atom after a detection of a lower state atom (scaled by $r\eta_b$) for $N_{\rm ex} = 7$ and $\nu = 0.054$. The curves are for $\eta = 100\%$ (thick line) and $\eta = 10\%$ (thin line). The vertical dotted lines indicate the trapping states for $n_0 = 0, \ldots, 4$.

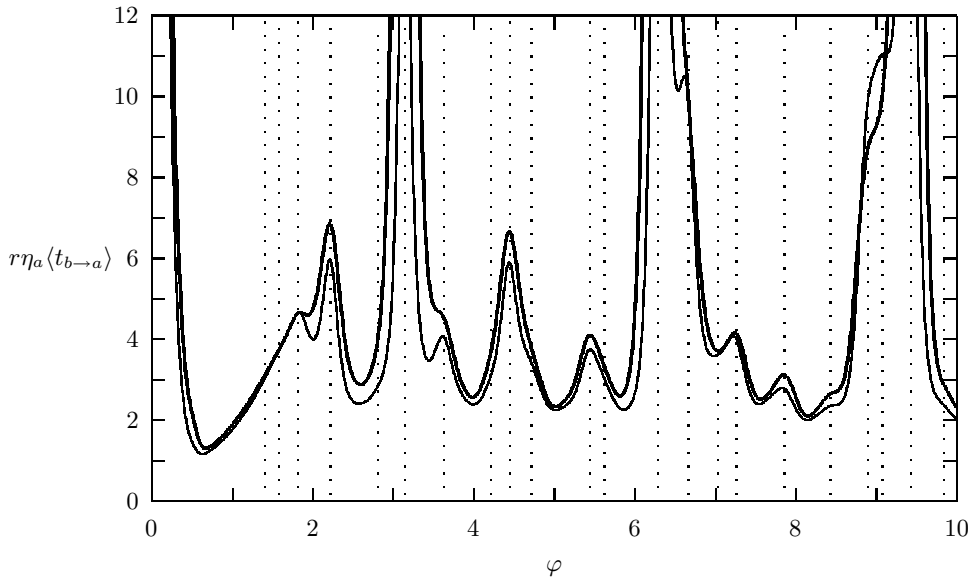

Figure 7.10: Mean waiting time $\langle t_{b\to a}\rangle$ until the next detection of a lower state atom after a detection of an upper state atom (scaled by $r\eta_a$) for $N_{\rm ex} = 7$ and $\nu = 0.054$. The curves are for $\eta = 100\%$ (thick line) and $\eta = 10\%$ (thin line). The vertical dotted lines indicate the trapping states for $n_0 = 0, \ldots, 4$.

upper state as expected, since almost every atom should leave the cavity in the upper state when the micromaser is operating at a trapping state. Figure 7.10 shows $\langle t_{b\to a}\rangle$, scaled by $r\eta_a$. Here the trapping states give rise to peaks in the average waiting time for the next detection of an atom in the lower state, though some trapping states have only a small effect on nearby peaks. The large peaks at $\varphi = \pi, 2\pi, 3pi$ are cut-off in the figure so that the other features can be seen. These peaks are featureless above what is shown in the figure. Figures 7.11 and 7.12 show the waiting times normalized by the uncorrelated values. Figure 7.12 shows some negative correlations in a vicinity of $\varphi = 9$.

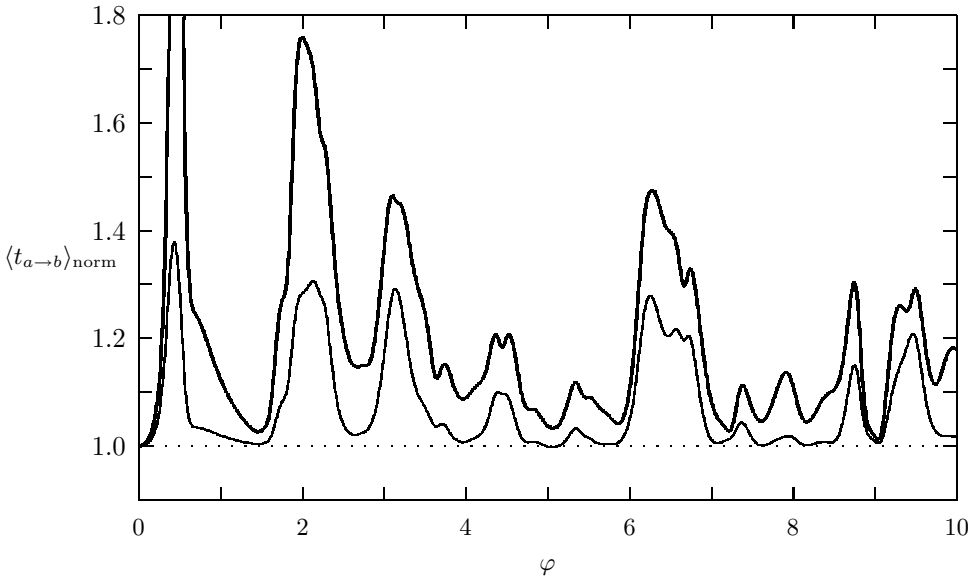

Figure 7.11: Mean waiting time $\langle t_{a\to b}\rangle$ until the next detection of an upper state atom after a detection of a lower state atom normalized to the uncorrelated value for $N_{\rm ex} = 7$ and $\nu = 0.054$. The curves are for $\eta = 100\%$ (thick line) and $\eta = 10\%$ (thin line).

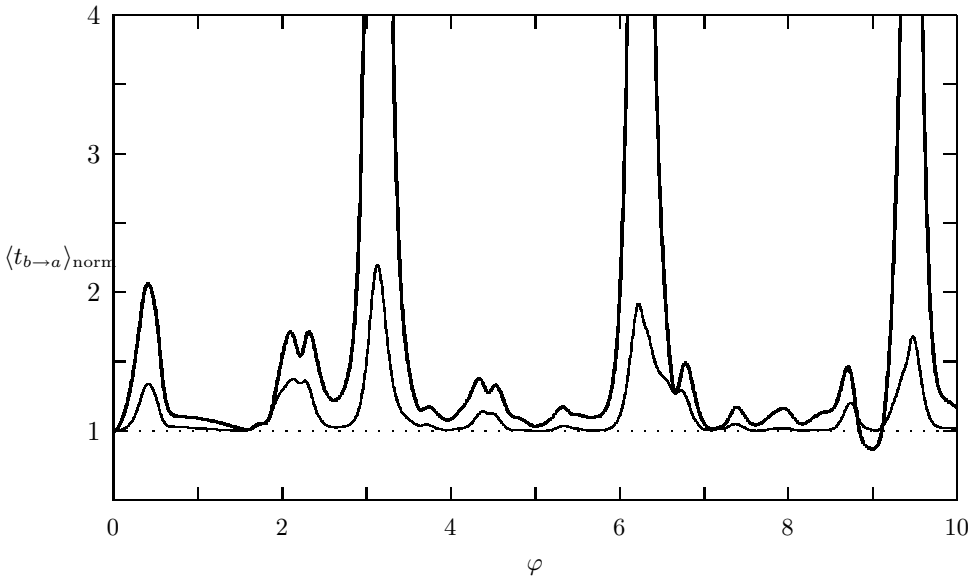

Figure 7.12: Mean waiting time $\langle t_{b\to a}\rangle$ until the next detection of a lower state atom after a detection of an upper state atom normalized to the uncorrelated value for $N_{\rm ex} = 7$ and $\nu = 0.054$. The curves are for $\eta = 100\%$ (thick line) and $\eta = 10\%$ (thin line).

Chapter 8

Conclusions

We have reviewed background material about electromagnetic fields inside of high-Q cavities and Rydberg atoms in electromagnetic fields. We have made small contributions to the theory of damping of the field by correcting the errors in the derivation of the field damping eigenstates by Briegel *et al.* [4] and finding a simpler approach to establishing the orthonormality of the eigenstates. We also made a contribution to the theory of damping of two-level atoms by using a density operator approach that does not assume zero temperature. We discussed the Jaynes-Cummings model of two-level atoms interacting with single mode electromagnetic fields and extended the theory to include a spacial-dependent atom-field coupling strength. We concluded that alone it would have no effect on the results of the experiments of Walther *et al.*[41, 50, 52, 54, 67].

In our development of the micromaser theory, we have derived an operator describing the continuous evolution of the micromaser field averaged over the arrival times of the injected atoms. This operator had been in use previously, but lacked a formal derivation. Our derivation also results in a more general form for the evolution operator including the effects of non-zero temperature, atomic depletion damping, and velocity averaging. Using this operator we derived a more general analytical expression for the steady state of the micromaser field than has been previously derived, and calculated the effects of atomic depletion damping with non-equal decay rates on the photon statistics as a function of the pumping parameter. We also extended the micromaser theory to include two-atom events and calculate the photon statistics of the micromaser field including two-atom events. Our results differ from the earlier results of Casagrande *et al.* [9]; however, a comparison of our results with the two extremes of atoms arriving in pairs and atoms arriving sequen-

tially and with a Monte Carlo simulation gives us confidence that our results are correct.

We discussed the detection statistics of measurements on the outgoing atoms of a micromaser system, and contributed to the discussion by deriving the sequence statistics and waiting-time statistics of the detection events. We derived the average number of successive detections of atoms in the upper and lower maser levels. We also showed that the average waiting times between detections of atoms in the same state are given by the uncorrelated rates of atomic detections, but that the average waiting-times between atoms in different states exhibit correlations.

We made numerous calculations of observable quantities including the atomic inversion, the Fano-Mandel funciton, the average number of successive detections of atoms in the upper and lower maser level, and the waiting-times between the detection of atoms in different states. In comparing our results for the atomic inversion and the Fano-Mandel function, we made an effort to perform a comprehensive comparison with the experimental results of Weidinger *et al.* [67], but the agreement remains very poor despite the excellent agreement between the theory and the earlier experiments. The theory might be extended further, although we do not anticipate that any further extension of the theory will improve agreement with the experiments of Ref. [67]. Our results for the average number of successive detections of atoms in the upper and lower maser levels show a sensitivity to the presence of trapping states. We conclude that measurements of these average numbers might provide a better alternative to measurements of the atomic inversion for observing trapping states.

In the future, we might consider a more comprehensive generalization of the Jaynes-Cummings model including extensions such as the atomic inversion damping, a spacial-dependent atom-field coupling strength (which may give a non-trivial result when including other effects as well), and the center-of-mass motion of the atom. Extending the model is valuable, due to its usefulness in many applications, but analytical results beyond what has already been achieved will prove difficult. We might also consider the finite interaction times in the micromaser, and study the return map that describes the micromaser field at successive atomic injections. We could consider more extensive

Monte Carlo simulations or try other methods for solving the dynamical equations of the micromaser field such as extensions of the eigenstate method of Briegel [4], or use of the matrix continued fraction method developed by Risken and Vollmer [55]. We might also consider other micromaser arrangements such as the pulsed micromaser of the more recent experiments by Varcoe *et al.* [61].

Bibliography

[1] I. Sh. Averbukh and N. F. Perelman. *Phys. Lett. A*, 10:449, 1989.

[2] P.J. Bardoff, E. Mayr, and W.P. Scleich. *Phys. Rev. A*, 51:4963, 1995.

[3] O. Benson, G. Raithel, and Herbert Walther. Quantum jumps of the micromaser field: Dynamic behavior close to phase transition points. *Phys. Rev. Lett.*, 72(22):3506–3513, May 1997.

[4] Hans-Jürgen Briegel and Berthold-Georg Englert. Quantum optical master equations: The use of damping bases. *Phys. Rev. A*, 47(4):3311–3329, Apr 1993.

[5] Hans-Jürgen Briegel, Berthold-Georg Englert, Christian Ginzel, and Schenzle Axel. *Phys. Rev. A*, 49:5019, 1994.

[6] Hans-Jürgen Briegel, Berthold-Georg Englert, Nicoletta Sterpi, and Herbert Walter. One-atom maser: Statistics of detector clicks. *Phys. Rev. A*, 49(4):2962–2985, Apr 1994.

[7] M. Brune, S. Haroche, V. Lefevre, J.M. Raimond, and N. Zagury. Quantum nondemolition measurements of small photon numbers by rydberg-atom phase-sesative detection. *Phys. Rev. Lett.*, 65(8):976–979, 1992.

[8] M. Brune, S. Haroche, J.M. Raimond, L. Davidovich, and N. Zagury. *Phys. Rev. A*, 45:5193, 1992.

[9] F. Casagrande, A. Lulli, and S. Ulzega. Collective effects and trapping states by a quantum-trajectory treatment of micromaser dynamics. *Phys. Rev. A*, 60(2):1582–1589, Aug 1999.

[10] J.I. Cirac and A.S. Parkins. *Phys. Rev. A*, 50:R4441, 1994.

[11] J.I. Cirac, A.S. Parkins, R. Blatt, and P. Zoller. Nonclassical states of motion in ion traps. *Adv. At. Mol. Opt. Phys.*, 37:237–296, 1996.

[12] J. D. Cresser and S. M. Pickles. *Phys. Rev. A*, 50:R925, 1994.

[13] J. D. Cresser and S. M. Pickles. A quantum trajectory analysis of the one-atom micromaser. *Quantum Semiclass. Opt.*, 8:73–104, 1996.

[14] F. W. Cummings. *Phys. Rev.*, 140:A1051, 1965.

[15] L. Davidovich, N. Zagury, M. Brune, J.M. Raimond, and S. Haroch. *Phys. Rev. A*, 50:R895, 1994.

[16] J. H. Eberly, N. B. Narozhny, and J. J. Sánchez-Mondragón. *Phys. Rev. Lett.*, 19:1323, 1980.

[17] Berthold-Georg Englert, Tserensodnom Gantsog, Axel Schenzle, Christian Wagner, and Herbert Walther. One-atom maser: Phase-sensitive measurements. *Phys. Rev. A*, 53(6):4386–4399, Jun 1996.

[18] Berthold-Georg. Englert, M. Löffler, O. Benson, B. Varcoe, M. Weidinger, and Herbert Walther. Entangled atoms in micromaser physics. *Fortschr. Phys.*, 46:897–926, 1998.

[19] U. Fano. Ionization yield of radiations. ii. the fluctuations of the number of ions. *Phys. Rev.*, 72(1):26–29, Jul 1947.

[20] P. Filipowicz, J. Javanainen, and P. Meystre. Theory of a microscopic maser. *Phys. Rev. A*, 34(4):3077–3087, Oct 1986.

[21] M. Frezberger, A.M. Herkommer, D.S. Krahmer, E. Mayr, and W.P. Schleich. Atom optics in quantized light fields. *Advances in Atomic, Molecular, and Optical Physics*, 41:143–180, 1999.

[22] Julio Gea-Banacloche. Collapse and revival of the state vector in the jaynes-cummings model: an example of state preparation by a quantum apparatus. *Phys. Rev. Lett.*, 65(27):3385–3388, Dec 1990.

[23] P. Goy, J. M. Raimond, M. Gross, and S. Haroche. *Phys. Rev. Lett.*, 50:1903, 1983.

[24] S. Haroche, M. Brune, and J. M. Raimond. Experiments with single atoms in a cavity: Entanglement, schrödinger's cats, and decoherence. *Philos. Trans. R. Soc. London A*, 355(1733):2367–2380, 1997.

[25] Ulrike Herzog. Statistics of photons and de-excited atoms in a micromaser with Poissonian pumping. *Phys. Rev. A*, 50(1):783–786, Jul 1994.

[26] Ulrike Herzog. Micromaser intensity correlations and atomic coincidence probabilities. *Appl. Phys. B*, 60:S21–S28, 1995.

[27] M.J. Holland, D.F. Walls, and P. Zoller. *Phys. Rev. Lett.*, 67:1716, 1991.

[28] J.D. Jackson. *Classical Electrodynamics*. John Wiley and Sons, Inc., New York, 1975.

[29] E. T. Jaynes and F. W. Cummings. *Proc. IEEE*, 51:89, 1963.

[30] David B. Johnson and W. C. Scheive. Detection statistics in the micromaser. *Phys. Rev. A*, 63:033808, Feb 2001.

[31] David B. Johnson and W. C. Schieve. Comment on "collective effects and trapping states by a quantum-trajectory treatment of micromaser dynamics". *Phys. Rev. A*, 67:027801, Feb 2003.

[32] P. L. Knight and Radmore P. M. *Phys. Lett.*, 26:342, 1982.

[33] Mikhail I. Kolobov and Fritz Haake. Collective effect in the microlaser. *Phys. Rev. A.*, 55(4):3033–3041, Apr 1997.

[34] Joachim Krause, Marlan O. Scully, and Herbert Walther. *Phys. Rev. A.*, 34:2032, 1986.

[35] Zheng-Dong Liu, Liang Zeng, and Shi-Yao Zhu. The evolution of a micromaser cavity field without the rotating-wave approximation. *J. Mod. Opts.*, 45(5):945–954, May 1998.

[36] Ning Lu. Micromaser spectrum: Trapped states. *Phys. Rev. A*, 47:1347, 1993.

[37] L. A. Lugiato, M. O. Scully, and Herbert Walther. Connection between microscopic and macroscopic maser theory. *Phys. Rev. A*, 36(2):740–743, Jul 1987.

[38] L. Mandel. Sub-poissonian photon statistics in resonance fluoresence. *Opt. Lett.*, 4(7):205–207, Jul 1979.

[39] Rebecca R. McGowan and William C. Schieve. *Phys. Rev. A.*, 56(3):2373–2384, Sep 1997.

[40] Rebecca R. McGowan and William C. Schieve. Theory of detection in the micromaser. *Phys. Rev. A*, 59(1):778–796, Jan 1999.

[41] D. Meschede, Herbert Walther, and G. Müller. One-atom maser. *Phys. Rev. Lett.*, 54(6):551–554, Feb 1985.

[42] P. Meystre. PhD thesis, Ecole Polytechnique Fédérale, Lausanne, 1974. (unpublished).

[43] P. Meystre. Cavity quantum optica and the quantum measurement process. *Progress in Opt.*, XXX:261–335, 1992.

[44] P. Meystre, G. Rempe, and Herbert Walther. Very-low-temperature behavior of a microscomaser. *Opt. Lett.*, 13(12):1078–1080, Dec 1988.

[45] Pierre Meystre. *Elements of Quantum Optics*. Cambridge University Press, New York, 1999.

[46] N. B. Narozhny, J. J. Sánchez-Mondragón, and J. H. Eberly. *Phys. Rev. A*, 39:236, 1981.

[47] Miguel Orszag, Ricardo Ramírez, Juan C. Retamal, and Carlos Saavedra. Quantum cooperative effects in a micromaser. *Phys. Rev. A*, 49:2933, 1994.

[48] H. Paul and Th. Richter. Bunching and antibunching of de-excited atoms leaving a micromaser. *Opt. Commun.*, 85(5,6):508–519, Oct 1991.

[49] Tran Quang, G. S. Agarwal, J. Bergou, M. O. Scully, H. Walther, K. Vogel, and W. P. Schleich. Calculation of the micromaser spectrum. i. green's function approach and approximate analytical techniques. *Phys. Rev. A*, 48:803, 1993.

[50] G. Raithel, O. Benson, and Herbert Walther. Atomic interferometry with the micromaser. *Phys. Rev. Lett.*, 75(19):3446–3449, Nov 1995.

[51] Georg Raithel, Christian Wagner, Lorenzo M. Narducci, and Marlan O. Scully. The micromaser: A proving ground for quantum physics. *Adv. At., Mol., Opt. Phys. Suppl.*, 2:57–121, 1994.

[52] Gerhard Rempe, F. Schmidt-Kaler, and Herbert Walther. Observation of sub-Poissonian statistics in a micromaser. *Phys. Rev. Lett.*, 64(23):2783–2786, Jun 1990.

[53] Gerhard Rempe and Herbert Walther. Sub-Poissonian atomic statistics in a micromaser. *Phys. Rev. A*, 42(3):1650–1655, Aug 1990.

[54] Gerhard Rempe, Herbert Walther, and Norbert Klein. Observation of quantum collapse and revival in a one-atom maser. *Phys. Rev. Lett.*, 58(4):353–356, Jan 1987.

[55] H. Risken and Vollmer H. D. Solutions and applications of tridiagonal vector recurrence relations. *Z. Physik B*, 39:339–346, 1980.

[56] M. O. Scully, Herbert Walther, G. S. Agarwal, T. Quang, and W. P. Schleich. *Phys. Rev. A.*, 44:5992, 1991.

[57] Marlan O. Scully and Willis E. Lamb. *Phys. Rev.*, 159:208, 1967.

[58] Marlan O. Scully and M. Suhail Zubairy. *Quantum Optics*. Cambridge University Press, New York, 1997.

[59] T. Sleator and H. Weinfurter. *Phys. Rev. Lett.*, 74:4087, 1995.

[60] D.T. Smithey, M. Beck, A. Faridani, and M.G. Raymer. *Phys. Rev. Lett.*, 70:1244, 1993.

[61] B.T.H. Varcoe, S. Brattke, M. Weidinger, and H. Walther. Preparing pure photon number states of the radiation field. *Nature*, 403:743–746, Feb 2000.

[62] K. Vogel, W. P. Schleich, M. O. Scully, and H. Walther. Calculation of the micromaser spectrum. ii. eigenvalue approach. *Phys. Rev. A*, 48:813, 1993.

[63] C. Wagner, R. J. Brecha, A. Schenzle, and Herbert Walther. *Phys. Bl.*, 48:465, 1992.

[64] C. Wagner, R. J. Brecha, A. Schenzle, and Herbert Walther. Phase diffusion and continuous quantum measurements in the micromaser. *Phys. Rev. A*, 46(9):R5350–R5353, Nov 1992.

[65] C. Wagner, R. J. Brecha, A. Schenzle, and Herbert Walther. *Phys. Rev. A*, 47:5068, 1993.

[66] Edda Wehner, Seno Raffaella, Sterpi Nicoletta, Berthold-Georg Englert, and Herbert Walther. Atom pairs in the micromaser. *Opt. Commun.*, 110:655, 1994.

[67] M. Weidinger, B. T. H. Varcoe, R. Heerlein, and H. Walther. Trapping states in the micromaser. *Phys. Rev. Lett.*, 82(19):3795–3798, May 1999.

[68] Shi-Yao Zhu, L.Z. Wang, and Heidi Fearn. Effect of atomic decay on micromasers. *Phys. Rev. A.*, 44(1):737–746, Jul 1991.

Vita

David Brian Johnson was born in 1973 and grew up in Richardson, Texas. He came to love learning to understand as much as he could about the universe and everything that goes on inside it. Studying Physics seemed to him the most efficient way of continuing his passion. He graduated with a B.S. in Physics at the University of Texas in 1995, and enrolled in Physics graduate studies at the University of Texas that same year.

Permanent address: 1905 Plymouth Rock
Richardson, Texas 75081

This dissertation was typeset with LaTeX[†] by the author.

[†]LaTeX is a document preparation system developed by Leslie Lamport as a special version of Donald Knuth's TeX Program.